Title
Self-Assembled, Peptide Based Biomaterials for Regenerative Medicine and Drug Delivery

Author
Black, Katie Anna

Publication Date
2014

Peer reviewed|Thesis/dissertation

Self-Assembled, Peptide Based Biomaterials for Regenerative Medicine and Drug Delivery

by

Katie Anna Black

A dissertation submitted in partial satisfaction of the

Requirements for the degree of

Joint Doctor of Philosophy
with University of California, San Francisco

in

Bioengineering

in the

Graduate Division

of the

University of California, Berkeley

Committee in charge:

Professor Matthew Tirrell, Chair
Professor Sanjay Kumar
Professor Ting Xu
Professor Tejal Desai

Spring 2014

Abstract

Self-Assembled, Peptide Based Biomaterials for Regenerative Medicine and Drug Delivery

By

Katie Anna Black

Joint Doctor of Philosophy
with the University of California, San Francisco

in Bioengineering

University of California, Berkeley

Professor Matthew Tirrell, Chair

A focus of the field of biomaterials is to use directed design to create new materials which replicate and enhance the intricate functions of the human body. Nature's own building blocks, peptides, are an ideal material to create self-assembling biomaterials as they are biodegradable, relatively easy to synthesize, and can be designed with a wide array of functions. In this dissertation, self-assembling peptide materials were optimized for two important medical applications: regenerative medicine and drug delivery.

Peptide amphiphiles (PAs), peptides conjugated to fatty acid tails, can self-assemble into both spherical micelles and worm-like micelles. PA worm-like micelles are of particular interest for regenerative medicine applications for their ability to form viscoelastic hydrogels at high concentration. Here we created PA hydrogel systems with active formation and stabilization triggers that are amenable to *in situ* gelation. Two different methods of *in situ* gel formation in PA systems were investigated, shear force and pH.

Shear-induced formation of worm-like micelles is demonstrated in the PA termed C_{16}-W3K. Before shearing, C_{16}-W3K PAs form spherical micelles in solution and exhibit little to no viscoelasticity. As the solution is subjected to simple shear flow with increasing shear rate, spherical micelles form elongated worm-like micelles up to microns in length. In the C_{16}-W3K PA system, shear force induced the change not only of the micelle structure but also of the peptide secondary structure simultaneously.

Worm-like micelle formation was also demonstrated using pH modulation, in the PA termed C_{16}GSH, which was designed with a branched peptide headgroup of histidine and serine amino acids. At low pH, the histidine side chains are protonated and hydrogen bonding does not occur, creating weakly elastic hydrogels. At pH 7.4, above the pKa of the histidine imidazole group, cooperative hydrogen bonding occurs, stabilizing the self-assembled worm-like micelles and creating a strong viscoelastic hydrogel. This unique architecture of C_{16}GSH makes it possible to create hydrogels spanning a wide range of stiffness (0.1-10 kPa). C_{16}GSH were optimized *in vitro* and *in vivo* for the application of peripheral nerve regeneration. Peripheral nerve injury is a debilitating condition for which new bioengineering solutions are needed. One

strategy to enhance regeneration inside nerve guide conduits is to fill the conduits with a hydrogel to mimic the native extracellular matrix found in peripheral nerves. C_{16}GSH hydrogels were compared to a commercially available collagen gel, which has been previously investigated as a nerve guide filler gel. Schwann cells, a cell type important in the peripheral nerve regenerative cascade, were able to spread, proliferate and migrate better on C_{16}GSH gels *in vitro* when compared to cells seeded on collagen gels. Moreover, C_{16}GSH gels were implanted subcutaneously in a murine model and were found to be biocompatible, degrade over time, and support angiogenesis without causing inflammation or a foreign body immune response. Taken together, these results help optimize and instruct the development of a new synthetic, hydrogel as a luminal filler for conduit-mediated peripheral nerve repair.

In the second half of this dissertation, peptide based complex coacervates were optimized for delivery of protein therapeutics. Complex coacervation is a liquid-liquid phase separation based on the electrostatic association of two oppositely charged polymers in aqueous solution. Coacervation results in micron sized droplets of a dense polymer-rich phase (coacervate) which is separate from the dilute polymer-poor solution phase (aqueous phase). Complex coacervates based on synthetic polypeptides have many desirable features for therapeutic protein delivery. They can be synthetically produced, can be made to be biocompatible and biodegradable, and their formation can be tuned by a wide array of parameters. In this dissertation, a method to encapsulate proteins by complex coacervation using polypeptides is explored.

Protein encapsulation with a model protein system: bovine serum albumin (BSA) was demonstrated. Rheological properties were studied to determine the viscoelasticity which may have implications for cell internalization. It was demonstrated that there is tradeoff between loading efficiency and total loading. Therefore, depending on the application, high loading capacity, up to 1:3 molar ratio of protein to polypeptide, or 100% loading of the protein can be achieved, depending on the process and cost of the protein which is often high. Encapsulated BSA retained its secondary structure when encapsulated and was released under conditions of low pH due to disassembly of the coacervate. Lastly, protein loaded coacervates were shown to be non-toxic in a cell viability assay.

Polypeptide complex coacervates show promise at encapsulating proteins for therapeutic delivery, but it is difficult to control their size and stability to due dynamic rearrangement and coalescence. To control the size and stability of polypeptide coacervates, the crosslinker EDC was used to create a peptide bond between the amino acid side groups of poly(L-lysine) (PLys) and poly(D/L-glutamic acid) (PGlu). By changing the ratio of PGlu to PLys colloidal stability was achieved without the need for an additional excipient. Surface charge of the particles was also controlled by this method. Final particle size was controlled by both molecular weight and concentration of the polypeptides. A span of particle diameter from to 272nm to 1.3 μm was achieved. Lastly, stability at low pH, where non-crosslinked coacervates disassemble, was demonstrated. A simple and tunable method to control particle size, such as the one presented here provides a possible solution to a major limitation in the field of drug delivery, control of particle size.

Dedication

This work is dedicated to my parents, Sean and Shelley Megley.

Table of Contents

List of Figures and Tables

Chapter 1

Chapter 2

Chapter 3

Chapter 4

Chapter 5

Acknowledgements

I am fortunate to have the support of colleagues, mentors, friends, and family along my journey to obtain a PhD, and to them, I owe a mountain of appreciation and thanks.

First, I'd like to thank my advisor, Matt Tirrell, for taking a chance on a 1st year graduate student even though it meant a move and a transfer to a new university. I am grateful for Matt's faith in my abilities as a scientist and the freedom I had in choosing the direction of my research.

I'd like to thank the members of the Tirrell group, both past and present, for their scientific guidance and camaraderie. The peptide amphiphile people: Badri A, EunJi Chung, Dan Krogstad, Brian Lin, Rachel Marullo, Laurie Mlinar, Won Suh, Amanda Trent, Bret Ulery and Emily Wonder. And of course the coaecervate people for also accepting me to "their side" of the lab: Matthew Kade, Sarah Perry, Dimitris Priftis, and Lorraine Leon. I also want to thank the incredible undergraduates I worked with and had the opportunity to mentor: Seema Desai, Jeremy Yip and William Byun. I have greatly benefited from the collaborative environment and excitement for science that the lab has.

The administrative staff at Berkeley deserves a special thanks, especially Rebecca Pauling, Kristin Olson, Terre Falciglia, Jennifer Teverbaugh, and Vonis Moore for sorting through the often confusing paperwork, space or funding situation so that I could focus on research.

In my time at Berkeley and in the wider bay area I have developed a group of amazing friends, a group of brilliant scientists, educators and other professionals with a passion for the outdoors. These friends with whom I have shared many weekend adventures, are people that I admire greatly and look forward to continuing our friendships (and adventures) for many years.

I'd like to thank my Grammy Joan. There is nothing more motivating than your grandmother's voice 3,000 miles away asking "how is your dissertation coming along?" She has always impressed upon me the value of education, and the importance in achieving your goals. Her care packages of cookies and candy made late nights of studying or writing much happier times.

I'd like to thank my parents, Sean and Shelley Megley and my sister, Colleen Megley for their lifetime of support. From the very earliest failed science projects through undergraduate and graduate school they have always supported my dreams. I'd like to thank them for inspiring my curiosity and love for math and science at a young age and for teaching me that anything is possible with a little hard work and dedication.

Lastly, and most importantly I'd like to thank my husband Matthew Black. His love, support and encouragement are what got to me to where I am today. There are no sufficient words to thank him enough for everything that he does. I "that" you.

Chapter 1: Background and Motivation

The field of biomaterials has grown rapidly in recent years and has made incredible improvements to human health.[1] From the earliest, relatively simple materials, such as sutures and stainless steel hip implants, scientists and clinicians have made great strides in improving biomaterials. Hip implants, for example, last longer than they did even five years ago due the development of composite materials to resist wear.[2] Historically, however, many biomaterials have been developed with a "top down" approach and still cannot come close to matching the complexity and capabilities of the body's own "biomaterials," such as nerves, red blood cells, and extracellular matrix.

In order to create more complex materials that can better mimic nature than many traditional techniques, many biomaterials under development utilize directed self-assembly, containing molecules that are designed to self-assemble into the desired structures.[3,4] When designed correctly, the molecules can self-assemble into complex, multifunctional nanomaterials easily and inexpensively. Nature's own building blocks, peptides, are an ideal material to create self-assembling biomaterials as they are biodegradable, relatively easy to synthesize, and can be designed with a wide array of functions. In this dissertation, self-assembling peptide materials were optimized for two important medical applications: regenerative medicine and drug delivery.

1.1 Peptide Amphiphiles for Regenerative Medicine

The human body has the capability to regenerate organs in some injuries but often lacks critical components to finish the process in others. One example where regeneration is particularly efficient is the liver, which can regenerate when more than 50% is removed.[5] However, in tissues such as skin, bone and nerve, regeneration is only possible for injuries less than a critical size. Above this critical point, scarring (in the case of skin and bone) or failure to attach (in the case of nerves) often occurs, which prevents regeneration. Still other tissues, such as cartilage, have inherently low regenerative potential due to the intrinsic biological features of the tissue.[6] In addition, other factors can reduce the regeneration potential of tissues including inflammation, scaring in the area, or age induced loss of progenitor cells.[7] Therefore, there is a great unmet medical need for biomaterials to aid the body in regeneration.

The field of regenerative medicine seeks to augment the body's regenerative process with materials to act as scaffolds for the body's regenerating cells. These scaffolds have unique requirements that vary based on the injury in question. Materials must come as close as possible to replicating the body's natural architecture in order to properly augment healing.

The extracellular matrix (ECM) is particularly important in directing the growth of cells as cells derive a wealth of information from their local microenvironment. In order to provide the regenerating cells with the correct signals, a biomaterial must recapitulate both the structure and function of the native ECM.[8,9] ECM is composed of two types of macromolecules: proteoglycans and fibrous structural proteins (collagen, lamin, fibronectin, vitronectin and elastin). Each tissue in the body differs in composition and structure of ECM, creating a characteristic microenvironment that is instructive to resident cells during development and regeneration.[10,11] The stiffness of ECM is another important property. Cells are able to "sense" stiffness by pulling on the matrix through contact points called focal adhesions. In a seminal paper, Engler, et al. demonstrated that matrix stiffness influences the differentiation of mesenchymal stem cells into neurons, myoblasts and osteoblasts.[12] This important result has

implications in regenerative medicine as adult stem cells are often integral in the healing process. Lastly, cells are able to degrade and remodel ECM in the body using secreted proteases. For a biomaterial to be compatible, it should degrade over time, as natural ECM does.

Peptide amphiphiles (PAs) have all the properties to form an ideal ECM substitute that can aid in regenerating cells. PAs can be designed to self-assemble into three dimensional hydrogels with a range of stiffness, can be designed to mimic the function of natural proteins, can easily be made to be multifunctional, and are biodegradable. PAs are molecules composed of a peptide segment (typically containing 5-20 amino acids) coupled to a fatty acid chain (12-18 carbons long). The hydrophilic (peptide) and hydrophobic (fatty acid tail) components of the PA cause them to self-assemble at low concentration due to hydrophobic interactions where the tail aggregates to minimize interactions with water.[13] PAs can assemble into a variety of structures including spherical micelles, long worm-like micelles, or liposomes depending on the PA design (Figure 1.1) .[14]

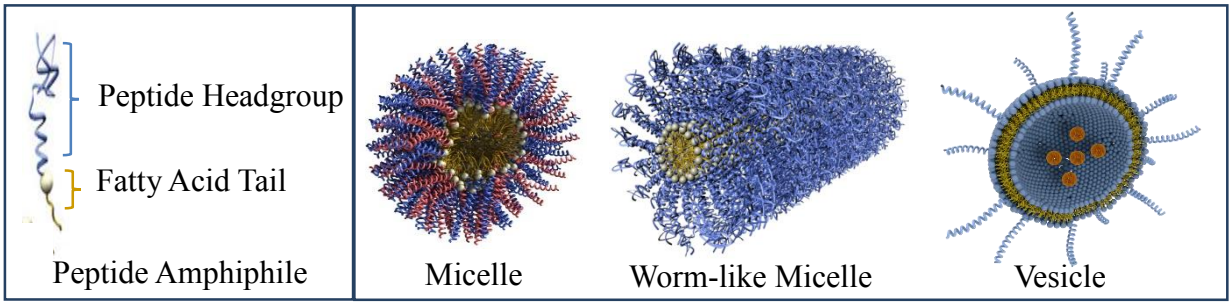

Figure 1.1: Peptide amphiphile (PA) molecule (left) which consist of a peptide conjugated to a fatty acid tail. In solution, PAs assemble into structures such as micelles, worm-like micelles or vesicles.

The self-assembled structures formed from PA's can mimic many of the beneficial properties of natural proteins found in the ECM. Self-assembled PA structures create a multivalent display of peptides, roughly 100 PA molecules per spherical micelle and many orders of magnitude more for the larger structures (worm-like micelles and vesicles), which can allow for numerous binding sites for cells. In addition, by simply mixing together different PA molecules, a multifunctional peptide display can be created.[15] This ability to mix and display peptides allows for the creation of multifunctional assembles that can, for example, both target a receptor on a cell and deliver a therapeutic.[16] Self-assemblies from PAs also have the ability to induce or stabilize the three-dimensional structure of the peptide headgroup, which is often lost when a short peptide is taken from a larger proteins. Our group and others, have used PAs to stabilize peptides into triple helices, α helices, and β sheets that resemble native protein molecular structures.[17–20] Recapitulation of the native protein secondary structure in the peptide headgroup creates biomimetic structures which effectively promote cell adhesion, spreading, migration, growth and differentiation *in vitro*.[20,21] Lastly, PAs are synthetically created from natural building blocks (amino acids and fatty acids), which allows enzymes present in the body to digest and recycle these molecules readily.

PAs can be designed to form different types of self-assembled structures. Most commonly, PAs form either soluble, spherical micelles or extended worm-like micelles that can intertwine to form hydrogels. Peptides with highly charged amino acids tend to occupy a large volume relative to the fatty acid tail and this cone-like shape forces a high curvature at the

peptide-lipid interface and tends to result in the formation of spherical micelles. Spherical PA micelles, due to their small size, are amenable for applications where circulation is necessary. Soluble PA micelles have been used in a multitude of applications including imaging[22,23], biomineralization[24,25], drug delivery[26,27], gene delivery[28,29], immunotherapy[30], and cancer therapeutics[31,32].

PAs with a proportional headgroup volume compared to tail section at the peptide-lipid interface tend to form cylindrical micelles, or worm-like micelles, and are desirable for mimicking the natural ECM. PAs that form worm-like micelles contain peptides with a smaller headgroup, especially those which are relatively linear, or contain interacting beta sheets. Specifically, β sheet hydrogen bonds in the first four amino acids closest to the worm-like micelle core are necessary to form cylindrical structures, and disruption of those bonds will result in the formation of spherical micelles instead.[33] Worm-like micelles which are typically nanometers in diameter and microns in length can entangle at a high concentration to form a viscoelastic hydrogel.[34,35] A stable hydrogel is defined as having a storage modulus (G') over loss modulus (G") ratio of greater than one at a dynamic frequency of 10Hz.

Worm-like micelles from PAs are an area of active research in many labs for regenerative medicine and tissue engineering applications.[36,37] In particular, PA hydrogels have shown promise in the area of neural-based tissue engineering. *In vitro*, neural progenitor cells cultured within a PA hydrogel differentiate into neurons, a necessary subtype for repair, while differentiation into astrocytes, a cell type associated with scarring, is suppressed.[38] When applied to a mouse spinal cord injury model, a PA gel was shown to improve regeneration and suppress scarring.[39,40] Despite the success with central nervous system (CNS) applications, PA hydrogels have not been used in peripheral nerve applications. Based on the success of PA gels with repair in the central nervous system, it was suggested in a recent review that PA gels would be well suited for the application of a filler gel for peripheral nerve injury.[15]

While PAs and worm-like micelles have seen much success in the lab, the ability to form gels *in situ* using an active trigger has not been realized. Most PA gels are formed instantaneously upon dissolution and then must be surgically inserted into the injury site. Injecting a preformed PA gel, especially where the application requires a stiff gel, is not practical and may cause fiber breakage creating an inhomogeneous gel. A preferred method would be the ability to inject a low viscosity solution into the injury site and have the gel form during injection. To this end, one study showed that by changing the amino acids at the core where β-sheet is promoted, to bulkier, charged residues, gelation time was increased. The authors suggest by tuning gelation time, the material could then be used as an injectable biomaterial.[41] Using time represents a passive trigger for gelation. Here we seek to create a PA hydrogel system with an active formation and stabilization trigger that is amenable to *in situ* gelation. In Chapters 2 and 3, two different *in situ* gelling PA systems are investigated and optimized for use in peripheral nerve regeneration, an application that has yet to be studied with PA hydrogels.

1.2 Complex Coacervation for Drug Delivery

Recent advances in molecular biology have enabled the discovery of a plethora of protein and peptide therapeutics. Due to their complexity, proteins can achieve functions that are difficult to accomplish with small molecule drugs. This has allowed proteins and peptides to be discovered or designed to interact with nearly any target with high specificity.[42] Protein therapeutics are now used to treat a variety of diseases, including diabetes[43] and cancer.[44]

Though protein therapeutics enjoy specificity and high potency, effective and efficient delivery remains challenging. When delivered intravenously, protein drugs suffer from low bioavailability and are easily degraded in the body. Proteins in the blood stream can be degraded by proteases, denatured, or targeted by the mononuclear phagocyte system for removal.[45] A method to encapsulate and protect proteins inside complex coacervates could enhance stability and aid in effective delivery of the therapeutic.

Complex coacervation is a liquid-liquid phase separation based on the electrostatic association of two oppositely charged polymers in aqueous solution. Coacervation results in micron sized droplets of a dense polymer-rich phase (coacervate) which is separate from the dilute polymer-poor solution phase (aqueous phase) (Figure 1.2). Over time or with centrifugal force, coacervate droplets can coalesce and form one continuous coacervate phase. This process was first observed using two natural polymers, gelatin and gum Arabic.[46] More recently, systems of complex coacervation have been explored for drug delivery using the naturally-occurring polymers alginate, chitosan, or heparin.[47,48] Examples of complex coacervation can be seen in nature, including the interaction of DNA and histone proteins[49] and in marine organisms (sandcastle worm gluing[50] and mussel fiber anchoring[51]). Complex coacervation has found industrial use in the areas of microencapsulation for food additives[52,53], electronic ink display[54], and protein purification[55].

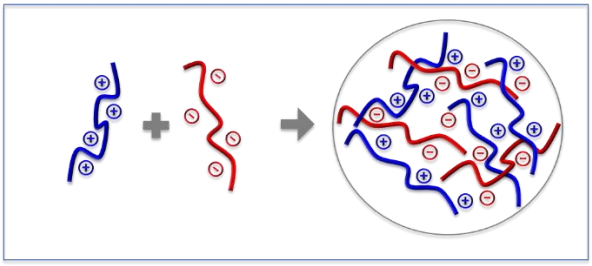

Figure 1.2: Schematic of complex coacervation

Complex coacervates formed by charged synthetic polypeptides offer a wide range of tunability and control of coacervate formation. Additionally *de novo* design with enhanced functionality and precise molecular control can be realized. Synthetically produced polypeptides such as poly(lysine) and poly(glutamic acid) are biocompatible and have been used in biomaterial applications such as coatings and covalent drug modifications.[56] Previous work identified the conditions under which these polypeptides form complex coacervates in solution.[57,58] In addition to polymer chemistry, salt concentration, pH, the ratio of polycation to polyanion, total polymer concentration and temperature are important system parameters that can be tuned to control coacervate formation. Additionally, it was found that polypeptide complex coacervates exhibit low interfacial tension, which may be useful for encapsulation of charged materials.[59,60]

Complex coacervates based on synthetic polypeptides have many desirable features for therapeutic protein delivery. They can be synthetically produced, can be made to be biocompatible and biodegradable, and their formation can be tuned by a wide array of parameters. While there are many polymer systems under development for protein delivery[61], complex coacervates have the distinct advantage that they are formed under mild, aqueous conditions. Despite this advantage and the fact that complex coacervates have been used in a wide range of commercial activities, there is very little work that has explored using coacervates

from polypeptides to encapsulate proteins as therapeutics. In Chapter 4, a method to encapsulate proteins by complex coacervation using polypeptides is explored. In Chapter 5, a modification to the system to increase the stability of the complex coacervates.

1.3 References

1. Sahoo, S. K., Parveen, S. & Panda, J. J. The present and future of nanotechnology in human health care. *Nanomedicine* **3,** 20–31 (2007).

2. Knight, S. R., Aujla, R. & Biswas, S. P. Total Hip Arthroplasty - over 100 years of operative history. *Orthop. Rev. (Pavia).* **3,** 72–74 (2011).

3. Zhang, S. Fabrication of novel biomaterials through molecular self-assembly. *Nat. Biotechnol.* **21,** 1171–8 (2003).

4. Kyle, S., Aggeli, A., Ingham, E. & McPherson, M. J. Production of self-assembling biomaterials for tissue engineering. *Trends Biotechnol.* **27,** 423–33 (2009).

5. Michalopoulos, G. K. & DeFrances, M. C. Liver Regeneration. *Science (80-.).* **276,** 60–66 (1997).

6. Cancedda, R., Dozin, B., Giannoni, P. & Quarto, R. Tissue engineering and cell therapy of cartilage and bone. *Matrix Biol.* **22,** 81–91 (2003).

7. Place, E. S., Evans, N. D. & Stevens, M. M. Complexity in biomaterials for tissue engineering. *Nat. Mater.* **8,** 457–70 (2009).

8. Lutolf, M. P. & Hubbell, J. a. Synthetic biomaterials as instructive extracellular microenvironments for morphogenesis in tissue engineering. *Nat. Biotechnol.* **23,** 47–55 (2005).

9. Huang, N. F. & Li, S. Regulation of the matrix microenvironment for stem cell engineering and regenerative medicine. *Ann. Biomed. Eng.* **39,** 1201–14 (2011).

10. Frantz, C., Stewart, K. M. & Weaver, V. M. The extracellular matrix at a glance. *J. Cell Sci.* **123,** 4195–200 (2010).

11. Daley, W. P., Peters, S. B. & Larsen, M. Extracellular matrix dynamics in development and regenerative medicine. *J. Cell Sci.* **121,** 255–64 (2008).

12. Engler, A. J., Sen, S., Sweeney, H. L. & Discher, D. E. Matrix elasticity directs stem cell lineage specification. *Cell* **126,** 677–89 (2006).

13. Israelachvili, J. N. *Intermolecular and surface forces*. (Academic Press, 1992).

14. Trent, A., Marullo, R., Lin, B., Black, M. & Tirrell, M. Structural properties of soluble peptide amphiphile micelles. *Soft Matter* **7,** 9572 (2011).

15. Tan, A., Rajadas, J. & Seifalian, A. M. Biochemical engineering nerve conduits using peptide amphiphiles. *J. Control. Release* **163,** 342–52 (2012).

16. Peters, D. *et al.* Targeting atherosclerosis by using modular, multifunctional micelles. *Proc. Natl. Acad. Sci. U. S. A.* **106,** 9815–9 (2009).

17. Yu, Y.-C., Berndt, P., Tirrell, M. & Fields, G. B. Self-Assembling Amphiphiles for Construction of Protein Molecular Architecture. *J. Am. Chem. Soc.* **118,** 12515–12520 (1996).

18. Fields, G. B. *et al.* Proteinlike Molecular Architecture : Biomaterial Applications for Inducing Cellular Receptor Binding and Signal Transduction. *Biopolymers* **47,** 143–151 (1998).

19. Yu, Y. C. *et al.* Structure and dynamics of peptide-amphiphiles incorporating triple-helical proteinlike molecular architecture. *Biochemistry* **38,** 1659–68 (1999).

20. Pakalns, T. *et al.* Cellular recognition of synthetic peptide amphiphiles in self-assembled monolayer films. *Biomaterials* **20,** 2265–79 (1999).

21. Dori, Y. *et al.* Ligand accessibility as means to control cell response to bioactive bilayer membranes. *J. Biomed. Mater. Res.* **50,** 75–81 (2000).

22. Morisco, A. *et al.* Micelles derivatized with octreotide as potential target-selective contrast agents in MRI. *J. Pept. Sci.* **15,** 242–50 (2009).

23. Bull, S. R., Guler, M. O., Bras, R. E., Meade, T. J. & Stupp, S. I. Self-assembled peptide amphiphile nanofibers conjugated to MRI contrast agents. *Nano Lett.* **5,** 1–4 (2005).

24. Hartgerink, J. D., Beniash, E. & Stupp, S. I. Self-assembly and mineralization of peptide-amphiphile nanofibers. *Science* **294,** 1684–8 (2001).

25. Spoerke, E. D., Anthony, S. G. & Stupp, S. I. Enzyme Directed Templating of Artificial Bone Mineral. *Adv. Mater.* **21,** 425–430 (2009).

26. Branco, M. C. & Schneider, J. P. Self-assembling materials for therapeutic delivery. *Acta Biomater.* **5,** 817–31 (2009).

27. Webber, M. J., Matson, J. B., Tamboli, V. K. & Stupp, S. I. Controlled release of dexamethasone from peptide nanofiber gels to modulate inflammatory response. *Biomaterials* **33,** 6823–32 (2012).

28. Bitton, R. *et al.* Self-assembly of model DNA-binding peptide amphiphiles. *Langmuir* **21,** 11888–95 (2005).

29. Tu, R. S. *et al.* Cooperative DNA binding and assembly by a bZip peptide-amphiphile. *Soft Matter* **6,** 1035 (2010).

30. Black, M. *et al.* Self-assembled peptide amphiphile micelles containing a cytotoxic T-cell epitope promote a protective immune response in vivo. *Adv. Mater.* **24,** 3845–9 (2012).

31. Standley, S. M. *et al.* Induction of cancer cell death by self-assembling nanostructures incorporating a cytotoxic peptide. *Cancer Res.* **70,** 3020–6 (2010).

32. Garg, A., Tisdale, A. W., Haidari, E. & Kokkoli, E. Targeting colon cancer cells using PEGylated liposomes modified with a fibronectin-mimetic peptide. *Int. J. Pharm.* **366,** 201–10 (2009).

33. Paramonov, S. E., Jun, H.-W. & Hartgerink, J. D. Self-assembly of peptide-amphiphile nanofibers: the roles of hydrogen bonding and amphiphilic packing. *J. Am. Chem. Soc.* **128,** 7291–8 (2006).

34. Greenfield, M. A., Hoffman, J. R., de la Cruz, M. O. & Stupp, S. I. Tunable mechanics of peptide nanofiber gels. *Langmuir* **26,** 3641–7 (2010).

35. Kern, F., Lequeux, F., Zana, R. & Candau, S. J. Dynamical Properties of Salt-Free Viscoelastic Micellar Solutions. *Langmuir* **10,** 1714–1723 (1994).

36. Cui, H., Webber, M. J. M. J. & Stupp, S. I. Self-Assembly of Peptide Amphiphiles: From Molecules to Nanostructures to Biomaterials. *Pept. Sci.* **94,** 1–18 (2009).

37. Webber, M. J., Berns, E. J. & Stupp, S. I. Supramolecular Nanofibers of Peptide Amphiphiles for Medicine. *Isr. J. Chem.* **53,** 1–25 (2013).

38. Silva, G. a *et al.* Selective differentiation of neural progenitor cells by high-epitope density nanofibers. *Science (80-.).* **303,** 1352–5 (2004).

39. Tysseling, V. M. *et al.* Self-assembling peptide amphiphile promotes plasticity of serotonergic fibers following spinal cord injury. *J. Neurosci. Res.* **88,** 3161–70 (2010).

40. Tysseling-Mattiace, V. M. *et al.* Self-assembling nanofibers inhibit glial scar formation and promote axon elongation after spinal cord injury. *J. Neurosci.* **28,** 3814–23 (2008).

41. Niece, K. L. *et al.* Modification of gelation kinetics in bioactive peptide amphiphiles. *Biomaterials* **29,** 4501–9 (2008).

42. Leader, B., Baca, Q. J. & Golan, D. E. Protein therapeutics: a summary and pharmacological classification. *Nat. Rev. Drug Discov.* **7,** 21–39 (2008).

43. DeWitt, D. E. & Hirsch, I. B. Outpatient insulin therapy in type 1 and type 2 diabetes mellitus. *J. Am. Med. Assoc.* **289,** 2254–2264 (2003).

44. Scott, A. M., Wolchok, J. D. & Old, L. J. Antibody therapy of cancer. *Nat. Rev. Cancer* **12,** 278–87 (2012).

45. Brown, L. R. Commercial challenges of protein drug delivery. *Expert Opin. Drug Deliv.* **2,** 29–42 (2005).

46. Bungenberg de Jong, H. B. & Kruyt, H. R. Coacervation (Partial Miscibility in Colloid Systems). *Proc. Sect. Sci, Koninkijke Ned. Akad. van Wet.* **32,** 849–856 (1929).

47. Sarmento, B. *et al.* Alginate/chitosan nanoparticles are effective for oral insulin delivery. *Pharm. Res.* **24,** 2198–206 (2007).

48. Chu, H., Gao, J., Chen, C.-W., Huard, J. & Wang, Y. Injectable fibroblast growth factor-2 coacervate for persistent angiogenesis. *Proc. Natl. Acad. Sci. U. S. A.* **108,** 13444–9 (2011).

49. Takahagi, M. & Tatsumi, K. Aggregative organization enhances the DNA end-joining process that is mediated by DNA-dependent protein kinase. *FEBS J.* **273,** 3063–75 (2006).

50. Stewart, R. J., Weaver, J. C., Morse, D. E. & Waite, J. H. The tube cement of Phragmatopoma californica: a solid foam. *J. Exp. Biol.* **207,** 4727–34 (2004).

51. Waite, J. H., Andersen, N. H., Jewhurst, S. & Sun, C. Mussel Adhesion: Finding the Tricks Worth Mimicking. *J. Adhes.* **81,** 297–317 (2005).

52. Shahidi, F., Han, X. Q. & Han, X. Encapsulation of Food ingredients. *Crit. Rev. Food Sci. Nutr.* **33,** 501–547 (1993).

53. King, A. H. in *Encapsulation Control. Release Food Ingredients* 26–39 (1995).

54. Song, J. K., Kang, H. C., Kim, K. S. & Chin, I.-J. Microcapsules by Complex Coacervation for Electronic Ink. *Mol. Cryst. Liq. Cryst.* **464,** 263–269 (2007).

55. Cooper, C. L., Dubin, P. L., Kayitmazer, A. B. & Turksen, S. Polyelectrolyte–protein complexes. *Curr. Opin. Colloid Interface Sci.* **10,** 52–78 (2005).

56. Shih, I.-L., Van, Y.-T. & Shen, M.-H. Biomedical applications of chemically and microbiologically synthesized poly(glutamic acid) and poly(lysine). *Mini Rev. Med. Chem.* **4,** 179–88 (2004).

57. Priftis, D. & Tirrell, M. Phase behaviour and complex coacervation of aqueous polypeptide solutions. *Soft Matter* **8,** 9396–9405 (2012).

58. Priftis, D., Megley, K., Laugel, N. & Tirrell, M. Complex coacervation of poly(ethylene-imine)/polypeptide aqueous solutions: thermodynamic and rheological characterization. *J. Colloid Interface Sci.* **398,** 39–50 (2013).

59. Priftis, D., Farina, R. & Tirrell, M. Interfacial Energy of Polypeptide Complex Coacervates Measured via Capillary Adhesion †. *Langmuir* **28,** 8721–9 (2012).

60. Spruijt, E., Sprakel, J., Cohen Stuart, M. A. & van der Gucht, J. Interfacial tension between a complex coacervate phase and its coexisting aqueous phase. *Soft Matter* **6,** 172 (2010).

61. Putney, S. & Burke, P. Improving protein therapeutics with sustained-release formulations. *Nat. Biotechnol.* **16,** 153–157 (1998).

Chapter 2: Shear Induced Transition from Spherical to Worm-Like Micelle in Peptide Amphiphile Solution

Associated Paper:

T Shimada, **K Megley**, M Tirrell, and A Hotta "Fluid Mechanical Shear Induces Structural Transitions in Assembly of a Peptide-Lipid Conjugate" *Soft Matter* 2011**, 7**, 8856-8861.

Abstract

Peptide amphiphiles (PAs) can self-assemble into both spherical micelles and worm-like micelles. The control of worm-like micelle formation in a PA solution is an area of active research, most often accomplished by modulating the temperature, salt content, or pH of the environment. In this chapter, shear-induced formation of worm-like micelles is demonstrated in the PA termed C_{16}-W3K. Before shearing, C_{16}-W3K PAs form spherical micelles in solution and exhibit little to no viscoelasticity. As the solution is subjected to simple shear flow, with increasing shear rate, spherical micelles form elongated worm-like micelles up to microns in length. The PA micelles change their structures from sphere to worm-like irreversibly and the resultant worm-like micelles are highly stable due to the β-sheet formation, i.e. intermolecular hydrogen bonding, in their peptide regions. In the C_{16}-W3K PA system, shear force induced the change not only of the micelle structure but also of the peptide secondary structure simultaneously. Such hierarchical transitions caused by simple shear make this PA system useful for application as an injectable tissue engineering matrix.

2.1 Introduction

Peptide amphiphiles (PA) are a class of synthetic molecules composed of a hydrophilic peptide segment (typically containing 5–30 amino acids) coupled to a hydrophobic tail (typically 12–18 carbons long), which may be single- or double-chained, natural fatty acid or lipid molecules, synthetic analogs or other hydrophobic segments.[1] The amphiphilicity of these molecules drives them to self-assemble in aqueous solution into structures such as spherical micelles, worm-like micelles, vesicles, monolayers, bilayers, nanotapes and ribbons due to hydrophobic interactions where the tails aggregate to minimize interactions with water.[2] It has been shown that self-assembly of the PAs can induce and/or stabilize secondary structure of the peptide headgroup into triple helices, α-helices, and β-sheets which resemble native protein molecular structures.[3–8] Recapitulation of the native protein secondary structure in the peptide headgroup creates biomimetic structures, which can be employed to promote cell adhesion, spreading, migration, growth and differentiation.[9–11] The native secondary structure generally enhances bio-activity.[12,13]

De novo design has been employed to select peptide sequences with propensity to form worm-like micelles, typically composed of alanine, valine or glycine amino acids.[14] Worm-like micelles are generally ~10 nanometers in diameter (the approximate length of two PA molecules) and have a polydisperse length distribution spanning many microns. In PAs where charged amino acids are utilized, worm-like micelle formation can be driven by pH or ion concentration changes.[15] It has also been shown that self-assembly into worm-like micelles is highly dependent on hydrogen bonding and amphiphilic packing. Specifically, in one class of PAs,[16] β-sheet

hydrogen bonds in the first four amino acids closest to the nanofiber core have been found to be necessary and sufficient to form and stabilize worm- like micelles, and disruption of those bonds will result in the formation of spherical micelles. The dimensions of the elongated worm-like micelles allow them to form entangled networks and display mechanical properties similar to those of a hydrogel.[17] A stable hydrogel can be operationally defined as having a storage modulus (G') to loss modulus (G") ratio of greater than 1 at a dynamic frequency of 10 Hz.[18]

In this work, a PA system termed C_{16}-W3K was investigated, which had been previously shown to transform with time (on the order of days) from spherical to worm-like micellar assemblies.[19] The C_{16}-W3K molecule is a 17-amino acid chain composed of thirteen alanines (A), with a tryptophan (W) (to allow absorbance measurements of concentration), and three spatially separated lysines (K) (to increase solubility in water) attached to a 16-carbon alkyl tail (Figure 2.1).

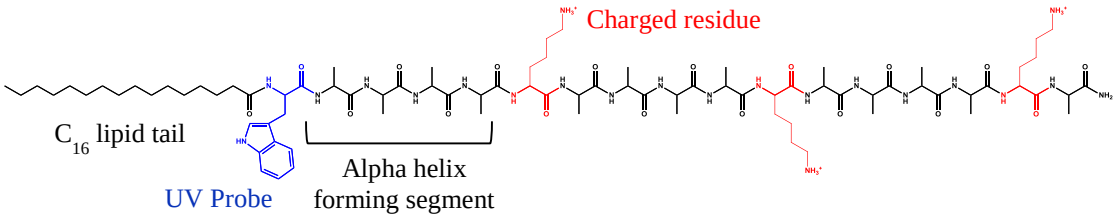

Figure 2.1: Chemical structure of the peptide amphiphile "C_{16}-W3K".

This arrangement of amino acids was chosen in particular due to the repeated alanine stretches and symmetrical arrangement of lysines that predisposes the peptide to form individual α-helices.[20] Previous work demonstrates that the PAs will first form spherical micelles and then over time (days at 25ºC and hours at 50ºC) undergo a transition to worm-like micelles with β-sheet character in the headgroup.[19] Here, it is demonstrated that the transition can be driven by fluid shear stress, effectively and instantaneously. It was found that at a specific shear rate (100 s^{-1}) the system experiences an irreversible jump in viscosity, and shows gel-like behavior in subsequent rheological tests. The measurements presented here show an abrupt transition at the micro-scale (the fibril formations) as well as on a molecular scale (the conformational α-helix to β-sheet transition) in the PA solution.

A bioactive system such as the one presented here, in which the gelation transition is driven by shear force, could be useful as an injectable matrix or scaffold for supporting tissue regeneration. Many PA systems have been investigated for use as matrices for applications such as bone, blood vessel or nerve tissue engineering.[21,22] However, most of these systems require nanofiber formation control by way of temperature or solution changes.[23] The present system transforms itself nearly instantaneously to a gel-like state in simple shear flow on exceeding a critical shear rate, which might be applied during the injection process itself.

2.2 Methods

Peptide amphiphile synthesis

Peptides were obtained as synthesized on resin, with side groups fully protected, from Synpep Corporation (Dublin, CA). Synthesis reagents N-hydrobenzotriazole (HOBt) and 2-(1H-benzotriazole-yl)- 1,1,3,3-tetramethyluroniumhexafluorophosphate (HBTU) were purchased from Novabiochem. All other chemical reagents were purchased from Sigma-Aldrich. The PA

C_{16}-W3K (Fig. 1) was made by conjugating the peptide to palmitic acid using the Fmoc solid-phase peptide-synthetic methods.[10] All PAs were deprotected and cleaved from the resin using a mixture of 95% by volume trifluoroacetic acid (TFA)/water solution. The PAs were then precipitated in cold methyl-tert-butyl-ether. The conjugates were purified by reverse phase high performance liquid chromatography (RP-HPLC) on a C4 column with gradients of acetonitrile in water with 0.1% trifluoroacetic acid (TFA). The identity of purified conjugates was verified by MALDI-TOF (Matrix Assisted Laser Desorption Ionization—Time of Flight) mass spectrometry. Purified samples were then lyophilized, resuspended by adding buffer (10mM sodium chloride with 1 mM sodium phosphate; pH 7.4) at room temperature at a PA concentration of 750μM (well above the CMC 2μM), and used immediately for analysis. The samples were soluble instantly in the buffer, and it was not necessary to stir the samples to dissolve the PA. All the following experiments were carried out in a similar fashion to prevent any sort of shear history before the experiments. At this neutral pH, the lysines in the PA are positively charged.

Rheology

Rheological measurements were carried out using an ARES- RFS rheometer (TA Instruments) with a cone and plate geometry (50mm in diameter with the cone angle of 0.04 radians) at 20ºC. The gap between the cone tip and the plate was kept constant at 0.05 mm. In each experiment, a new solution of the PA was prepared so that the time evolution of the solution could be neglected. Each testing required a sample volume of 1.4mL. A unidirectional shear rate sweep was used to determine viscosity as a function of shear rate (ranging from 1 to 1000 s^{-1}). Amplitude sweeps were performed to determine the linear viscoelastic range. Storage modulus (G') and loss modulus (G") were determined using an oscillatory frequency sweep over the frequency range of 0.1 Hz < u < 100 Hz.

Circular Dichroism

The peptide secondary structure was studied by circular dichroism (CD) on a Jasco J-815 Circular Dichroism Spectropolarimeter at 25ºC. The PA solutions before and after the rheological testing were used for the CD measurements. Data were collected from 190nm to 250nm at 1nm intervals. All reported spectra are the result of averaging three scans.

Cell Culture

Cell culture reagents were purchased from Gibco (Life Technologies, Carlsbad, CA) unless otherwise noted. Pre-sheared solutions of C_{16}-W3K were cast into 96 well plates at a height of 1mm. A confluent layer of NIH 3T3 fibroblasts (ATCC) was trypsinized with 0.25% Trypsin–EDTA for one minute and neutralized with calf bovine serum (CBS) supplemented Dulbecco's Modified Eagle Medium (DMEM) with 1% v/v penicillin-streptomycin. The cells were then seeded on the hydrogels at a density of 1.6×10^4 cells per cm^2 (16 hour time point) or 7.9×10^3 cells per cm^2 in media (72 hour timepoint). The low density seeding would allow for extended viability studies. Cells were cultured at 37ºC, in a humidified atmosphere with 5% CO2. At hour 16 and 72 cell cultures were removed from the incubator and Presto Blue Cell Viability Kit was used to measure cell viability as compared to a control well containing no gel, only cells.

2.3 Results

2.3.1 Shear induced gelation

Figure 2.2 shows the first, second and third scans of a single C_{16}-W3K sample of viscosity versus shear rate the using unidirectional shear. For shear rates ranging from 10^0 to 10^2 s^{-1}, the viscosity was constant (10^{-3} Pa s), near the value for pure water. In this range, viscosity was independent of shear rate; the solution behaved as a Newtonian fluid.[18] At the shear rate of 10^2 s^{-1}, an abrupt increase in viscosity was observed, which implies that a phase transition occurred in the PA solution. After the critical shear rate, the solution demonstrated shear-thinning behavior, indicating a network formation of entangled fibers. The viscosity of the second cycle increased dramatically, nearly 1000 times higher at the shear rate of 1 s^{-1} than the viscosity during the first scan (i.e. initial solution). The third and fourth cycle closely reproduced the second one, indicating no further structural change. From these results, we presume that the solution irreversibly changed from a very dilute suspension of spherical micelles, rheologically indistinguishable from water, into a highly viscous solution with entangled worm-like micelles, during the rheological testing.

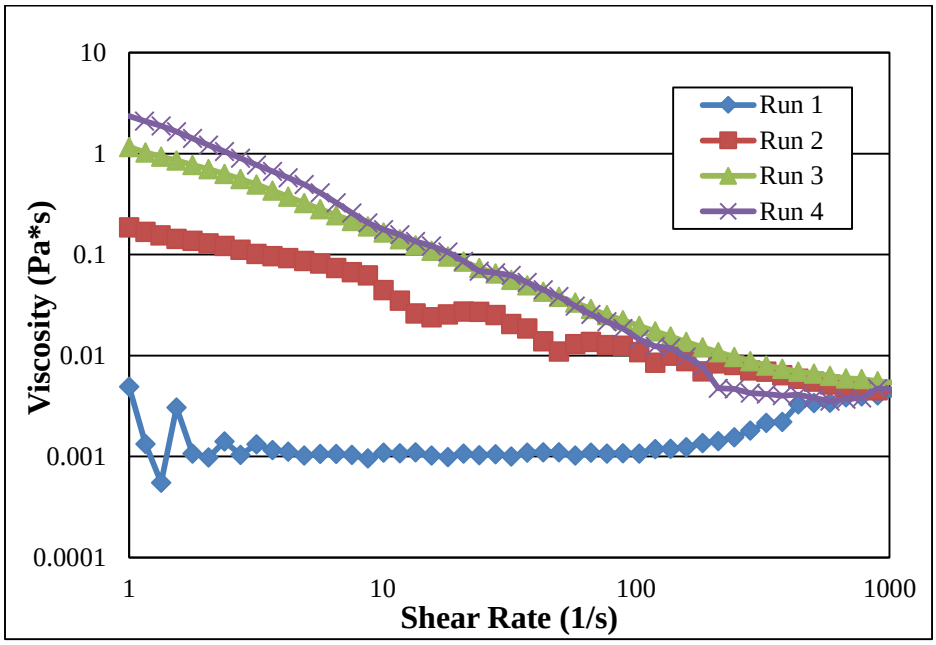

Figure 2.2: Viscosity measurements of the C_{16}-W3K solution in the first, second, third and fourth cycles of testing for the same sample. The abrupt transition was observed only during the first cycle. The succeeding three cycles almost traced the same viscosity line. The viscosity of the second and the third cycles increased by nearly 1000 times at a strain rate of 1 s^{-1}.

In Figure 2.3, the results of the oscillatory frequency sweep are shown for the solution before and after the rheological testing. Before the transition (red symbols), the storage modulus (G') and the loss modulus (G") were barely detectable, indicating that the liquid behaved as Newtonian fluid. Above the frequency of 10^0, the loss modulus became higher than the storage modulus with $G' \approx \omega^2$ and $G'' \approx \omega$, indicating that the sample behaved as a weakly viscoelastic

liquid. The storage modulus (G') and the loss modulus (G") of the sample after the testing (blue symbols) were higher by one-thousand fold to ten-thousand fold than those of the sample before the testing. After the transition, the storage modulus was constant and higher than the loss modulus throughout the range of frequency, indicating that, at this stage, the solid elastic-like behavior dominated the viscous components. In addition, the modulus was relatively independent of frequency across the range tested, characteristic of a soft networked elastic solid, in this case, a hydrogel.

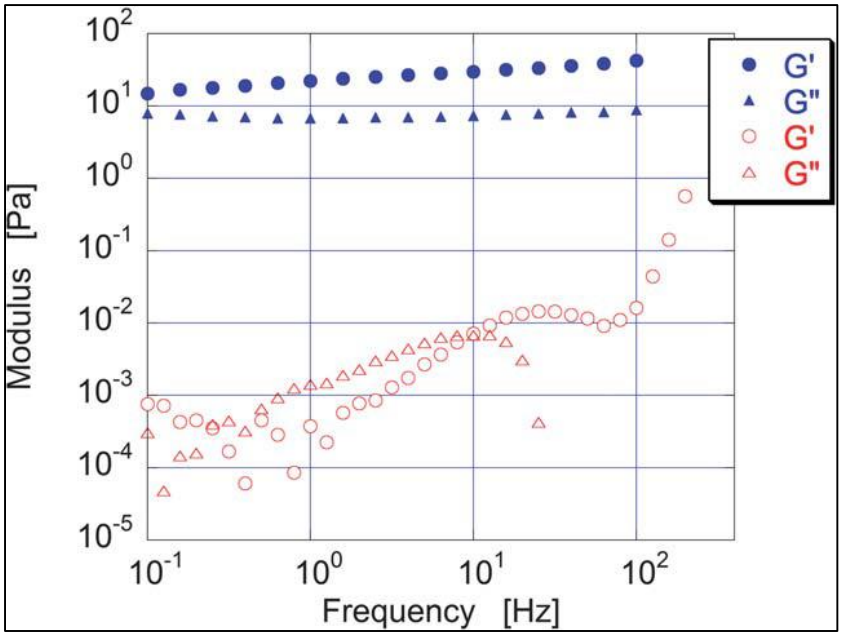

Figure 2.3: Oscillatory testing of the C_{16}-W3K solutions before (open, red symbols) and after (closed, blue symbols) the transition was induced by the simple shear test.

2.3.2 Relationship between stiffness and concentration

Gels of C_{16}-W3K made with increasing concentration of PA were sheared to induce gelation (as described above) and stiffness was measured. Storage modulus (G') from the frequency sweep test (at a frequency of 10 Hz) for each concentration of C_{16}-W3K is reported in Figure 2.4. For concentrations up to 1000μM, storage modulus (G') increased up to 72 Pa with increasing concentration. For concentrations above 1000μM, stiffness decreased.

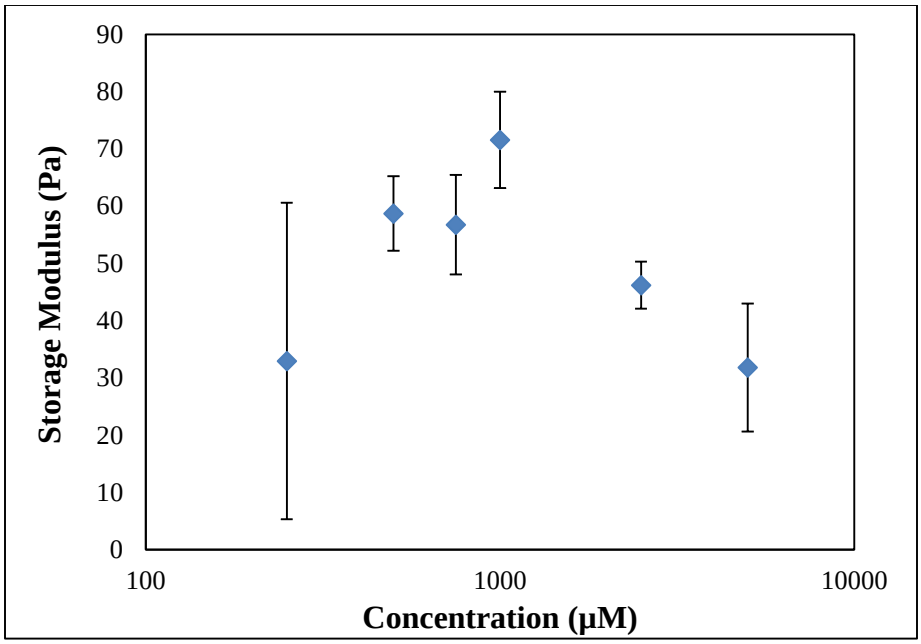

Figure 2.4: Storage modulus as a function of concentration, tabulated from individual frequency sweep tests (frequency = 10 Hz) for each concentration of pre-sheared gel.

2.3.3 Bulk shear force induces a change in peptide secondary structure

Circular Dichroism (CD) was used to study the secondary structure in the peptide headgroup. Figure 2.5 shows the CD spectra of the PA solutions measured before (red) and after (blue) the rheological testing. The CD spectrum of the sample before rheological testing exhibited two minima at 204 nm and 222 nm, indicating that initially the C_{16}-W3K formed α-helical and random-coil secondary structures in solution. In contrast, the spectrum measured after the rheological testing presented a typical spectrum of the β-sheet structure in the solution, with a single minimum shifted towards 218 nm (Figure 2.5). Using linear addition of basis spectra modeling, the contributions of each secondary structure was calculated (Table 2.1). Thus it was found that the sample experienced a transition in molecular conformation from α-helical with random coil structures to predominantly β-sheet structures during the rheological testing. In addition this secondary structure transition was stable 20 and 43 days after rheological testing.

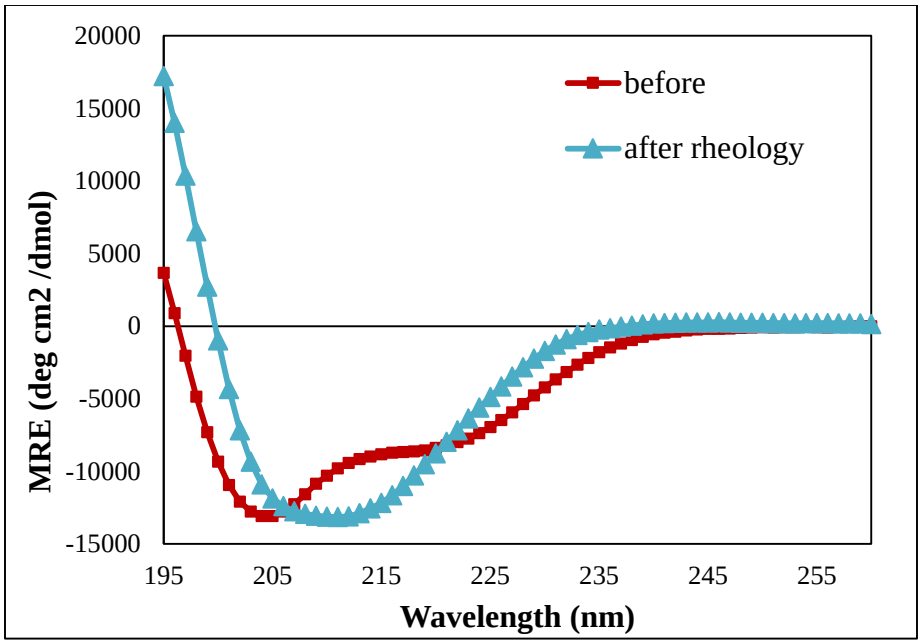

Figure 2.5: The CD spectra of the C_{16}-W3K solution measured before (red) and after (blue) the rheological testing. The red curve has its peaks at 204nm and 222nm representing α-helical and random coil structures and the blue curve shifts towards a peak of 218nm representing the β-sheet structure.

MRE Fit Modeling			
	α-helix	Random coil	β-sheet
Before	18.4%	41.5%	40.2%
After	0%	27.7%	72.3%
20 days after	0%	23.2%	76.8%
43 days after	0%	25.6%	74.4%

Table 2.1: MRE fit modeling results for the CD spectra of the C_{16}-W3K solution measured before, immediately after, 20 days, and 43 days after rheological testing.

2.3.4 *In vitro* biocompatibility

To assess the material biocompatibility, an in vitro cell viability test was performed. NIH 3T3 cells were cultured on top of C_{16}-W3K, C_{16}-W3K-RGDS, and combinations thereof. After a period of 16 and 72 hours, cell viability was measured. At 16 hours cells grown on all variations

of C_{16}-W3K and C_{16}-W3K-RGDS had statistically similar viability to that of the control, tissue culture plastic (ANOVA). At 72 hours, cells had significantly lower viability than the control (Figure 2.6) (Dunnett's Test, $p<0.01$).

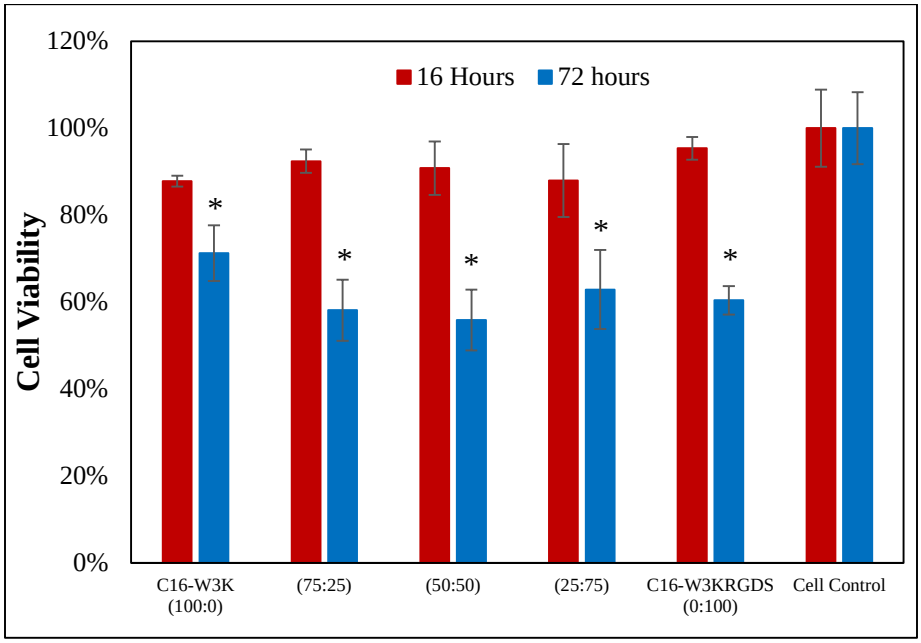

Figure 2.6: Cell viability of NIH 3T3 cells grown on gels of C_{16}-W3K, C_{16}-W3KRGDS, or a mixture. Time points include 16 and 72 hours. *Dunnett's Test, statistically different than control, $p<0.01$.

2.4 Discussion

PA based hydrogels have great potential in the area of tissue engineering. For this application, PA's must be carefully designed to form worm-like micelles with gelation control and tunable mechanical properties. One strategy has been to use four alanine amino acids next to the tail region, at the core of the micelle to induce β-sheet hydrogen bonding and stabilize a worm-like micelle structure. Such arrangements typically require additional salt or heat to force the transition from spherical to worm-like micelle. In cases where tissue engineering matrices need to be injectable, this method is not ideal. Here, an alternative gelation mechanism is explored: the application of bulk shear force. For this work a PA, C_{16}-W3K, with three alanaine repeat stretches which transitions slowly on the order of weeks to a gel like state was used. Methods of forcing that transition to happen instantaneously were demonstrated using rheological testing. An in situ gelation mechanism such as the application of shear force, could be readily translated into clinical use as shear force is experienced when solutions are injected through the narrow nozzle of a needle.

Solutions of the PA C_{16}-W3K showed an abrupt increase in viscosity and gelation at a critical shear rate during the rheological testing. It is known that some dilute cationic surfactant systems, such as CTAB (hexadecyltrimethylammonium bromide) and CTAT (cetyltrimethylammonium p-toluensulfonate), also exhibit the abrupt increases in viscosity at a critical shear rate during rheological testing and the structures formed under shear have been

studied using small angle neutron scattering with shear, light scattering, birefringence and cryo-TEM.[24–28] In these studies, the common requirements for the surfactant systems are (1) concentration which is very low, but above the CMC, where partially worm-like micelles can be formed and (2) strong electrostatic repulsion in the charged micelles. These conditions closely match the C_{16}-W3K system as the concentration of C_{16}-W3K is low (750μM) but above its CMC (2μM) and has three lysines residues which are positively charged at pH 7.4.

The application of shear during the rheological testing induced the transition of the micelle structures in the solution from spherical to worm-like micelles, and thus creating non-Newtonian and gel-like properties. In the initial test of viscosity using a simple unidirectional shear test, the C_{16}-W3K solutions had roughly the viscosity of water, and had no dependence on shear rate. At a critical shear rate of 100 1/s, a jump in viscosity was measured, indicating a structural transition in the solution. Subsequent viscosity tests on the same solution showed a 10,000 fold increase in viscosity and a shear thinning dependence on shear rate indicating an entangled gel of worm-like micelles had formed. Additional viscosity tests matched the shear thinning behavior of the second test, indicating that the structural change was permanent. Evidence of a sol-gel transition was also seen using dynamic oscillatory rheological testing. A frequency sweep of the C_{16}-W3K solution before the transition showed a barely detectable modulus, with the two components of modulus (storage and loss) crossing over. A frequency sweep of a C_{16}-W3K solution that had been transitioned via the simple shear test, had a higher modulus, and storage component G', higher than the loss component G" indicating an elastic hydrogel. Using rheological tests, a structural transition from spherical to worm-like micelles was observed.

The effect of increasing concentrations of C_{16}-W3K on gel stiffness was studied. For gels up to 1000 μM, stiffness increased with concentration. Above 1000 μM, the stiffness of C_{16}-W3K actually decreased. This phenomenon can be explained by the differences in behavior for semi-dilute and concentrated worm-like micelles surfactants. In the semi dilute range the micelles are isotopic in orientation and it is expected the solution behave as a viscoelastic liquid, scaling with concentration. As solutions in this semi-dilute regime are sheared, breakup and reformation of micelles occurs. In the concentrated regime above 1000 μM, ordering of the micelles occurs creating a nematic phase. As solutions in this concentrated regime are sheared, elastic modulus (G') decreases due to lack of isotropic entanglements.[24,29] Maximum stiffness values of 72 Pa are in agreement with most PA gel systems reported in literature,[30] though are significantly less stiff than some newly developed systems able to reach stiffnesses of ~1000 Pa.[31]

Through the CD measurements, it was found that, in addition to the wormlike micelle formation, the peptide W3K in C_{16}-W3K simultaneously changed the secondary structure from predominantly α-helix with random coils to mainly β-sheet during the rheological testing. Previous work showed that the β-sheet formation also takes days at 25ºC.[19] However in this experiment with rheological testing, the secondary structural change occurs in a short time, indicating that the α-helix and random coil to β-sheet transition in the peptide is also induced by the mechanical shear in the rheological testing. Although some polypeptides have been reported to undergo α-helix to β-sheet transitions triggered by external stimulation such as changes in pH or redox, the microscopic α-helix to β-sheet transition in polypeptides induced by macroscopic forces such as fluid mechanical shear has not been reported, to our knowledge. Since the direct effect of macroscopic mechanical shear on the peptide secondary structure in the molecular scale

cannot be reasonable, it is presumed that the micellar structural change induced by shear triggers the peptide structural change.

The worm-like micelles of other cationic surfactants formed by induction of shear are stable under active shear stress and disappear again when the shear force is stopped. However, our results indicate that the C_{16}-W3K PA worm-like micelles remain after shear is removed. The irreversibility and the high stability of the micelles results from the intermolecular hydrogen bonding in the β-sheet structure of the peptide existing in the micelle shell. The CD results clearly show the new β-sheet formation through the rheological testing is stable for long time periods (1.5 months). The micelle structure and the peptide secondary structure are determined cooperatively to minimize the whole energy of the system. In some PA systems, induction and stabilization of peptide secondary structures by micelle formation have been reported.[3–5,7,8] The micelle formation changes the local environment around the peptides in the PA, affecting the peptide secondary structures. The similar process may happen in our C_{16}-W3K system. The peptide W3K is stable in α-helix and random coil when the C_{16}-W3K forms spherical micelle. However, when the micelle structure is forced to change by mechanical shear to be worm-like, the peptides may adjust the secondary structure to β-sheet that is most stable in the new environment.

Biocompatibility was assessed with a model fibroblast cell line, NIH 3T3. Pre-sheared gels of C_{16}-W3K, C_{16}-W3KRGDS and combinations of the two, were added to the bottom of 96 well plates and cells were seeded on top. At time points of 16 and 72 hours, a dye was used to determine the number of viable cells. At 16 hours, cells on C_{16}-W3K and C_{16}-W3KRGDS variants had statistically similar viability to that of the control, tissue culture plastic. At 72 hours however, a decline in cell viability was apparent, for all variants of the C_{16}-W3K gels. A possible explanation is that as monomer PAs exist in equilibrium with the worm-like micelles, PA monomers which have a positive charge could associate with and disrupt the negatively charged cell membranes. This effect has been seen in other work in our group with other peptide amphiphiles.[32]

2.5 Conclusions

In this work, a novel method to induce multi-scale supramolecular structures in a PA solution through mechanical shear was introduced. Upon dissolution the C_{16}-W3K PA formed spherical micelles with a low solution viscosity. With the application of shear, spherical micelles elongated to form worm-like micelles, able to entangle and give rise to a viscoelastic hydrogel. The macroscopic transition was also accompanied by a secondary structure transition in the peptide head group from α-helical to β-sheet. The detailed investigation of the conformational transitions in our designed C_{16}-W3K PAs may well provide useful information about how to design other shear responsive peptide amphiphile systems.

For the application of tissue engineering, biomaterials must match closely the stiffness, architecture, and function of native extracellular matrix of the tissues in question. With a maximum storage modulus of 72 Pa, the C_{16}-W3K system would not be suitable for repair of even the softest tissues in the body, for example brain tissue which has a stiffness of 1,000 Pa.[33] In addition, at time points of 72 hours, a slight decline in cell viability was observed for cells grown on C_{16}-W3K gels. Taken together, though the C_{16}-W3K is an interesting system for the study of PA design, it is not suitable for the application of tissue engineering. In the following chapter these limitations will be taken into consideration in the redesign of a PA system for

tissue engineering. Specific attention will be paid to stability of the matrix, range of stiffness, and biocompatibility.

2.6 References

1. Hartgerink, J. D., Beniash, E. & Stupp, S. I. Peptide-amphiphile nanofibers: a versatile scaffold for the preparation of self-assembling materials. *Proc. Natl. Acad. Sci. U. S. A.* **99,** 5133–8 (2002).

2. Tu, R. S. & Tirrell, M. Bottom-up design of biomimetic assemblies. *Adv. Drug Deliv. Rev.* **56,** 1537–63 (2004).

3. Yu, Y.-C., Berndt, P., Tirrell, M. & Fields, G. B. Self-Assembling Amphiphiles for Construction of Protein Molecular Architecture. *J. Am. Chem. Soc.* **118,** 12515–12520 (1996).

4. Fields, G. B. *et al.* Proteinlike Molecular Architecture : Biomaterial Applications for Inducing Cellular Receptor Binding and Signal Transduction. *Biopolymers* **47,** 143–151 (1998).

5. Yu, Y. C. *et al.* Structure and dynamics of peptide-amphiphiles incorporating triple-helical proteinlike molecular architecture. *Biochemistry* **38,** 1659–68 (1999).

6. Pakalns, T. *et al.* Cellular recognition of synthetic peptide amphiphiles in self-assembled monolayer films. *Biomaterials* **20,** 2265–79 (1999).

7. Forns, P., Lauer-Fields, J. L., Gao, S. & Fields, G. B. Induction of protein-like molecular architecture by monoalkyl hydrocarbon chains. *Biopolymers* **54,** 531–46 (2000).

8. Malkar, N. B., Lauer-Fields, J. L., Juska, D. & Fields, G. B. Characterization of peptide-amphiphiles possessing cellular activation sequences. *Biomacromolecules* **4,** 518–28 (2003).

9. Dori, Y. *et al.* Ligand accessibility as means to control cell response to bioactive bilayer membranes. *J. Biomed. Mater. Res.* **50,** 75–81 (2000).

10. Berndt, P., Fields, G. B. & Tirrell, M. Synthetic lipidation of peptides and amino acids: monolayer structure and properties. *J. Am. Chem. Soc.* **117,** 9515–9522 (1995).

11. Winger, T. M., Ludovice, P. J. & Chaikof, E. L. Lipopeptide conjugates: biomolecular building blocks for receptor activating membrane-mimetic structures. *Biomaterials* **17,** 437–41 (1996).

12. Tu, R. S. *et al.* Cooperative DNA binding and assembly by a bZip peptide-amphiphile. *Soft Matter* **6,** 1035 (2010).

13. Missirlis, D. *et al.* Linker Chemistry Determines Secondary Structure of p53(14-29) in Peptide Amphiphile Micelles. *Bioconjug. Chem.* 465–475 (2010). doi:10.1021/bc900383m

14. Zhang, S. Fabrication of novel biomaterials through molecular self-assembly. *Nat. Biotechnol.* **21,** 1171–8 (2003).

15. Hartgerink, J. D., Beniash, E. & Stupp, S. I. Self-assembly and mineralization of peptide-amphiphile nanofibers. *Science* **294,** 1684–8 (2001).

16. Paramonov, S. E., Jun, H.-W. & Hartgerink, J. D. Self-assembly of peptide-amphiphile nanofibers: the roles of hydrogen bonding and amphiphilic packing. *J. Am. Chem. Soc.* **128,** 7291–8 (2006).

17. Kern, F., Lequeux, F., Zana, R. & Candau, S. J. Dynamical Properties of Salt-Free Viscoelastic Micellar Solutions. *Langmuir* **10,** 1714–1723 (1994).

18. Mezger, T. *The Rheology Handbook: For Users of Rotational and Oscillatory Rheometers*. (Vincentz Network, 2006).

19. Shimada, T., Lee, S., Bates, F. S., Hotta, A. & Tirrell, M. Wormlike micelle formation in peptide-lipid conjugates driven by secondary structure transformation of the headgroups. *J. Phys. Chem. B* **113,** 13711–4 (2009).

20. Marqusee, S., Robbins, V. H. & Baldwin, R. L. Unusually stable helix formation in short alanine-based peptides. *Proc. Natl. Acad. Sci. U. S. A.* **86,** 5286–90 (1989).

21. Sargeant, T. D. *et al.* Hybrid bone implants: self-assembly of peptide amphiphile nanofibers within porous titanium. *Biomaterials* **29,** 161–71 (2008).

22. Hosseinkhani, H., Hosseinkhani, M., Khademhosseini, A., Kobayashi, H. & Tabata, Y. Enhanced angiogenesis through controlled release of basic fibroblast growth factor from peptide amphiphile for tissue regeneration. *Biomaterials* **27,** 5836–44 (2006).

23. Mart, R. J., Osborne, R. D., Stevens, M. M. & Ulijn, R. V. Peptide-based stimuli-responsive biomaterials. *Soft Matter* **2,** 822–835 (2006).

24. Berret, J., Gamez-Corrales, R., Oberdisse, J., Walker, L. & Lindner, P. Flow-structure relationship of shear-thickening surfactant solutions. *Europhys. Lett.* **41,** 677–682 (1998).

25. Ohlendorf, D., Interthal, W. & Hoffman, H. Surfaetant systems for drag reduction: physico-chemical properties and rheological behaviour. *Rheol. Acta* **25,** 468–486 (1986).

26. Wunderlich, I., Hoffmann, H. & Rehage, H. Flow birefringenee and rheological measurements on shear induced micellar structures. *Rheol. Acta* **26,** 532–542 (1987).

27. Liu, C. & Pine, D. Shear-Induced Gelation and Fracture in Micellar Solutions. *Phys. Rev. Lett.* **77,** 2121–2124 (1996).

28. Truong, M. T. & Walker, L. M. Quantifying the Importance of Micellar Microstructure and Electrostatic Interactions on the Shear-Induced Structural Transition of Cylindrical Micelles. *Langmuir* **18,** 2024–2031 (2002).

29. Berret, J. in *Mol. Gels* 667–720 (2006).

30. Anderson, J. M., Andukuri, A., Lim, D. J. & Jun, H.-W. Modulating the gelation properties of self-assembling peptide amphiphiles. *ACS Nano* **3,** 3447–54 (2009).

31. Greenfield, M. A., Hoffman, J. R., de la Cruz, M. O. & Stupp, S. I. Tunable mechanics of peptide nanofiber gels. *Langmuir* **26,** 3641–7 (2010).

32. Missirlis, D., Teesalu, T., Black, M. & Tirrell, M. The non-peptidic part determines the internalization mechanism and intracellular trafficking of Peptide amphiphiles. *PLoS One* **8,** e54611 (2013).

33. Pettikiriarachchi, J. T. S., Parish, C. L., Shoichet, M. S., Forsythe, J. S. & Nisbet, D. R. Biomaterials for Brain Tissue Engineering. *Aust. J. Chem.* **63,** 1143 (2010).

Chapter 3: pH Sensitive Peptide Amphiphile Hydrogels for the Application of Peripheral Nerve Regeneration

Associated Papers:

B Lin, **K Megley**, N Viswanathan, D Krogstad, L Drews, Y Qian, and M Tirrell "pH-responsive branched peptide amphiphile hydrogel designed for applications in regenerative medicine with potential as injectable tissue scaffolds" *Journal of Materials Chemistry*, **2012**, 22, 19447-19454.

K Black, B Lin, E Wonder, S Desai, E Chung, B Ulery, R Katari, and M Tirrell "Biocompatibility and optimization of a peptide amphiphile hydrogel for applications in peripheral nerve regeneration" *Tissue Engineering Part A, (submitted)*

Abstract:

Peripheral nerve injury is a debilitating condition for which new bioengineering solutions are needed. Autografting, the gold standard in treatment, involves sacrifice of a healthy nerve and results in loss of sensation or function at the donor site. One alternative solution to autografting is to use a nerve guide conduit, designed to physically guide the nerve as it regenerates across the injury gap. Such conduits are effective for short gap injuries, but fail to surpass autografting in long gap injuries. One strategy to enhance regeneration inside conduits in long gap injuries is to fill the guide conduits with a hydrogel to mimic the native extracellular matrix found in peripheral nerves. In this work, a peptide amphiphile based hydrogel was optimized for peripheral nerve repair. Hydrogels consisting of the peptide amphiphile C_{16}GSH were compared to a commercially available collagen gel. Schwann cells, a cell type important in the peripheral nerve regenerative cascade, were able to spread, proliferate and migrate better on C_{16}GSH gels *in vitro* when compared to cells seeded on collagen gels. Moreover, C_{16}GSH gels were implanted subcutaneously in a murine model and were found to be biocompatible, degrade over time, and support angiogenesis without causing inflammation or a foreign body immune response. Taken together, these results help optimize and instruct the development of a new synthetic, hydrogel as a luminal filler for conduit-mediated peripheral nerve repair.

3.1 Introduction

Peripheral nerve injury (PNI) is a debilitating condition which affects 2.8% of trauma patients, and can result in lifelong disability.[1] Autografting, the current gold standard treatment for PNI, involves removal of a piece of a healthy sensory nerve from elsewhere in the body (often the sural nerve, a sensory nerve of the lower leg) and attachment to the severed nerve ends, in order to guide regeneration.[2] Autografting is limited by availability of expendable donor nerves and results in a second injury with loss of sensation at the donor site.[3] To address the inherent limitations of autografting, nerve guide conduits have been developed as an alternative. Nerve guide conduits are hollow tubes that, when used to connect the two severed ends of a nerve injury, aid in neural repair by directing axons towards the distal stump and minimizing infiltration of scar tissue.[4] Conduits have been created from both natural and synthetic sources and four conduits have been approved by the FDA for use in limited gap length injuries.[5,6] Nerve

guides have shown comparable efficacy in 20-25mm injuries but are inferior to autografts in long gap injuries.[7,8]

In order to surpass the efficacy of autografts, especially in long gap repair, improvements must be made to the hollow tube design of current nerve guide conduits.[9,10] One strategy to enhance regeneration is to fill the tube with a material such as a hydrogel in order to promote cell growth. In designing a hydrogel to enhance peripheral nerve regrowth, the natural progression of regeneration must be considered. During the regeneration process, macrophages and fibroblasts first enter the injury space to remove debris and deposit an extracellular matrix framework, respectively. Schwann cells then detach from the proximal nerve to proliferate and migrate into the injury gap towards the distal nerve stump. Following the Schwann cells, new axons sprout from the severed proximal nerve stump and reconnect to the distal nerve stump, completing the regeneration process.[11] Thus, an ideal conduit gel filler should mimic the peripheral nerve environment and enhance the activity of regenerating Schwann cells. Collagen and laminin have both been investigated as potential luminal gel fillers for this application.[12–14] Though collagen gels have had some success, there are difficulties in precise control of the stiffness and Type I collagen gels sourced from animals have been shown to produce a deleterious immune response in patients.[15]

Synthetically based hydrogels are ideal to allow precise control of mechanical and biochemical properties while avoiding potential negative immune responses. One type of material, the peptide amphiphile (PA), is an attractive material to fill this need based on their ease of synthesis, modular design, and self-assembly properties.[16] PAs are made by conjugating short peptide sequences to fatty acid tails. The hydrophilic (peptide) and hydrophobic (fatty acid tail) components of the PA cause them to self-assemble at low concentrations into spherical micelles, long worm-like micelles, or liposomes depending on the PA design.[17] Worm-like micelles which are typically nanometers in diameter and microns in length can entangle at a high concentration to form a viscoelastic hydrogel.[18] PAs have been used in a variety of biomedical applications including imaging[19,20], biomineralization[21,22], drug delivery[23,24], gene delivery[25,26], immunotherapy[27], cancer therapeutics[28,29] and regenerative medicine.[30] In particular, PAs designed to form worm-like micelles that give rise to hydrogels have shown promise in the area of neural-based tissue engineering, such as spinal cord injury[31,32] and cavernous nerve injury.[33] Based on this encouraging evidence, it was suggested in a recent review that PA gels would be well suited for the application of a filler gel for peripheral nerve injury.[16]

In this work, the PA C_{16}GSH (Figure 1) was investigated for material properties and biocompatibility. C_{16}GSH hydrogels respond to pH changes due to hydrogen bonding between neighboring serine and histidine amino acids located on arms of neighboring monomers. At low pH, the histidine side chains are protonated and hydrogen bonding does not occur, creating weakly elastic hydrogels. At pH 7.4, above the pKa of the histidine imidazole group, cooperative hydrogen bonding occurs, stabilizing the self-assembled worm-like micelles and creating a strong viscoelastic hydrogel.[34] This unique architecture of C_{16}GSH makes it possible to create hydrogels spanning a wide range of stiffness. The C_{16}GSH hydrogel was optimized through a series of *in vitro* and *in vivo* tests to serve as a filler gel material to be used in conjunction with a nerve guide conduit for peripheral nerve regeneration. A commercially available collagen gel was used as a benchmark, as collagen gels have been shown to be beneficial both *in vitro* and *in vivo* for peripheral nerve injury.[35,36] First, a series of *in vitro* tests designed to mimic *in vivo* conditions was used to evaluate the hydrogel's ability to promote spreading, proliferation, and migration of Schwann cells. Following *in vitro* optimization, an *in vivo* subcutaneous

implantation model was used to investigate the biocompatibility and degradation rate of the hydrogels. Used together, this set of *in vitro* and *in vivo* tests provide a useful methodology by which to screen and optimize hydrogels for peripheral nerve regeneration applications. The work reported here represents a critical step in developing a hydrogel for peripheral nerve regeneration prior to the use of a small animal injury model. Ultimately, the creation and use of an improved filler gel material in conjunction with hollow synthetic nerve guides will allow clinicians to repair long gap peripheral nerve injuries without the undesirable side effects of the current state of the art treatment, autografting.

3.2 Materials and Methods

Peptide amphiphile synthesis

The GSH peptide was purchased fully protected on rink-amide resin (China Tech Peptides Co., Suzhou, China) or synthesized on rink-amide resin (Anaspec Fremont, CA) using an automated PS3 Benchtop Peptide Synthesizer (Protein Technologies, Tucson, AZ) solid phase peptide synthesizer. Fatty acid tails were conjugated to the lysine residue of the peptide as described previously[34] to create C_{16}GSH PAs (Figure 1). The synthesis products were precipitated in diethyl ether and purified to above 90% purity on a Shimadzu CBM-20A high performance liquid chromatography (HPLC) system, in reverse phase, employing a Waters Symmetry 300 semi-preparative C8 column. Product identity was confirmed by mass spectrometry employing an Applied Biosystems 4700 Proteomics Analyzer and purity was determined using analytical HPLC with a Waters Symmetry 300 analytical column. Exact concentrations were determined by UV spectroscopy[37], and it was determined that the peptides accounted for 60% of the measured mass of peptide salts. This correction was taken into account when considering molarity.

Hydrogel preparation

C_{16}GSH stock solutions were prepared at 2wt% in MilliQ water at pH 4 and sterilized by filtration through a 0.8/0.2μm Supor® Membrane filter (Pall Life Sciences, Port Washington, NY). PA solutions were heated to 50°C and sonicated for 5 minutes to ensure complete dissolution. PA solutions were then cooled to room temperature and further diluted with MilliQ water to specified concentrations before use. For *in vivo* studies, C_{16}GSH stock solutions were diluted to 2 and 0.2wt% in water, raised to pH 6.5 using 1M NaOH (Sigma Aldrich, Milwaukee, WI) and loaded into 1mL sterile syringes. A buffer solution of 2X PBS was added and mixed thoroughly to achieve a concentration of 1 and 0.1wt%, respectively, and a pH of 7.4.

Type I bovine collagen (Sigma Aldrich, Milwaukee, WI) was used as received (0.3wt%). Manufacturer's instructions were followed for the gelling procedure. Briefly, the acidic collagen solution was mixed 8:1 with 10X phosphate buffered saline (PBS) and the pH was adjusted to 7.4 using 1μL drops of 0.1M NaOH. Collagen solutions were kept on ice prior to use to prevent gelation. Collagen solutions were gelled by incubation at 37°C for 1 hour.

Rheology

Oscillatory shear rheology was performed on an Anton Paar Physica MCR 301 using a 25mm top plate. The measurement distance was set to 1mm and the samples were measured in a humidity chamber set to 20ºC. Samples were prepared in MilliQ water and measured at pH 4 ± 1 and 9 ± 1. For the high pH experiments, PA solutions were loaded at pH 4 and raised to the

higher pH with a minimal amount of NaOH, in situ, then equilibrated for 20 minutes in the humidity chamber for temperature, humidity, and pH stabilization prior to measurement. Collagen samples were prepared in MilliQ water and 10X PBS as previously described (Sigma Aldrich, Milwaukee, WI) and kept on ice until use. Collagen solutions were equilibrated for 1 hour at 37ºC in the humidity chamber prior to measurement.

Amplitude sweeps were performed and determined that 1% strain was within the linear viscoelastic range for both materials. Frequency sweeps were performed between 1 and 10 Hz. Two sweeps were performed for each sample and the data from the second sweep is reported. To approximate the Young's modulus (E) from the shear modulus (G'), the following relationship was used:

$$E = 2G'(1 + \nu)$$

The Poisson's ratio (ν) was assumed to be 0.5 since the hydrogel is an incompressible material.

Cell culture

Cell culture reagents were purchased from Gibco (Life Technologies, Carlsbad, CA) unless otherwise noted. Rat Schwannoma cells, RT4-D6P2T (ATCC, Manassas, VA) were cultured in Dulbecco's Modified Eagle Medium (DMEM) supplemented with 10% Fetal Bovine Serum (FBS) and 1% penicillin-streptomycin (P-S). Cells were incubated at 37°C in an atmosphere of 5% CO_2. Cell experiments were performed using passage 5-10 cells.

Scanning electron microscopy (SEM)

C_{16}GSH solutions were cast onto glass coverslips (10µL/coverslip) and allowed to equilibrate for 20 minutes. Gel crosslinking was achieved by adding 1µL of 0.1M NaOH and waiting 30 minutes. Coverslips were placed at the bottom of an eight well chamber slide (Nunc, Thermo Scientific, Waltham, MA) and washed three times with PBS and three times with serum free DMEM. Schwann cells were trypsinized, suspended in complete medium, and added at a density of 5,000 cells per well. Cells were allowed to attach and spread for a period of 24 hours. Samples were then washed with PBS and fixed with 4% formaldehyde for 15 minutes. Samples were fixed a second time with 2% glutaraldehyde in 0.1M sodium cacodylate buffer, washed three times with 0.1M sodium cacodylate buffer, and post fixed in 1% osmium tetroxide in 0.1M sodium cacodylate buffer for 1 hour. Samples were again washed three times with 0.1M sodium cacodylate to remove excess osmium tetroxide and exposed to a gradient of increasing ethanol in water until 100% ethanol was reached. Samples were then subjected to critical point drying on a Tousimis AutoSamdri-815, Series A. Dried samples were sputter coated with platinum using a Tousimis sputter coater. Scanning electron microscopy was performed on a Hiatchi S-5000 high resolution, cold field emission SEM.

Cell proliferation

C_{16}GSH solutions were cast into Corning half-area 96 well plates (Sigma Aldrich, Milwaukee, WI) at a volume of 30µL per well resulting in a solution of approximately 1mm in height. Solution was allowed to rest for 20 minutes before gel crosslinking was initiated by the addition of 1µL of 50% NaOH. Gels were then washed 10 times with PBS. Gels were sterilized with 5X P-S in PBS for 1 hour. Gels were washed with DMEM (without serum) 5 times and incubated at 37°C for 1 hour. Schwann cells were added to wells at a density of 2,500 cells per well in complete medium. After 24 hours of growth, cells were imaged on a Nikon Eclipse

TE200 microscope. After 48 hours, PrestoBlue® (Invitrogen, Carlsbad, CA) was added to the wells to achieve a final concentration of 10% by volume. After 3 hours of incubation, fluorescence was read on a Tecan plate reader (560nm excitation /590nm emission).

Migration

C_{16}GSH solution was loaded into the inlet ports of Iuvo™ Microchannel 5250 plates (Thermo Scientific, Waltham, MA) 1mm wide x 5.25mm long x 140µm high. Solution was allowed to rest for 20 minutes before gel crosslinking was initiated by adding 1µL of 0.1M NaOH to the outlet port. After 1 hour, gels inside the channels were washed 5 times with PBS by adding 3µL to the inlet port allowing 5 minutes for passive pumping to occur. Gels inside the channels were sterilized with 5X P-S in PBS for 1 hour, washed with DMEM (without serum) 5 times, and incubated at 37°C for 1 hour. Schwann cells were added at a density of 2,000 cells per channel to the outlet port in complete medium. Each microchannel was then checked visually to ensure cells were only present in the outlet port area. Cells were allowed to migrate across gel filled channels for 6 days and media was replenished on days 2 and 5. On day 6, media was removed, and cells were fixed and stained with Hoechst 33242 (Sigma) and FITC-Phalloidin (Invitrogen). Images of migration were taken on a Zeiss LSM 700 laser scanning confocal microscope. ImageJ software was used to count cell nuclei that had migrated into the channel from the outlet port.

Subcutaneous biocompatibility

Female BALB/c mice (Charles River Laboratories, Sulzfeld, Germany) were housed five animals per cage, kept with water ***ad libitum***, exposed to an artificial light–dark regime, and fed with regular chow. To assess the biocompatibility of the C_{16}GSH hydrogels, 38 BALB/c mice were given subcutaneous implantations of one of the four following materials: 0.1wt% C_{16}GSH hydrogel (n=10), 1wt% C_{16}GSH hydrogel (n=10), collagen gel (n=9), or a sham-operated phosphate buffered saline (PBS) control (n=9). The C_{16}GSH hydrogels were prepared as previously described in 1mL syringes and stored at 37°C overnight. Collagen gel was prepared as described earlier with solution being pre-loaded into 1mL syringes and heated to 37°C overnight to induce gelation.

Mice were anaesthetized using isoflurane (1.5-3% in O_2), their interscapular region shaved, and a small incision (~ 2cm) made on the right dorsal side. A sterile 1 mL syringe was used to inject 100 µL under the skin without a needle. The incision was then closed with two 4.0 silk sutures (Ethicon, Somerville, NJ). All animal procedures followed NIH guidelines for the care and use of laboratory animals, and were approved by the University of Chicago's Institutional Animal Care and Use Committee (protocol no. 72297, Chicago, IL, USA).

Histology and immunohistochemistry

Mice were euthanized at time points of 3, 10 and 30 days post implantation in order to study early (day 3 and 10) and late (day 30) *in vivo* response. Following euthanization, the implantation bed and surrounding tissues were explanted, and blood samples were collected from the thoracic cavity. The explants were fixed in 10% neutral buffered formalin for 8 hours, dehydrated in a graded series of ethanol, transferred to xylene, and embedded in paraffin. The samples were then sectioned into 5 - 7µm thick slices, deparaffinized and rehydrated. Sections were stained with hematoxylin and eosin (H&E) or processed for immunohistochemistry.

To assess host immune response and vascularization, rat anti-mouse CD45 antibody (1:10, BD, Franklin Lakes, NJ, 550539), rat anti-mouse F4/80 antibody (1:200, AbD Serotec, Oxford, UK, MCA497GA), and goat polyclonal anti-mouse CD31 antibody (1:200, Santa Cruz Biotechnology, Santa Cruz, CA sc-1506) were used to detect leukocytes, macrophages, and endothelial cells, respectively. Tissue sections were deparaffinized in xylene and rehydrated through serial dilutions of ethanol. Sections were then incubated in antigen retrieval buffer (DAKO, Glostrup, Denmark S1699) and heated at 97° C for 20 minutes in a steamer. Primary antibodies were applied to the sections and incubated in a humidified chamber at room temperature for one hour. Slides were washed with PBS and incubated for 30 minutes at room temperature with the secondary antibodies. Secondary antibodies included rat adsorbed biotinylated horse anti-mouse IgG antibody (1:100, Vector laboratories, Burlingame, CA BA-2001), biotinylated rabbit anti-rat IgG antibody **(**10 μg/ml, Vector laboratories, BA-4001), and biotinylated horse anti-goat IgG antibody **(**1:200, Vector laboratories, BA-9500). Finally, antigen-antibody binding was detected by the Elite kit (PK-6100, Vector Laboratories) and the DAB (DAKO, K3468) system. All sections were evaluated using bright field microscopy (Leica DMI6000 B, Wetzlar, Germany).

Enzyme-linked immunosorbent assay (ELISA)

Blood samples were collected and the serum was separated out by centrifugation. Serum was kept at -80°C until time of use. Circulating IgG was assayed using an ELISA kit (Bethyl Laboratories, Montgomery, TX). Briefly, microtiter plates were coated with goat anti-mouse IgG-Fc for 1 hour at room temperature. Plates were washed with 50mM Tris, 0.14M NaCl, and 0.05% Tween 20 and then blocked with 50mM Tris, 0.14M NaCl, and 1% BSA for 30 minutes. Samples and reference serum were serially diluted in 50mM Tris, 0.14M NaCl, 1% BSA, and 0.05% Tween 20. Following 1 hour of incubation and washing steps, a HRP-conjugated anti-IgM or anti-IgG detection antibody was added. After addition of substrate solution, the reaction was stopped with 0.18M H_2SO_4. The absorbance was measured at 450nm on a Tecan plate reader. A four parameter fitting equation was used according to manufacturer instructions to convert absorbance to concentration using reference serum as a standard.

Statistical Analysis

Experimental values were expressed as means ± standard deviation. Statistical significance was calculated using a one way ANOVA with Tukey or Dunnett's post hoc correction with $p<0.05$ or $p<0.01$ as indicated.

3.3 Results

3.3.1 pH Dependent Gelation and Morphological Analysis

C_{16}GSH was designed as a double headed PA with two arms having histidine and serine residues, joined by glycine linker regions and a lysine amino acid off of which a 16 carbon fatty acid tail was conjugated (Figure 3.1). Below pH 6, the histidine sidechains are predominately pronated and at pH 7.4, physiological pH, above 90% of the imidazole side chains are in their basic form and capable of hydrogen bonding.[38] Serine amino acids have a side chain hydroxyl functionality which can participate in hydrogen bonding and is relatively insensitive to pH. Thus, at low pH, C_{16}GSH assembled into wormlike micelles, but with little stabilization in the peptide

headgroup, creating a weakly viscous liquid. When the pH is raised to physiological conditions (pH 7.4) histidine and serine amino acids from neighboring PAs can participate in cooperative hydrogen bonding, effectively crosslinking the peptide headgroups. Physically this transition was manifested in the switch from weakly viscous gel, to strong self-supporting hydrogel (Figure 3.2).

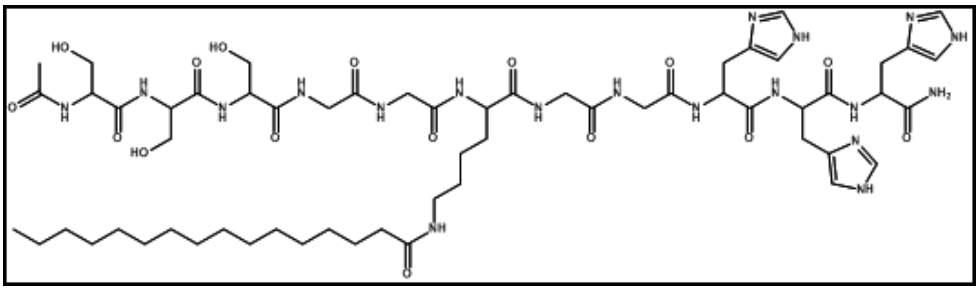

Figure 3.1: Chemical structure of the peptide amphiphile "C_{16}GSH". Three amino acid repeats form arms of histidine and serine residues, joined by glycine linker regions and a lysine on which a 16 carbon fatty acid tail was attached.

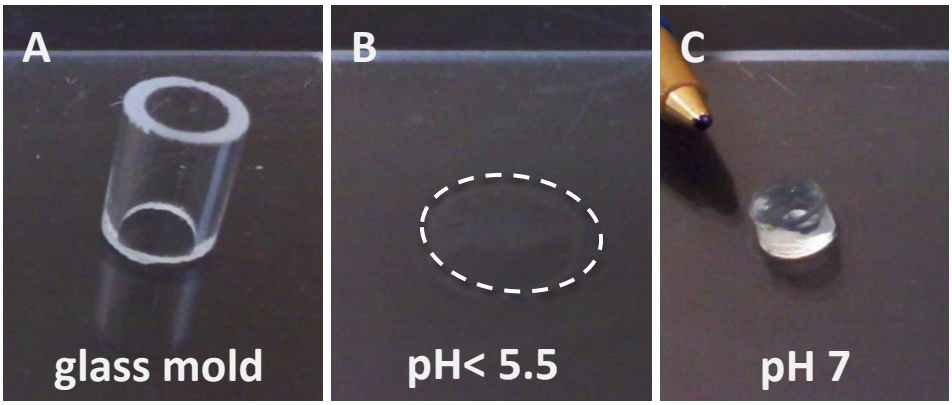

Figure 3.2: Physical demonstration of C_{16}GSH gelation. 0.2wt% C_{16}GSH was cast in glass molds (A) and left at low pH (B) or raised to pH 7 (C). At pH <5.5, the solution is a viscous liquid and flows outward when the mold is removed (as indicated by dashed lines). At pH 7, C_{16}GSH forms a self-supporting hydrogel.

Morphology of the C_{16}GSH hydrogel was studied using SEM. At pH 7.4, C_{16}GSH forms a fibrous and entangled matrix, similar to that of a type 1 collagen gel. As concentration is increased, fiber density also increased, forming a dense, entangled matrix (Figure 3.3).

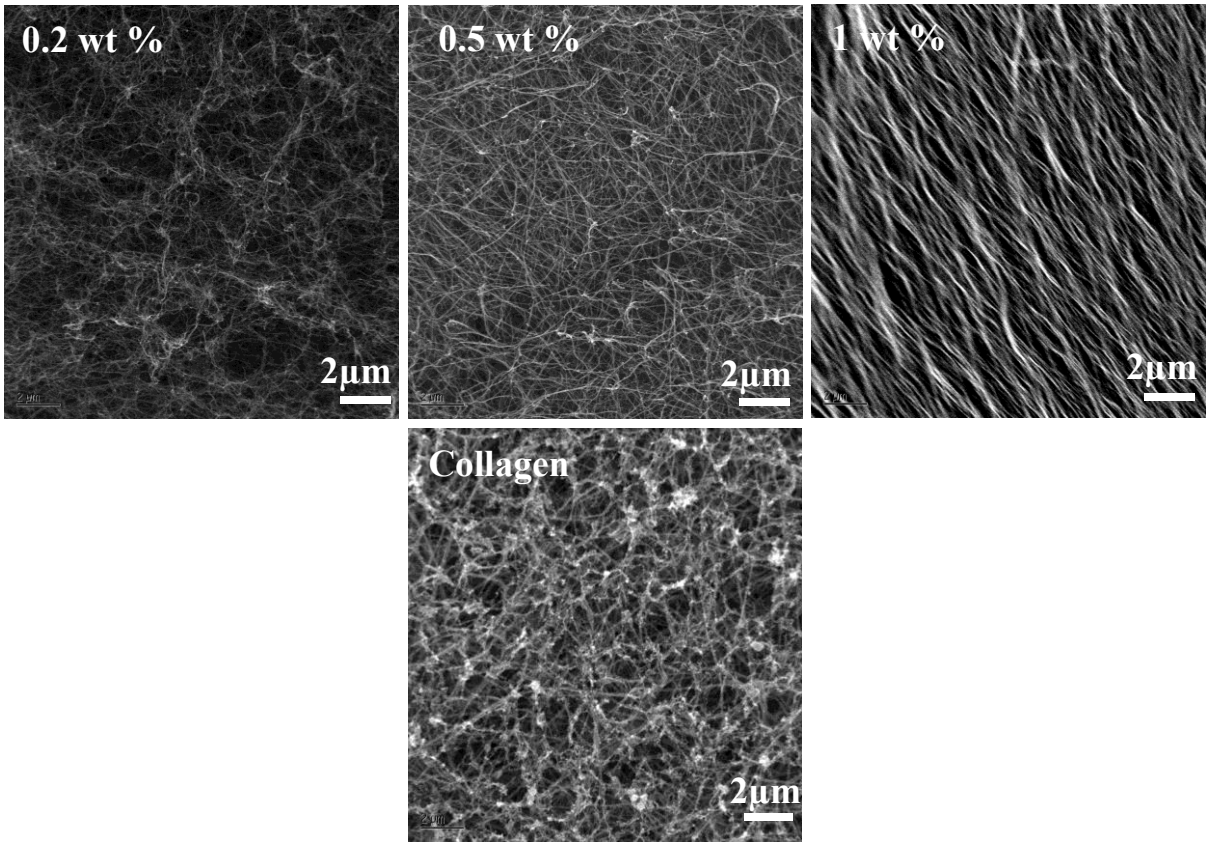

Figure 3.3: SEM Images of C_{16}GSH gels (top panel) at varying concentrations (0.2, 0.5, and 1 wt%). Collagen gel (bottom) prepared as directed (0.3wt%).

3.3.2 Mechanical Properties

Mechanical properties of the C_{16}GSH hydrogel system were studied using rheology. Samples were loaded onto the rheometer at low pH, and measured using oscillatory frequency sweep test. Samples were then raised to pH 7 by addition of base and allowed to equilibrate for 20 minutes before measurement. At pH 5, as concentration is increased modulus stays low, indicative of a weakly elastic gel (Figure 3.4). At pH 7, increasing the concentration of C_{16}GSH directly correlates to an increase in the storage modulus of the material spanning a range from 0.3kPa at a concentration of 0.05wt% up to 9.7kPa at the highest concentration tested, 1wt%.[34] Collagen, prepared according to the manufacturer's instructions, has a storage modulus of 1kPa and a concentration of 0.3wt% (Table 3.1). Thus at a bulk concentration of 0.3wt%, C_{16}GSH is approximately 6 times stiffer than the collagen gel. Conversely, at a stiffness of 1kPa, collagen (0.3wt%) is a denser gel than C_{16}GSH at equivalent stiffness (0.1wt%).

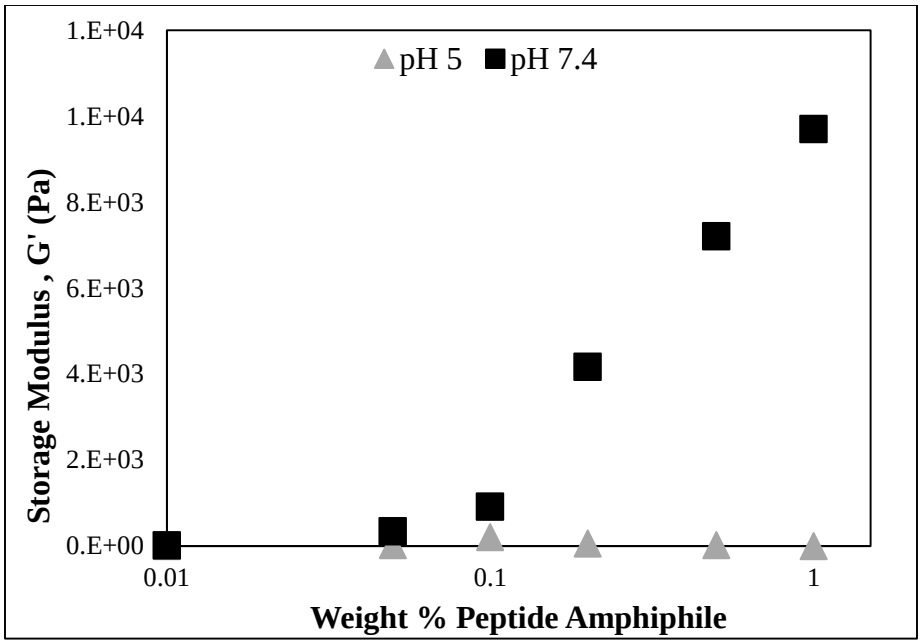

Figure 3.4: Scaling of storage modulus with PA concentration at pH 5 (grey triangles), and pH 7 (black squares).

Material	Weight %	Storage Modulus, G' (Pa)	Young's Modulus, E (Pa)
C_{16}GSH	1wt%	9.66×10^3	2.90×10^4
	0.5wt%	7.19×10^3	2.16×10^4
	0.2wt%	4.16×10^3	1.25×10^4
	0.1wt%	9.16×10^2	2.75×10^3
	0.05wt%	3.37×10^2	1.01×10^3
Collagen	~0.3wt%	1.07×10^3	3.21×10^3

Table 3.1: Materials properties of C_{16}GSH and collagen hydrogels.

3.3.3 Schwann Cell Spreading

In order to investigate how cells interact with the materials, Schwann cells were grown on C_{16}GSH hydrogels and the control surface, collagen, for 18 hours and imaged using bright field microscopy. For this work, rat Schwannoma cells, which have been shown in previous work to be similar to primary Schwann cells, were used.[39]. As stiffness was increased, less spreading was observed (Figure 3.5A-C). Cells spread most on the softest gel (0.1wt%, G'=0.92kPa) (Figure 3.5D).

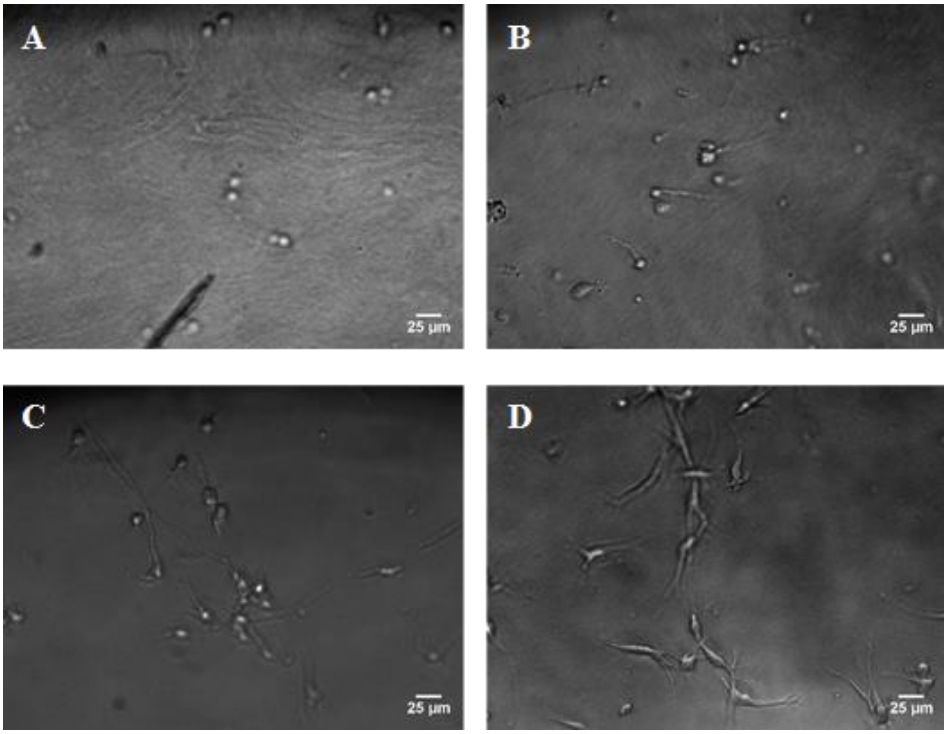

Figure 3.5: Stiffness dependent spreading of Schwann cells on C_{16}GSH hydrogels of (A) 1wt%, (B) 0.5wt%, (C) 0.2wt%, and (D) 0.1wt%.

Cells were also grown on gels for 24 hours and processed for SEM. From these images, it is possible to visualize the gel fibers. Cells grown on 0.1wt% C_{16}GSH gels were able to attach, spread, and migrate as evident by the appearance of broken fibers near the trailing edge of the cells (Figure 3.6A). On collagen, cells were able to attach but exhibited less spreading than was seen with the 0.1wt% C_{16}GSH gel (Figure 3.6B). C_{16}GSH and collagen at these concentrations have roughly equivalent stiffness (Table 3.1).

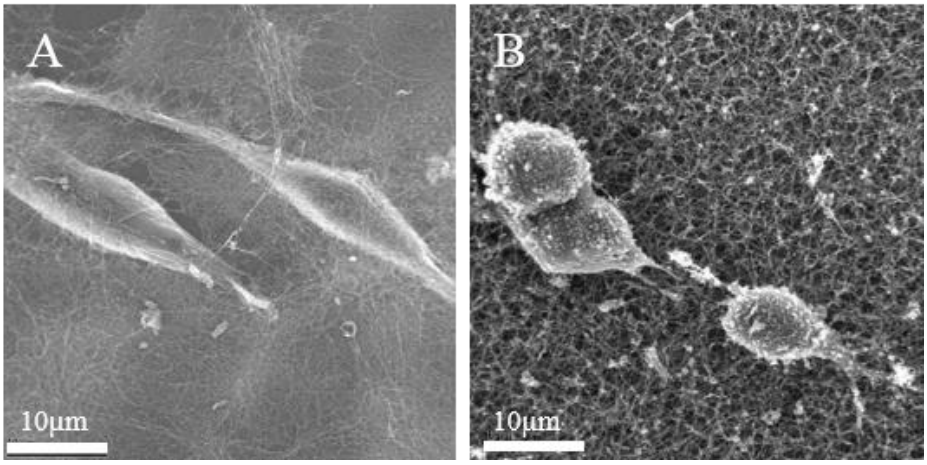

Figure 3.6: Scanning electron micrographs of cell spreading on (A) 0.1 wt% C16GSH and (B) collagen gels after 24 hours.

3.3.4 Schwann Cell Proliferation

Proliferation assays were utilized as a measure of cell biocompatibility. Schwann cells were grown on gel surfaces for two days, after which, proliferation was quantified. Viable cell number on all concentrations of C_{16}GSH gel was higher than that of proliferation on collagen gel, a result that was found to be statistically significant (ANOVA, Dunnett's Test, $p<0.01$) (Figure 3.7). No statistical difference was found between C_{16}GSH concentrations.

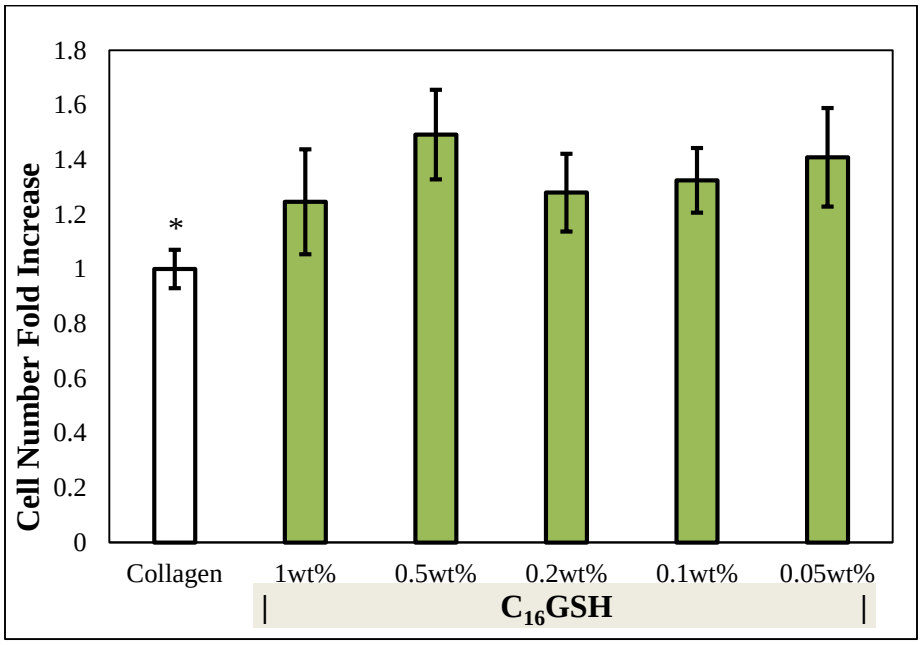

Figure 3.7: Proliferation of Schwann cells on collagen and C_{16}GSH gels after 48 hours (Mean +/- SD, * $p<0.01$, ANOVA, Dunnett's test). At all concentrations, cells proliferate statistically more on all concentrations of C_{16}GSH gels than on collagen.

3.3.5 Schwann Cell Migration

To better mimic the cellular environment during peripheral nerve repair, a microchannel experiment was used to measure Schwann cell migration (Figure 3.8). Cells were seeded at the open inlet of closed channels, 1mm wide, 140µm high and 5.25mm long, filled with hydrogel. Cells were allowed to grow and migrate through the microchannel in response to crowding at the inlet and availability of nutrients (no additional growth factors were added). After a period of 6 days, roughly equivalent to the cellar migration phase *in vivo*[11], representative images show a longitudinal slice of the microchannel where cells have migrated from the inlet port (white arc) along the channel through a C_{16}GSH or a collagen hydrogel (Figure 3.9). When the channel was filled with a collagen gel (Figure 3.9A), only a few cells migrated into the channel. Comparatively, when C_{16}GSH was used at 0.2wt% (Figure 3.9B), a large increase in migrated cells was seen. Additionally, cells exhibit a spindle like morphology and alignment along the direction of the channel. Using a 0.05wt% C_{16}GSH increases cell migration into the hydrogel filled channel (Figure 3.9C).

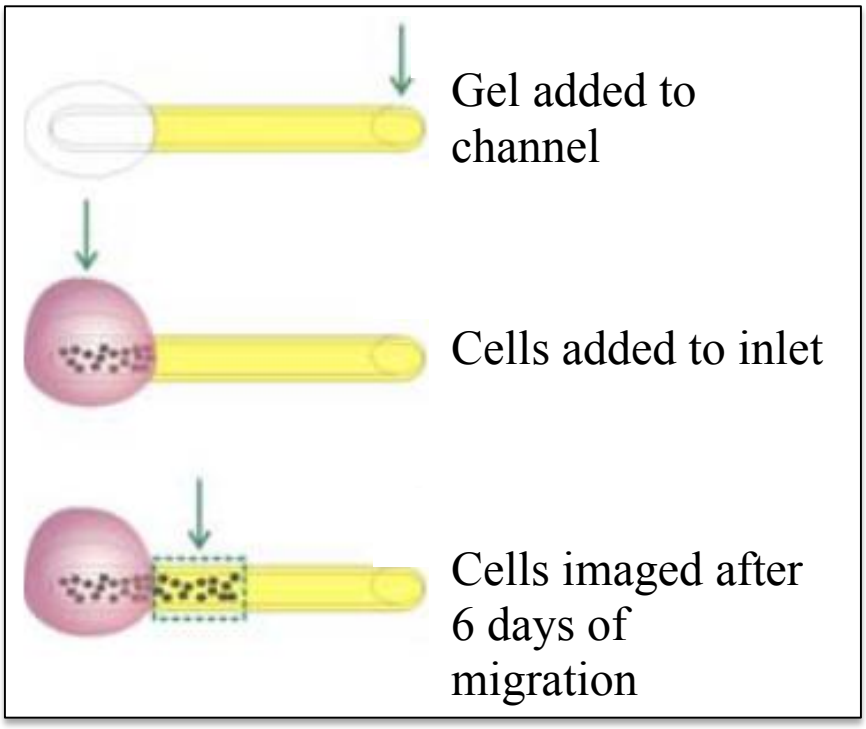

Figure 3.8: Diagram of 3D cell migration experiment. Gel was added to the channel via passive pumping and cross-linked in situ by adding base. Cells were added to the inlet port and allowed to migrate through the channel in 3D.

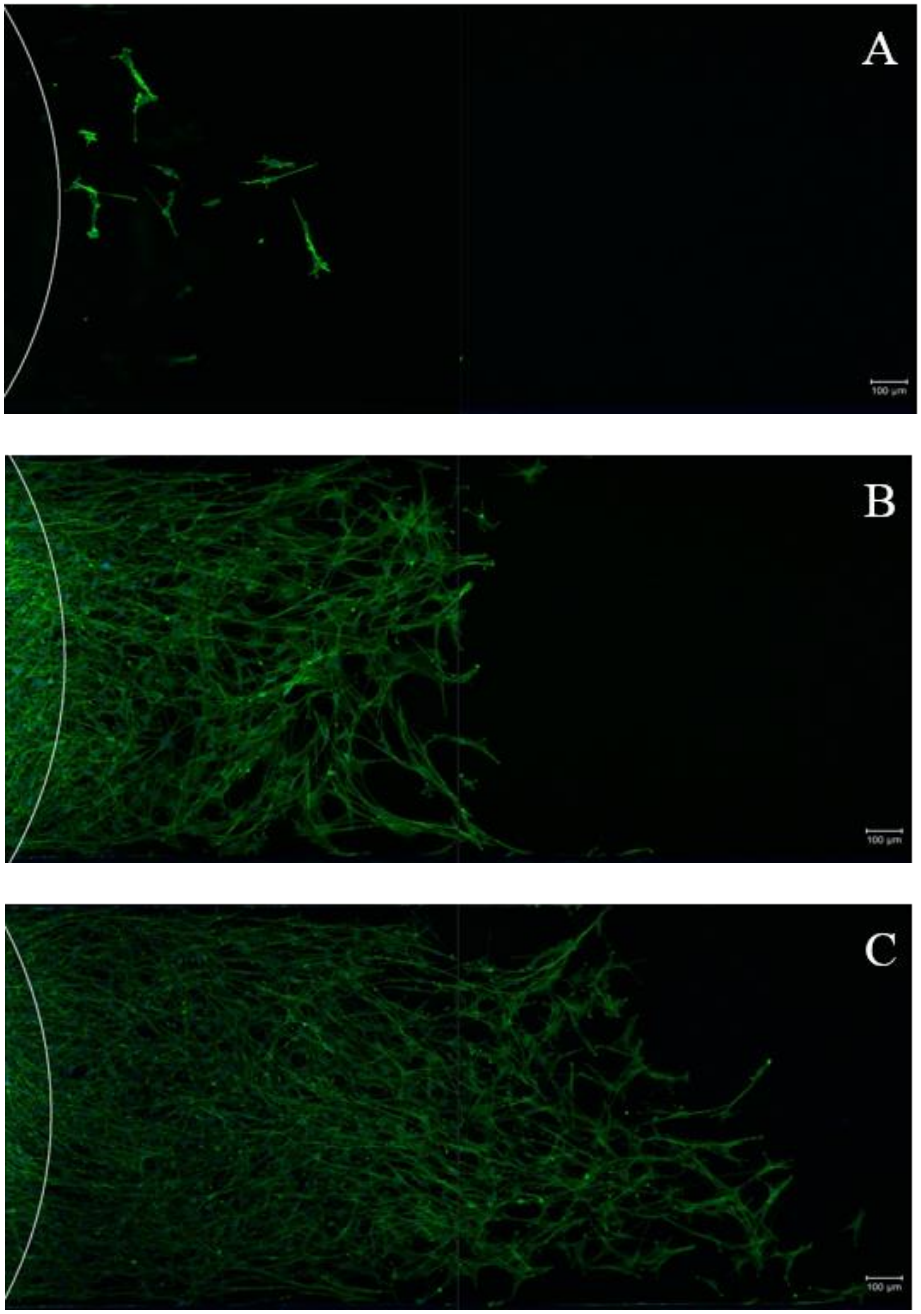

Figure 3.9: Representative images of Schwann cells migrating through microchannels filled with collagen (A), 0.2wt% (B) or 0.05wt% (C) C_{16}GSH hydrogels. Cells have migrated from the inlet area (white arc) on the left towards the right over a period of 6 days without additional growth factors.

Total number of migrated cells for each condition was analyzed using ImageJ software (Figure 3.10). For channels filled with collagen or 0.5wt% C_{16}GSH, only a few cells were able to migrate into the channel, likely due to the high density of fibers present, seen previously in SEM.[34] At 0.2wt% C_{16}GSH, a critical porosity was achieved where cell migration was permitted. The greatest number of migrating cells occurred at 0.05wt% C_{16}GSH.

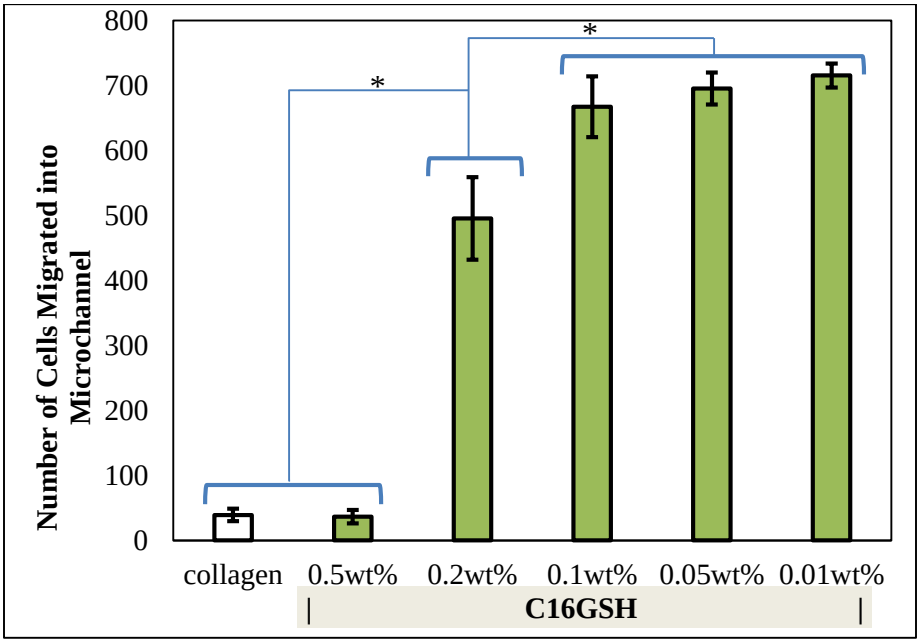

Figure 3.10: Migration of Schwann cells through 3D michrochannels of collagen or C_{16}GSH gels. Calculated number of cells entering the microchannel from the entrance port for each gel as calculated using ImageJ software. (Mean +/- SD, * $p<0.01$, ANOVA, Dunnett's test).

3.3.6 *In Vivo* Subcutaneous Biocompatibility

To assess the biocompatibility and degradation of the C_{16}GSH hydrogels *in vivo*, a murine subcutaneous implantation model was used. Gels were inserted into the subcutaneous space on the dorsal, scapular region (Figure 3.11). No evidence of irritation, redness or swelling was observed at the site of subcutaneous implantation for any of the test groups over the course of the study. The gels were implanted in the subcutaneous space and not restrained, thus movement and relocation of the gel was expected. During histological analysis, clear evidence of the 1wt% C_{16}GSH gel was seen at day 3 and 10, and with a smaller area at day 30 (Figure 3.12). The softer 0.1wt% C_{16}GSH and collagen gels were not clearly visible in histology slides. This result was expected considering the soft nature of the 0.1wt% C_{16}GSH and collagen gels and the freedom of movement possible for the unconfined gel in the subcutaneous space. However, in future studies in the application of interest, peripheral nerve regeneration, the gel would be confined to a solid tube and attached to either end of a severed nerve and therefore not able to dissipate within body.

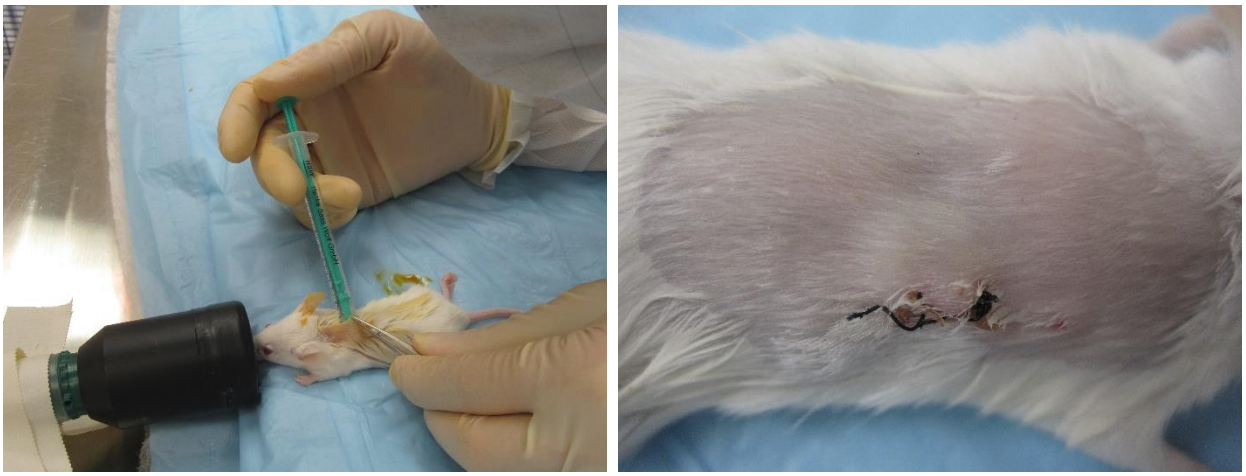

Figure 3.11: Subcutaneous implantation procedure for C_{16}GSH and collagen hydrogels (left) and surgical site on day 3 (right) showing no signs of inflammation or infection.

At day 3, a large area of 1wt% C_{16}GSH was seen with some infiltrating cells; fibroblasts and macrophages (Figure 3.12). The presence of macrophages at the edge of the implanted gel was confirmed by positive (brown) staining against F4/80. At this time point, there was no visible fibrous capsule formation at the gel interface and no evidence of multinucleated giant cells.

At day 10, cells migrated into roughly 30% into the gel and started to degrade the material (Figure 3.12). At this time point there was also positive F4/80 staining indicating the presence of macrophages. Interestingly, at day 10, robust blood vessel formation can be seen inside the gel area indicating that the gel was able to support angiogenesis. Functional blood vessel formation is confirmed by the presence of red blood cells within the lumen of the blood vessel (black arrows, Figure 3.13).

By day 30, the gel was mostly degraded and only a small, thin section of gel was visible. At this late time point, the 1wt% C_{16}GSH gel was almost completely integrated into the surrounding tissue and the presence of macrophages was greatly reduced as indicated by a lack of F4/80 staining (Figure 3.12)

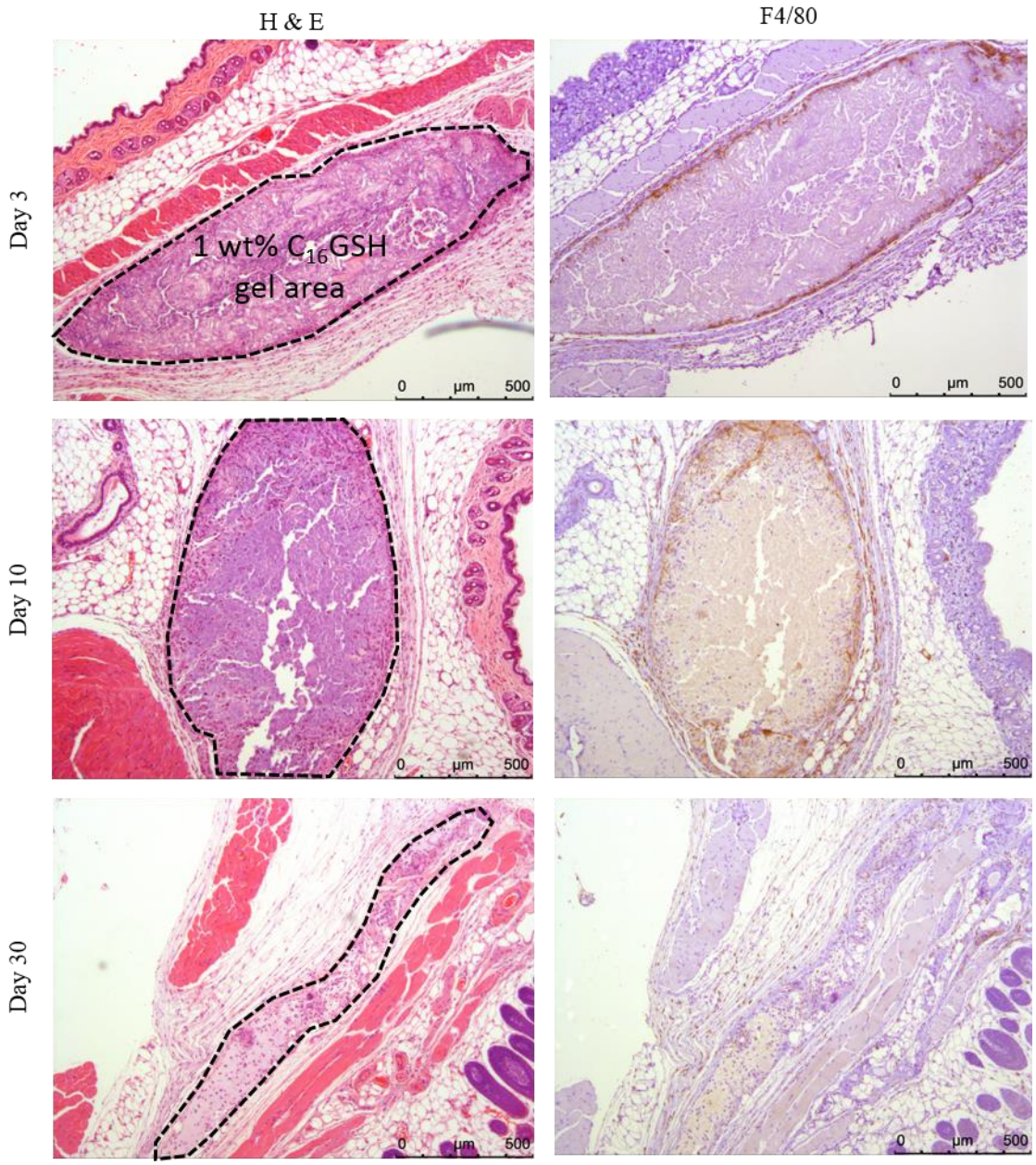

Figure 3.12: Histological images of 1wt% C_{16}GSH hydrogels implanted subcutaneously at day 3, 10, and 30. Dashed outlines indicate the gel implant area. Over a 30 day period gels are infiltrated by cells and degrade (H&E Staining). Presence of macrophages is confirmed with F4/80 staining at days 3 and 10, and is significantly reduced by day 30.

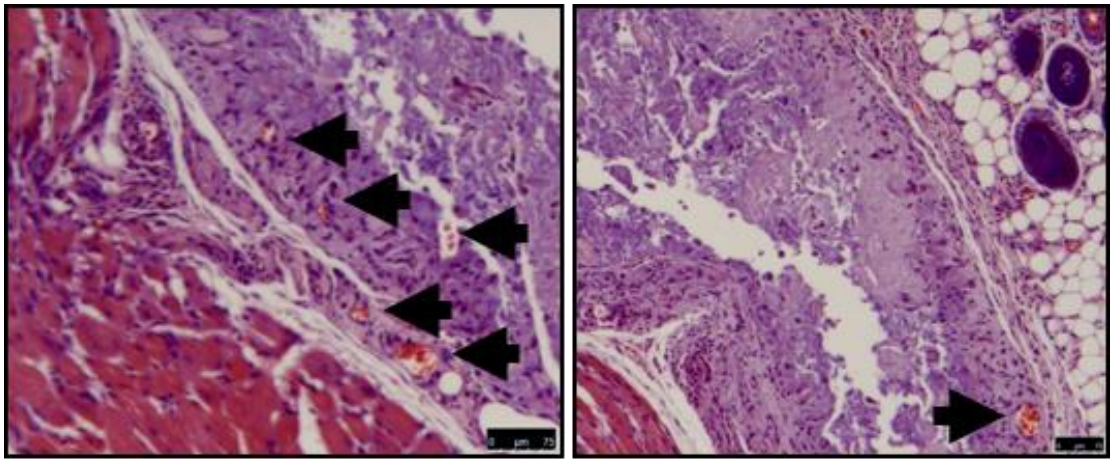

Figure 3.13: Day 10 histological images of 1wt% C_{16}GSH implanted gels showing spontaneous development of blood vessels within the gel (black arrows). Scale bar is 75µm**.**

3.3.7 Systemic Immune Response

To investigate if subcutaneous implantation caused any adverse systemic effects, an ELISA was used to measure the levels of circulating total IgG in the blood at each time point. At each time point, no statistical difference was measured between treatment groups.

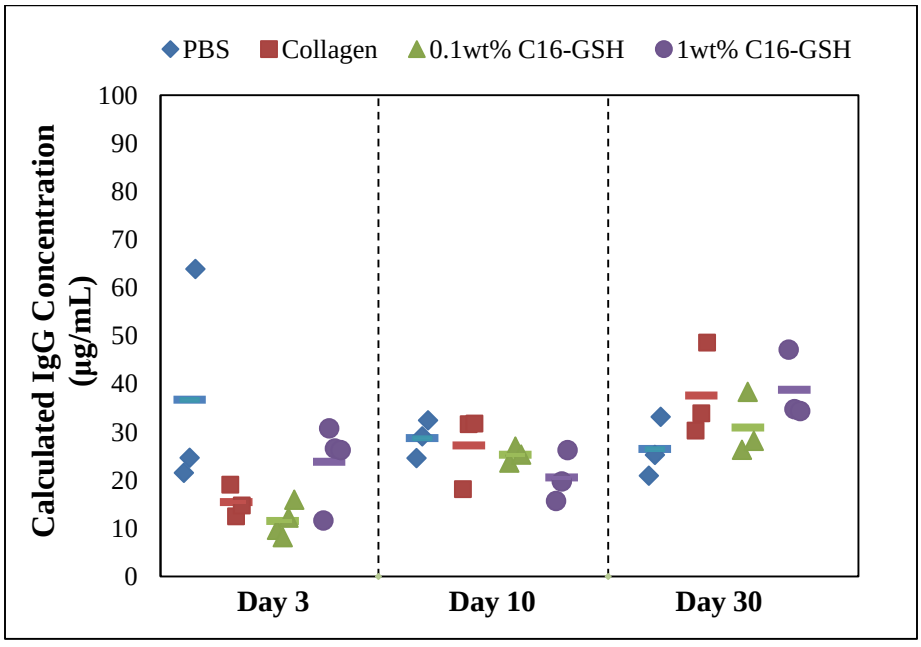

Figure 3.14: Systemic antibody production as measured by total IgG ELISA. No statistical difference was measured between treatment groups within each time point (ANOVA with Tukey Post Hoc Correction).

3.4 Discussion

In order to achieve the same efficacy as nerve autografting, the current standard of care, nerve guide conduits need to be improved beyond their current hollow tube design. Several strategies have been put forward, including intraluminal channels, cellular supplementation and hydrogels.[40] Several natural hydrogel materials have been studied to fill this need including collagen, laminin, and hyaluronic acid.[10] Collagen hydrogels in particular have shown some efficacy both *in vitro* and *in vivo* for peripheral nerve regeneration and thus provide a useful benchmark for this work.[12–14] Here we develop a synthetic hydrogel based on the self-assembly of peptide amphiphiles for the application of nerve guide conduit filler.

Upon dissolution at neutral pH, the PA C_{16}GSH assembled into a fibrous entangled matrix (Figure 3.3). At physiological pH, amino acids in the head group of the PA participate in cooperative hydrogen bonding which effectively crosslinks the worm-like micelle assembly. By increasing the concentration, a span of moduli can be achieved ranging from a storage modulus of 0.3 to 10 kPa (Figure 3.4). This large range in stiffness is possible because the PA hydrogels scale with concentration by increasing the fiber density and entanglements. This range of stiffness far surpasses most reported PA hydrogels ~0.1-1 kPa.[18,41] For comparison, collagen as supplied (0.3wt%) had a modulus of 1kPa (Table 3.1). With collagen, scaling the concentration of the material to scale the modulus is limited due to the nature of collagen self-assembly as fibers gel by associating in a triple helix.[42]

Schwann cells, considered the first responders of peripheral nerve repair, must spread, proliferate and migrate into the injury space in order to guide neurons and achieve functional repair. Thus, a hydrogel designed for peripheral nerve repair applications must enhance the activity of this cell population. Here we show that Schwann cells spread and elongated best on the lowest concentration of C_{16}GSH gels tested (0.1wt%) (Figure 3.5). On gels of equivalent stiffness, Schwann cells spread more on C_{16}GSH than on collagen (Figure 3.6). The importance of fiber density is highlighted since at these concentrations, C_{16}GSH and collagen have equivalent stiffnesses; however spreading was greatly improved on the C_{16}GSH surface which has a lower fiber density. Additionally, the Schwann cells display a polarized spindle morphology which is consistent with a migratory phenotype.[43]

As a measure of cell viability, proliferation of cells grown on the surface of gels were measured after two days. At all concentrations of C_{16}GSH, Schwann cells proliferated more than on collagen gels (Figure 3.7). Interestingly, there is no statistical difference or trend between the varying concentrations of C_{16}GSH gels. This result suggests that although cell proliferation is a commonly used *in vitro* test, it may not be sufficient in analyzing subtle differences in cell preference based on substrate stiffness.

With the eventual goal of peripheral nerve regeneration inside a hollow conduit filled with gel, a 3D michrochannel migration assay was used to best mimic conditions that the cells face *in vivo* (Figure 3.8). Using a 3D microchannel assay, large differences in cell migration were evident between gel concentrations that were not evident in the simple 2D proliferation assay. For collagen and 0.5wt% C_{16}GSH, very few cells were able to migrate, likely due to the increased density of the gels. At 0.2wt% C_{16}GSH, the density and stiffness of the gel is permissive to migration and a large increase in the number of cells migrated into the microchannel was seen (Figure 3.9). Migration was maximized at a C_{16}GSH concentration of 0.01wt% (Figure 3.10). The rate of cell migration and gel wt% preference *in vivo* may change

with the addition of other cell types and digesting enzymes. The trend however, is informative for the design of hydrogels for this application.

Lastly, C_{16}GSH gels were implanted subcutaneously and shown to degrade and support regeneration without causing inflammation or a foreign body immune response. Cells migrated well into the tissue, including macrophages, which play an important role in tissue regeneration.[44] At the border between native tissue and the PA gel implant, there was no evidence of a fibrous capsule or chronic inflammation, in the form of multinucleated giant cells (Figure 3.11).[45] After 10 days of implantation, new blood vessel formation was evident inside the gel implant (Figure 3.12). This result is important as previous peptide amphiphile based gels required the use of growth factors to promote angiogenesis.[46] Robust blood vessel formation is a key process in peripheral nerve regeneration, and the presence of new blood vessels has been shown to improve nerve regeneration *in vivo*.[47] By 30 days, the gel has mostly been degraded or integrated into the surrounding tissue. In sum, PA gels are able to support cell ingrowth, blood vessel formation and degradation.

Finally, systemic immune response was analyzed by measuring circulating IgG levels at each time point. Elevated levels of IgG would indicate an adaptive immune response by the body to foreign materials.[48] However, we found no statistical difference between the sham operated PBS group and the C_{16}GSH and collagen gel implant groups (Figure 9). This result indicates that implantation of both the C_{16}GSH and collagen gels did not cause a systemic immune response.

3.5 Conclusions

With this set of *in vitro* and *in vivo* assays, a PA hydrogel, C_{16}GSH, was studied and compared to a benchmark of collagen gel for the application of a luminal filler for conduit-mediated peripheral nerve repair. In each *in vitro* assay, designed to replicate *in vivo* conditions, the C_{16}GSH gel surpassed the collagen gel control in enhancing the activity of Schwann cells. When implanted *in vivo*, C_{16}GSH did not cause any local or systemic immune response. Future work will continue to develop the C_{16}GSH hydrogels as a conduit filler using a small animal peripheral nerve injury model.

3.6 References

1. Noble, J., Munro, C. & Prasad, V. Analysis of upper and lower extremity peripheral nerve injuries in a population of patients with multiple injuries. *J. Trauma* **45,** 116–122 (1998).

2. Ray, W. Z. & Mackinnon, S. E. Management of nerve gaps: autografts, allografts, nerve transfers, and end-to-side neurorrhaphy. *Exp. Neurol.* **223,** 77–85 (2010).

3. Mackinnon, S. New directions in peripheral nerve surgery. *Ann. Plast. Surg.* **22,** 257–273 (1989).

4. Seckel, B. Enhancement of peripheral nerve regeneration. *Muscle Nerve* **13,** 785–800 (1990).

5. Meek, M. F. & Coert, J. H. US Food and Drug Administration/Conformit Europe-approved absorbable nerve conduits for clinical repair of peripheral and cranial nerves. *Ann. Plast. Surg.* **60,** 110–6 (2008).

6. Kehoe, S., Zhang, X. F. & Boyd, D. FDA approved guidance conduits and wraps for peripheral nerve injury: a review of materials and efficacy. *Injury* **43,** 553–72 (2012).

7. Bell, J. & Haycock, J. Next generation nerve guides: materials, fabrication, growth factors, and cell delivery. *Tissue Eng. Part B Rev.* **18,** 116–128 (2011).

8. Angius, D. *et al.* A systematic review of animal models used to study nerve regeneration in tissue-engineered scaffolds. *Biomaterials* **33,** 8034–9 (2012).

9. Chalfoun, C. T., Wirth, G. A & Evans, G. R. D. Tissue engineered nerve constructs: where do we stand? *J. Cell. Mol. Med.* **10,** 309–17 (2006).

10. Lin, Y. C. & Marra, K. G. Injectable systems and implantable conduits for peripheral nerve repair. *Biomed. Mater.* **7,** 024102 (2012).

11. Belkas, J. S., Shoichet, M. S. & Midha, R. Peripheral nerve regeneration through guidance tubes. *Neurol. Res.* **26,** 151–60 (2004).

12. Satou, T. *et al.* A morphological study on the effects of collagen gel matrix on regeneration of severed rat sciatic nerve in silicone tubes. *Pathol. Int.* **36,** 199–208 (1986).

13. Madison, R., da Silva, C. F., Dikkes, P., Chiu, T. H. & Sidman, R. L. Increased rate of peripheral nerve regeneration using bioresorbable nerve guides and a laminin-containing gel. *Exp. Neurol.* **88,** 767–72 (1985).

14. Chamberlain, L. J., Yannas, I. V, Hsu, H. P., Strichartz, G. R. & Spector, M. Near-terminus axonal structure and function following rat sciatic nerve regeneration through a collagen-GAG matrix in a ten-millimeter gap. *J. Neurosci. Res.* **60,** 666–77 (2000).

15. Charriere, G., Bejot, M., Schnitzler, L., Ville, G. & Hartmann, D. J. Reactions to a bovine collagen implant. *J. Am. Acad. Dermatol.* **21,** 1203–1208 (1989).

16. Tan, A., Rajadas, J. & Seifalian, A. M. Biochemical engineering nerve conduits using peptide amphiphiles. *J. Control. Release* **163,** 342–52 (2012).

17. Trent, A., Marullo, R., Lin, B., Black, M. & Tirrell, M. Structural properties of soluble peptide amphiphile micelles. *Soft Matter* **7,** 9572 (2011).

18. Greenfield, M. A., Hoffman, J. R., de la Cruz, M. O. & Stupp, S. I. Tunable mechanics of peptide nanofiber gels. *Langmuir* **26,** 3641–7 (2010).

19. Morisco, A. *et al.* Micelles derivatized with octreotide as potential target-selective contrast agents in MRI. *J. Pept. Sci.* **15,** 242–50 (2009).

20. Bull, S. R., Guler, M. O., Bras, R. E., Meade, T. J. & Stupp, S. I. Self-assembled peptide amphiphile nanofibers conjugated to MRI contrast agents. *Nano Lett.* **5,** 1–4 (2005).

21. Hartgerink, J. D., Beniash, E. & Stupp, S. I. Self-assembly and mineralization of peptide-amphiphile nanofibers. *Science* **294,** 1684–8 (2001).

22. Spoerke, E. D., Anthony, S. G. & Stupp, S. I. Enzyme Directed Templating of Artificial Bone Mineral. *Adv. Mater.* **21,** 425–430 (2009).

23. Branco, M. C. & Schneider, J. P. Self-assembling materials for therapeutic delivery. *Acta Biomater.* **5,** 817–31 (2009).

24. Webber, M. J., Matson, J. B., Tamboli, V. K. & Stupp, S. I. Controlled release of dexamethasone from peptide nanofiber gels to modulate inflammatory response. *Biomaterials* **33,** 6823–32 (2012).

25. Bitton, R. *et al.* Self-assembly of model DNA-binding peptide amphiphiles. *Langmuir* **21,** 11888–95 (2005).

26. Tu, R. S. *et al.* Cooperative DNA binding and assembly by a bZip peptide-amphiphile. *Soft Matter* **6,** 1035 (2010).

27. Black, M. *et al.* Self-assembled peptide amphiphile micelles containing a cytotoxic T-cell epitope promote a protective immune response in vivo. *Adv. Mater.* **24,** 3845–9 (2012).

28. Standley, S. M. *et al.* Induction of cancer cell death by self-assembling nanostructures incorporating a cytotoxic peptide. *Cancer Res.* **70,** 3020–6 (2010).

29. Garg, A., Tisdale, A. W., Haidari, E. & Kokkoli, E. Targeting colon cancer cells using PEGylated liposomes modified with a fibronectin-mimetic peptide. *Int. J. Pharm.* **366,** 201–10 (2009).

30. Webber, M. J., Berns, E. J. & Stupp, S. I. Supramolecular Nanofibers of Peptide Amphiphiles for Medicine. *Isr. J. Chem.* **53,** 1–25 (2013).

31. Tysseling, V. M. *et al.* Self-assembling peptide amphiphile promotes plasticity of serotonergic fibers following spinal cord injury. *J. Neurosci. Res.* **88,** 3161–70 (2010).

32. Tysseling-Mattiace, V. M. *et al.* Self-assembling nanofibers inhibit glial scar formation and promote axon elongation after spinal cord injury. *J. Neurosci.* **28,** 3814–23 (2008).

33. Bond, C. W. *et al.* Peptide amphiphile nanofiber delivery of sonic hedgehog protein to reduce smooth muscle apoptosis in the penis after cavernous nerve resection. *J. Sex. Med.* **8,** 78–89 (2011).

34. Lin, B. F. *et al.* pH-responsive branched peptide amphiphile hydrogel designed for applications in regenerative medicine with potential as injectable tissue scaffolds. *J. Mater. Chem.* **22,** 19447–19454 (2012).

35. Dubey, N., Letourneau, P. C. & Tranquillo, R. T. Guided neurite elongation and schwann cell invasion into magnetically aligned collagen in simulated peripheral nerve regeneration. *Exp. Neurol.* **158,** 338–50 (1999).

36. Ceballos, D. *et al.* Magnetically aligned collagen gel filling a collagen nerve guide improves peripheral nerve regeneration. *Exp. Neurol.* **158,** 290–300 (1999).

37. Kuipers, B. J. H. & Gruppen, H. Prediction of molar extinction coefficients of proteins and peptides using UV absorption of the constituent amino acids at 214 nm to enable quantitative reverse phase high-performance liquid chromatography-mass spectrometry analysis. *J. Agric. Food Chem.* **55,** 5445–51 (2007).

38. Pasc, A., Akong, F. O., Cosgun, S. & Gérardin, C. Differences between β -Ala and Gly-Gly in the design of amino acids-based hydrogels. *Bellstein J. Org. Chemsitry* **6,** 973–977 (2010).

39. Hai, M., Muja, N., DeVries, G. H., Quarles, R. H. & Patel, P. I. Comparative analysis of Schwann cell lines as model systems for myelin gene transcription studies. *J. Neurosci. Res.* **69,** 497–508 (2002).

40. Huang, Y.-C. & Huang, Y.-Y. Biomaterials and strategies for nerve regeneration. *Artif. Organs* **30,** 514–22 (2006).

41. Anderson, J. M., Andukuri, A., Lim, D. J. & Jun, H.-W. Modulating the gelation properties of self-assembling peptide amphiphiles. *ACS Nano* **3,** 3447–54 (2009).

42. Piechocka, I. K., van Oosten, A. S. G., Breuls, R. G. M. & Koenderink, G. H. Rheology of heterotypic collagen networks. *Biomacromolecules* **12,** 2797–805 (2011).

43. Wang, Y., Teng, H.-L. & Huang, Z. Intrinsic migratory properties of cultured Schwann cells based on single-cell migration assay. *PLoS One* **7,** 1–11 (2012).

44. Xia, Z. & Triffitt, J. T. A review on macrophage responses to biomaterials. *Biomed. Mater.* **1,** R1–9 (2006).

45. Mikos, A., McIntire, L., Anderson, J. & Babensee, J. Host response to tissue engineered devices. *Adv. Drug Deliv. Rev.* **33,** 111–139 (1998).

46. Ghanaati, S. *et al.* Dynamic in vivo biocompatibility of angiogenic peptide amphiphile nanofibers. *Biomaterials* **30,** 6202–12 (2009).

47. Hobson, M. I., Green, C. J. & Terenghi, G. VEGF enhances intraneural angiogenesis and improves nerve regeneration after axotomy. *J. Anat.* **197,** 591–605 (2000).

48. Anderson, J. M. Mechanisms of inflammation and infection with implanted devices. *Cardiovasc. Pathol.* **2,** 33–41 (1993).

Chapter 4: Protein Encapsulation via Polypeptide Complex Coacervation

Associated Papers:

D Priftis, **K Megley**, N Laugel and M Tirrell. "Complex coacervation of poly(ethylene imine)/polypeptide in aqueous solutions: Thermodynamic and rheological characterization" *Journal of Colloid and Interface Science,* 398 (2013) 39-50.

K Black, D Priftis, S Perry, J Yip, W Byun, and M Tirrell. "Protein Encapsulation via Complex Coacervation of Polypeptides" *(submitted)*

Abstract:

Proteins have gained increasing success as therapeutic agents, however challenges exist in effective and efficient delivery. In this work, a simple and versatile method is presented for encapsulating proteins via complex coacervation with oppositely charged polypeptides. Here we demonstrate encapsulation with a model protein system: bovine serum albumin. Rheological properties were studied to determine the viscoelasticity which may have implications for cell internalization. Efficiency of uptake, preservation of secondary structure, and conditions of release were studied in order to further our understanding of the incorporation of proteins into complex coacervates. The biocompatibility of our complex coacervate system and the interaction with cells were also studied. A simple system such as encapsulating proteins with polypeptide coacervates has great potential use in the field of drug delivery.

4.1 Introduction

Recent advances in molecular biology have enabled the discovery of a plethora of protein and peptide therapeutics. Protein therapeutics are now used to treat a variety of diseases, including diabetes[1] and cancer.[2] Though protein therapeutics enjoy specificity and high potency, effective and efficient delivery remains challenging. When delivered intravenously, protein drugs suffer from low bioavailability and are easily degraded in the body. Proteins in the blood stream can be degraded by proteases, denatured, or targeted by the mononuclear phagocyte system for removal.[3]

Various strategies have been developed to improve the delivery of proteins, including chemical modification with polyethylene glycol and encapsulation into liposomal or polymeric carriers.[3–5] One polymeric carrier system, poly(lactic-co-glycolic acid) (PLGA) has received significant of attention due to its biocompatibility and ability to degrade by hydrolysis over time.[6] PLGA has been shown to effectively encapsulate a wide range of proteins including insulin for the treatment of diabetes,[7] and is also approved by the FDA for use in human growth hormone delivery to treat deficiencies in pediatric patients.[8] One of the major drawbacks of PLGA nanoparticles is inefficient drug loading, typically 1% active ingredient per particle by mass.[6] PLGA particles are typically formed using a solvent emulsion or nanoprecipitation method. Though this system has had much success, the conditions under which the particles are formed, using harsh solvents, may cause denaturing and inactivity of the protein.[9]

An alternative to the harsh processing conditions of PLGA is to use self-assembling polymer constructs based on the phenomenon of complex coacervation. Complex coacervates are formed when oppositely charged polyelectrolytes are mixed in aqueous solution. Coacervation results in a liquid-liquid phase separation in which a dense polymer-rich phase (coacervate) separates from the dilute polymer-poor solution phase (aqueous phase). This process was first observed using natural polymers gelatin and gum Arabic.[10] More recently, systems of complex coacervation have been explored for drug delivery using such naturally-occurring polymers as alginate and chitosan.[11] Though this method shows promise, the process of encapsulation, tunable parameters, and biocompatibility are not well understood. Additionally there is a need to expand coacervate-based drug delivery platforms to include synthetic systems, so as to enable *de novo* design with enhanced functionality and precise molecular control.

Synthetic polypeptides and polymers offer a wide range of tunablity, and control of coacervate formation based on the diversity of amino acid sequences used. Synthetically produced polypeptides such as the ones used here, *i.e.*, poly(lysine) (PLys) and poly(glutamic acid) (PGlu), are biocompatible and have been used in biomaterial applications such as coatings and covalent drug modifications.[12] PLys and Polyethylenimine (PEI) have been used effectively for transfection and gene delivery.[13] Previous work identified the conditions under which these polypeptides form complex coacervates in solution.[14,15] In addition to polymer chemistry, salt concentration, pH, the ratio of polycation to polyanion, total polymer concentration and temperature are important system parameters that can be tuned to control coacervate formation. Additionally, it was found that polypeptide complex coacervates exhibit low interfacial tension, which may be useful for encapsulation of charged materials.[16,17]

Here we present a versatile method to encapsulate proteins by complex coacervation using polypeptides. First, the dynamic mechanical properties of the coacervates were studied using rheology. Recently it was found that uptake of nanoparticles, both in efficiency and mechanism is directly linked to the particle's elastic modulus.[18] Uptake efficiency was measured by separating the dense coacervate phase from the corresponding solution phase and quantifying the excess protein present in solution. Preservation of secondary structure and conditions of release were also examined, as these present challenges to the field of protein delivery. Lastly, the interaction of the protein-loaded coacervates with cells was studied as an initial test for the feasibility of using this system clinically.

4.2 Materials and Methods

Materials

Polypeptides used in this study PLys (N=400 and N=100), PGlu (N=400 and N=100), and poly(D,L-aspartic acid) PAsp (N=400) were purchased from Alamanda Polymers, Inc. (Huntsville, AL). PEI (N=400) was purchased from Sigma-Aldrich (St. Louis, MO). All other materials were purchased from Sigma-Aldrich (St. Louis, MO) unless otherwise noted. All water was dispensed from a Milli-Q water purification system at a resistivity of 18.2 MΩ cm. The polypeptides were used as received without any further purification. Separate stock solutions of 1 wt % of each polypeptide and protein were prepared in water. The pH was then adjusted to 7.0 ± 0.05 by adding small amounts of 1M NaOH or HCl. Phosphate buffered saline (PBS) at 10x was used for dilution.

Formation of Complex Coacervates

For the purpose of rheological measurements complex coacervates were formed by mixing the polycation (PEI) and polyanion (PGlu or PAsp) in aqueous solutions with concentrated NaCl to form a final concentration of 0.2wt% polymer and 100-600 mM NaCl. The complex coacervate mixtures are prepared in microcentrifuge vials and are vigorously shaken with a vortex after each separate component was added. The order of mixing was kept the same for all experiments. Samples were then centrifuged in order to achieve rapid separation of the dense coacervate phase. Samples were centrifuged for 15 minutes 10,000 rpm using a microcentrifuge. After centrifugation, the supernatant solution phase was carefully removed by using a micropipette while the coacervate phase (transparent gel) was used for rheological measurements.

Complex coacervates with encapsulated protein were formed by mixing Plys with the protein of interest (BSA) to form an intermediate complex in a concentrated PBS solution and then adding PGlu to form the coacervate in aqueous solutions with a final salt concentration of 1x phosphate buffered saline (PBS). PLys and PGlu were always used with equal degrees of polymerization (either N=400 or N=100). The polyelectrolyte mixtures are prepared in microcentrifuge vials and were vigorously vortexed after the addition of each component. The order of mixing was kept the same for all experiments. All complex coacervates were prepared immediately before use and studied at room temperature (25ºC).

Samples were used directly as a suspension or centrifuged in order to achieve rapid separation of the dense coacervate phase. Samples were centrifuged for 15 minutes 10,000 rpm using a microcentrifuge. After centrifugation, the supernatant solution phase was carefully removed by using a micropipette while the coacervate phase (transparent gel) was left at the bottom of the vial.

Samples used to determine protein encapsulation were formulated with 15 μM of each polypeptide (PLys and PGlu) and increasing amounts of BSA spanning a molar ratio of 0.05 to 0.5 BSA to total polypeptide.

Rheology

Rheological measurements were performed on a Physica MCR 301 rheometer fitted with a parallel plate geometry (8 mm in diameter). PEI/PGlu or PEI/PAsp coacervate samples were loaded onto the plate and allowed to equilibrate for 10 min. A steady shear rate sweep was preformed to measure viscosity. Strain sweep tests were carried out to determine the linear viscoelastic range (0–10%). Oscillatory tests were used to determine the storage modulus (G') and loss modulus (G") while varying the frequency from 0.1 to 100 rad/s with a constant strain of 1% or 5%.

Optical Microscopy

An optical microscope (Nikon, Eclipse TE 200) was used to image the protein-loaded coacervates. The coacervate mixture was placed on a glass slide to image the droplets using both brightfield and fluorescence.

Protein Quantification

To determine the loading capacity for the coacervate system, samples were prepared and then immediately centrifuged. A Bradford assay (Bio Rad Hercules, CA) was then used to determine the protein content of the solution supernatant (*i.e.*, the protein that was not encapsulated) as compared to a control with no polypeptides and the same amount of protein.

Samples were prepared in triplicate and each sample measured three times in a Costar® 96 well plate (Sigma) for a total of nine measurements per condition.

Circular Dichroism (CD)

To determine the secondary structure of free versus encapsulated protein, circular dichroism was used. Samples were prepared as described previously, 0.05 BSA to total polypeptide was chosen as at that concentration 100% of the protein is encapsulated. Samples were measured on a Jasco J-815 Circular Dichroism Spectropolarimeter with a 1 cm quartz cuvette at 25ºC. Measurements were performed from 250 nm to 190 nm. An average of three scans is reported.

Turbidity

Turbidity, or the absorption of light at 500 nm, was used a measure of total coacervate formation. Turbidity (T) is defined by T=-ln(I/I_0), with I_0 = incident light intensity and I = intensity of light passed through the sample volume. Neither polypeptide (PGlu or PLys) absorbs light at 500 nm. The fluorescein (FITC) label on BSA absorbs light at 500 nm (FITC excitation = 490 nm and excitation = 525 nm), so turbidity at each pH was corrected by subtracting the turbidity of BSA-FITC alone. A plate reader equipped with a UV spectrophotometer (Tecan, Infinite M200) was employed and samples were measured in triplicate in a Costar® non-binding 96 well plate (Sigma). Turbidity was then converted to % disassembled in order to describe amount of coacervate released under conditions of decreasing pH by assuming 0% released corresponded to turbidity at pH 7.4 using equation [4.1] below where $T_{7.4}$ is the turbidity reading at pH 7.4 and T_x corresponds to turbidity at a given pH X:

$$\%\ Dissasembled\ Coac. = \left[\frac{T_{7.4} - T_x}{T_{7.4}}\right] \times 100\% \qquad [4.1]$$

Cell Viability

Cell culture reagents were purchased from Gibco (Life Technologies, Carlsbad, CA) unless otherwise noted. A confluent layer of NIH 3T3 fibroblasts (ATCC, Manassas, VA) was trypsinized with 0.25% Trypsin-EDTA for five minutes and neutralized with calf bovine serum (CBS) supplemented Dulbecco's Modified Eagle Medium (DMEM) with 1% v/v penicillin-streptomycin. The cells were then seeded into 96-well plates (Thermo Scientific, Waltham, MA) at a density of $1.6x10^4$ cells/cm^2 and allowed to attach overnight at 37°C in a humidified atmosphere with 5% CO_2. BSA-loaded coacervates, BSA alone, coacervates alone, PLys and PGlu were added to wells at a concentration of 15 µM polypeptide each and 3 µM BSA. After 24 hours, wells were washed twice with PBS, and PrestoBlue® (Invitrogen, Carlsbad, CA) a metabolic assay was added to the wells to achieve a final concentration of 10% by volume in media. After 3 hours of incubation, fluorescence was read on a Tecan plate reader (560 nm excitation / 590 nm emission).

For the purpose of imaging, cells were seeded in 8-well chamber slides (Nunc®, Thermo Scientific, Waltham, MA) at a density of $1.6x10^4$ cells/cm^2 and allowed to attach overnight. BSA-loaded coacervates were added to wells at a concentration of 30 µM total polypeptide and 3 µM BSA. After 24 hours, wells were washed three times with PBS, fixed with 4% paraformaldehyde in PBS for 15 minutes and washed three times with PBS. Cells and the associated BSA loaded coacervates were imaged on an optical microscope (Nikon, Eclipse TE 200) using both brightfield and fluorescence.

4.3 Results

4.3.1 Materials characterization of complex coacervates

Rheological measurements were employed to investigate how changes in the salt concentration of the mixtures influenced the mechanical properties of the coacervates. The viscosity of PEI/PGlu coacervates was determined by carrying out steady shear experiments of samples prepared with different salt concentrations. As salt concentration was increased, a decrease in viscosity was observed (Figure 4.1)

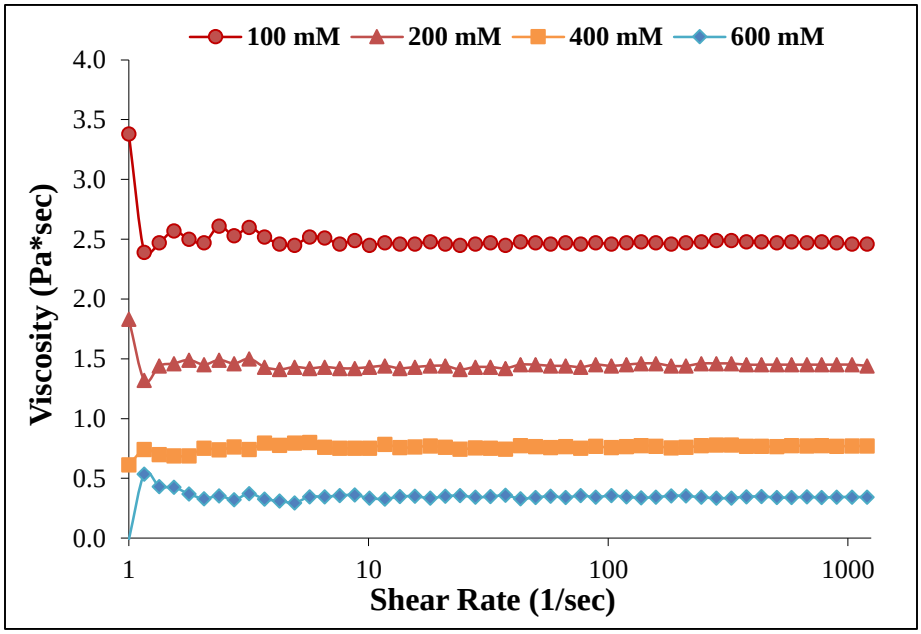

Figure 4.1: Viscosity as a function of shear rate for PEI/PGlu coacervates prepared with varying NaCl concentrations (N=400, pH 7.4) .

A dynamic frequency sweep test was used to measure the viscoelastic behavior of the coacervates. The storage (G') and loss (G") moduli were measured as a function of frequency for PEI/PAsp coacervates formed with various salt concentrations. Similar results were found for PEI/PGlu coacervates (data not shown). The experiments were performed at a constant strain of 1%, which was found to be in the linear regime. The viscoelastic behavior was strongly dependent on the salt concentration (Figure 4.2). For the coacervate formed with the lower salt concentration (Figure 4.2A), the loss (viscous) modulus (G") had higher values compared to the storage (elastic) modulus (G'), for all frequencies tested. As the salt concentration was increased the loss modulus decreased, creating a crossover point of the two moduli (Figure 4.2C). Coacervates prepared with lower salt are more viscous while coacervates prepared with higher salt are more elastic. The shift in the crossover point of G' and G" with changing salt concentration, as seen in Figure 4.2, points to the change in relaxation time scales of the coacervates. In an analogous fashion to the commonly used time–temperature superposition, in Figure 4.3, frequency sweep curves were shifted to create time-salt superposition master curves

that can predict behavior at a wide range of time scales not accessible by conventional rheological measurements.

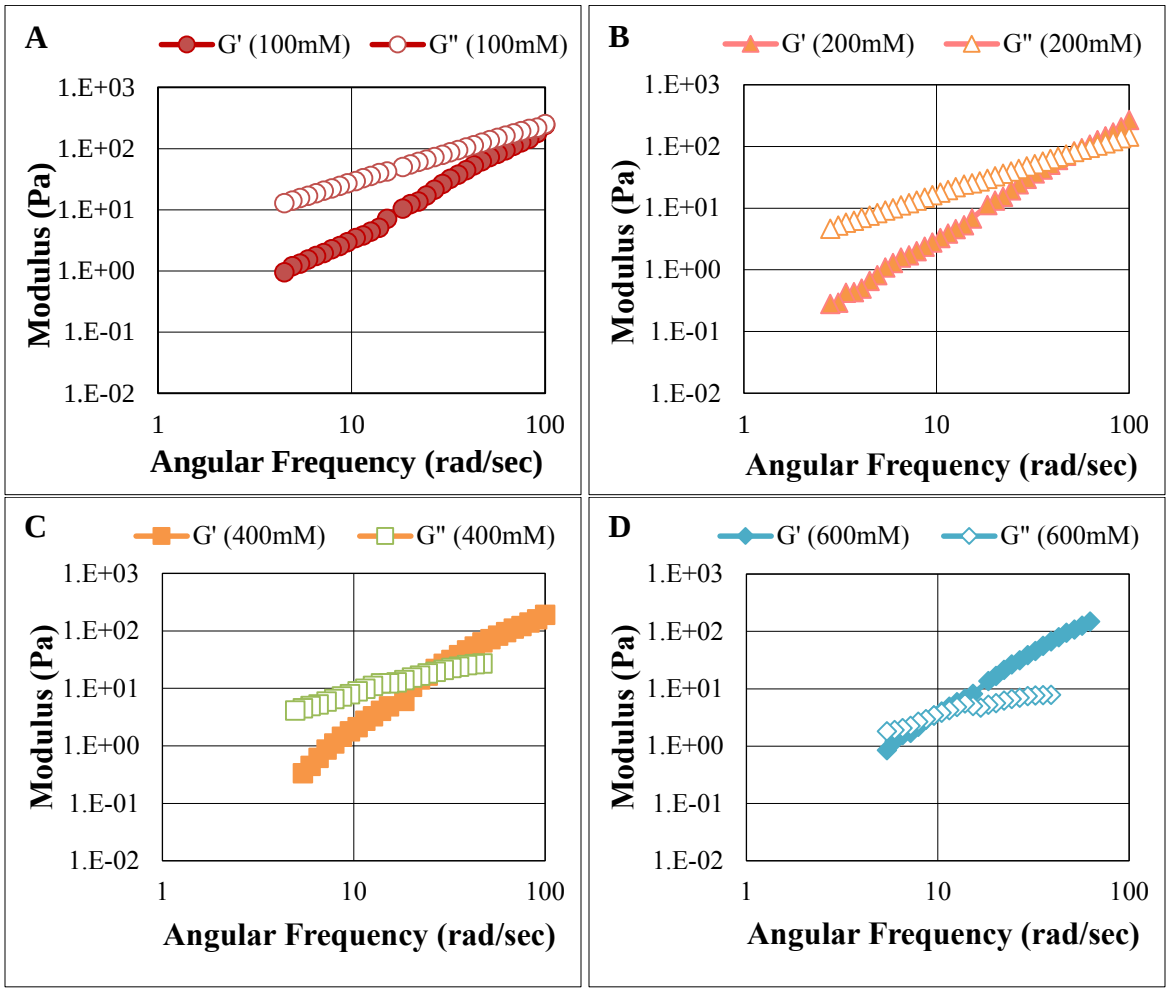

Figure 4.2: Storage (G') and loss (G") modulus versus angular frequency of PEI/PAsp coacervates formed with 100 (A), 200 (B), 400 (C) and 600 (D) mM total NaCl concentration (N=400, pH=7.4).

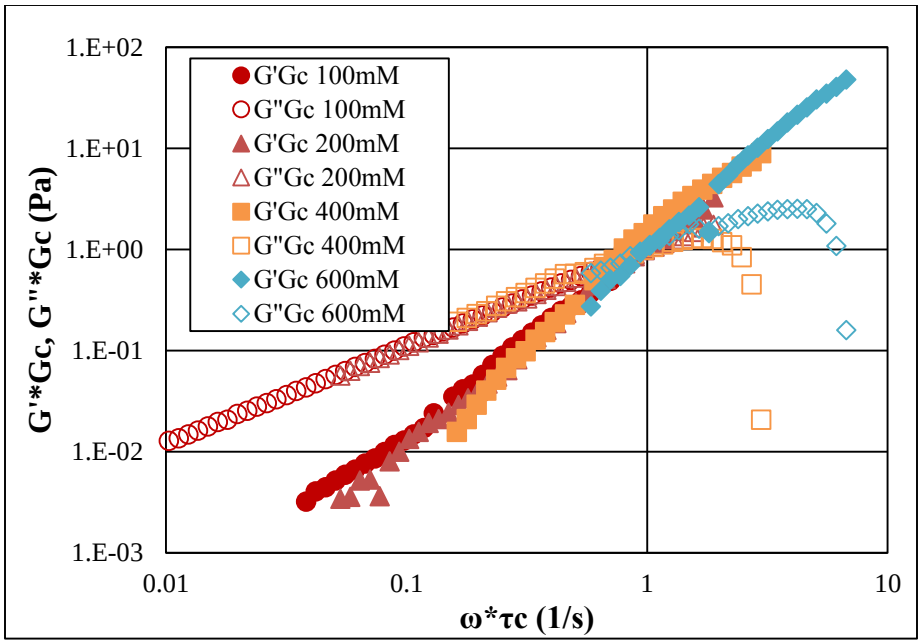

Figure 4.3: Time-salt superposition master curve created by shifting frequency sweep curves in Figure 4.2 by shift factors Gc and τc.

4.3.2 Encapsulation of BSA using polypeptide coacervates

Charged proteins can be encapsulated via complex coacervation using benign, aqueous conditions (phosphate buffered saline (PBS), pH 7.4). First, the protein of interest, bovine serum albumin (BSA), and the polycation, poly(L-lysine) (PLys), were mixed to form an intermediate complex based on the electrostatic interaction of the positively charged PLys with BSA, which has a net negative charge at neutral pH. In order to visualize the encapsulated protein, a fluorescently tagged FITC-BSA construct was used. Next the polyanion, poly(D/L-glutamic acid) (PGlu), was added and protein-containing complex coacervates were formed (Figure 4.4). The successful encapsulation of protein was confirmed visually using optical microscopy based on the colocalization of the green fluorescence signal from the protein with the coacervate droplet (Figure 4.5).

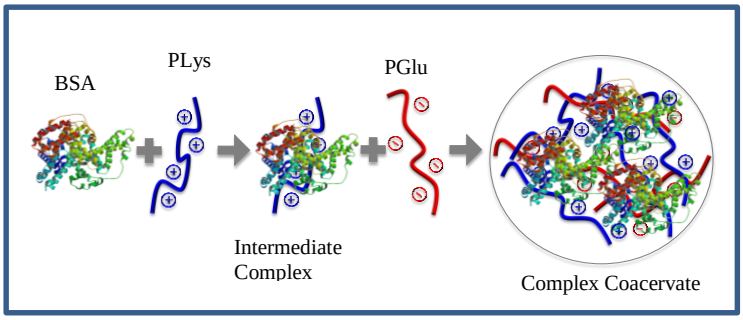

Figure 4.4: Diagram of the preparation of polypeptide complex coacervates with encapsulated BSA. First BSA and PLys are mixed creating an intermediate complex. Next, PGlu is added and complex coacervate droplets with encapsulated BSA are formed.

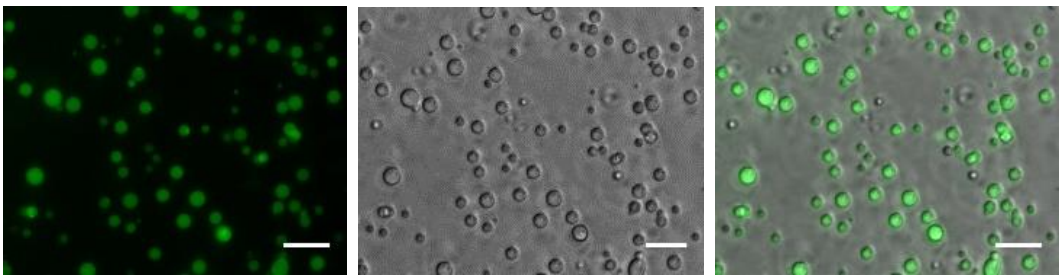

Figure 4.5: Optical micrographs of FITC-BSA encapsulation within coacervate droplets shown in fluorescence (left), brightfield (center) and overlay (right). Colocalization of fluorescence within the droplets confirms protein encapsulation. Scale bar represents 15μm.

The efficiency of protein encapsulation was measured using a Bradford protein colorimetric assay. Briefly, coacervates were formed as described above, keeping the concentration of PLys and PGlu constant while steadily increasing the amount of BSA. Encapsulation was measured by separating the coacervates from the solution phase by centrifugation and then quantifying the amount of protein remaining in the solution phase (*i.e.*, not encapsulated). Values were compared to a control with no PLys or PGlu (Figure 4.6). At a ratio of 0.05 BSA per polypeptide (or 20 polypeptides per BSA molecule), 100% of the added BSA is encapsulated. As the ratio of BSA to polypeptide is increased, the total amount of BSA encapsulated increases up to a maximum of 0.31 BSA per polypeptide, representing 63% encapsulation efficiency.

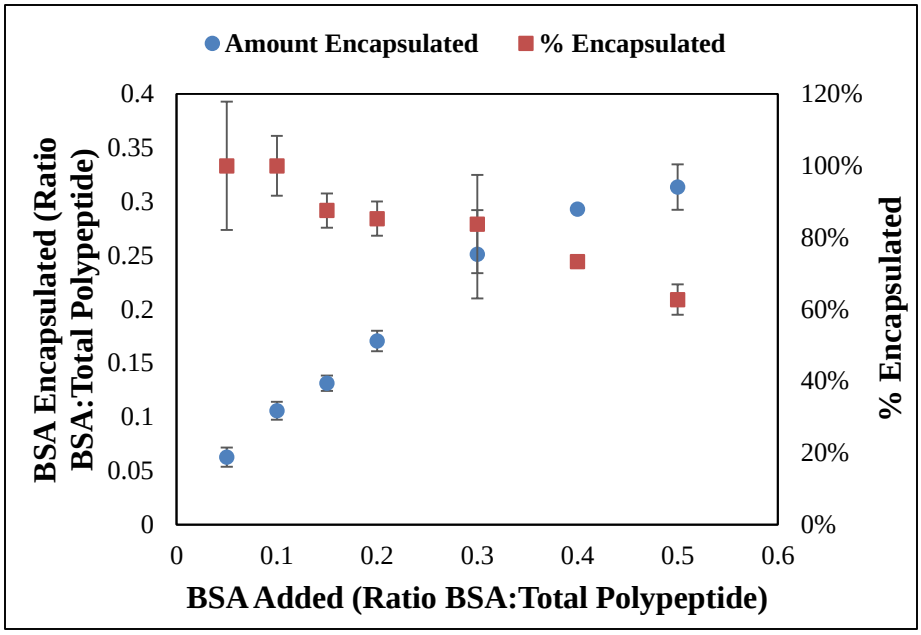

Figure 4.6: Encapsulation efficiency of BSA in a polypeptide coacervate system. As the ratio of BSA to polypeptide is increased, more BSA was encapsulated but efficiency of encapsulation ecreased. Error bars represent standard deviation.

4.3.3 Secondary structure stabilization of encapsulated BSA

Preservation of secondary structure is an important criteria for protein delivery as structure can related directly to activity and function. The potential for variations in protein structure was examined using circular dichroism. BSA is an alpha helical protein, as evidenced by the two characteristic minima at 208 and 222 nm.[19] A similar alpha helical structure was observed for BSA encapsulated in coacervates (Figure 4.7). The observed decrease in intensity was likely the result of loss of signal due to scattering from the droplets.

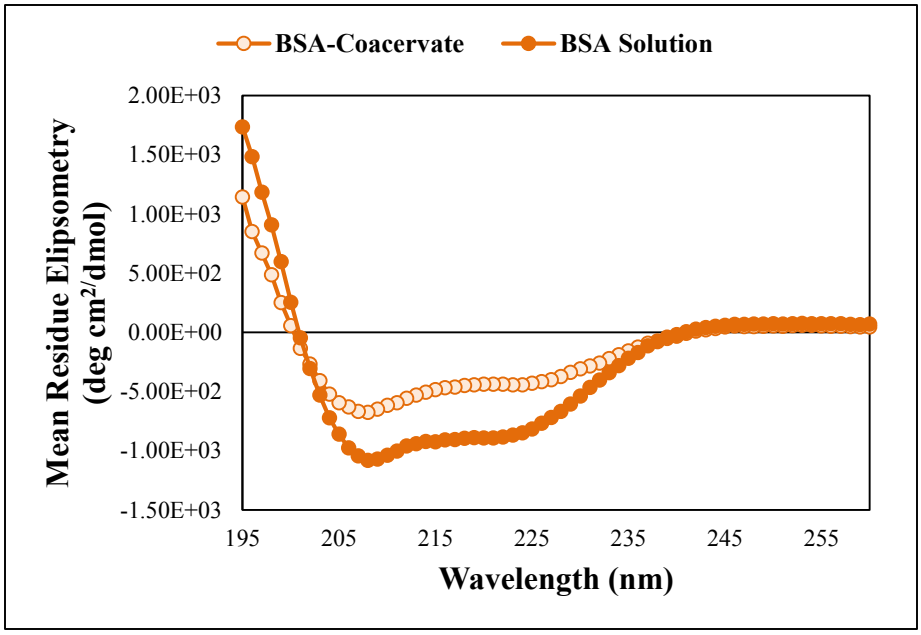

Figure 4.7: CD spectra of free (filled) and encapsulated (open) BSA showing characteristic dual minima of 208 and 222 indicative of alpha helical secondary structure. Encapsulation was performed at a ratio of 0.05 BSA to polypeptide to ensure 100% encapsulation (N = 400, Salt = 1X PBS, pH = 7.4).

4.3.4 pH triggered release of BSA from coacervates

Polypeptide complex coacervates form as a result of electrostatic associations between oppositely-charged amino acid side chains, and thus are sensitive to changes in pH. This pH responsiveness makes them ideal for drug delivery because they can disassemble and trigger the release cargo upon entry into a low pH environment, such as in the endosome or lysosome of cells. Turbidity was used as a measure of total complex formation. As pH was decreased, the complex coacervates disassembled and were fully disassembled by pH 2 (Figure 4.8). With decreasing pH, the PGlu carboxylic acid side chains, (pKa= 4.25) become increasingly protonated, thus weakening the electrostatic interaction between PGlu and PLys. Shorter polypeptides (N=100) showed lower stability as a function of pH. An inflection point in the disassembly curve of polypeptides with N=100 occurs at pH = 5 and for longer chains, N=400 at pH = 4 (Figure 4.9). Polypeptide molecular weight thus provides an additional parameter for controlling protein release.

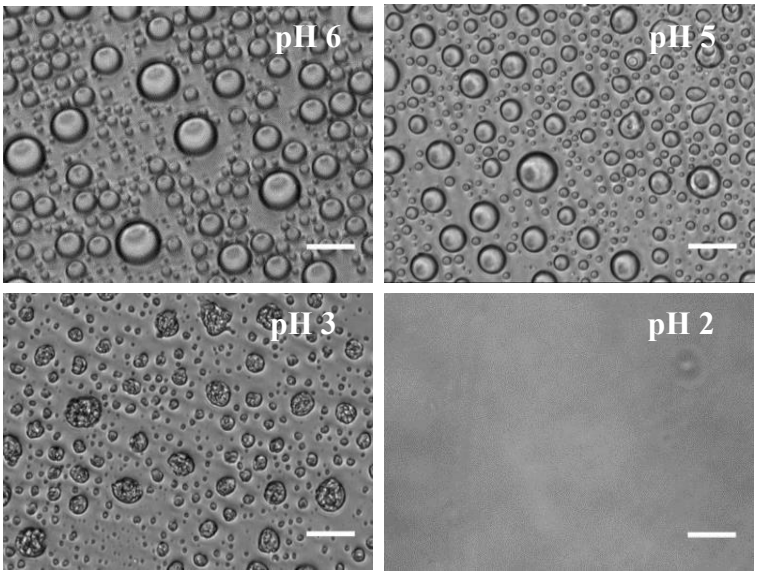

Figure 4.8: Representative optical micrographs of coacervates as a function of decreasing pH (N=400). Scale bars represent 25μm.

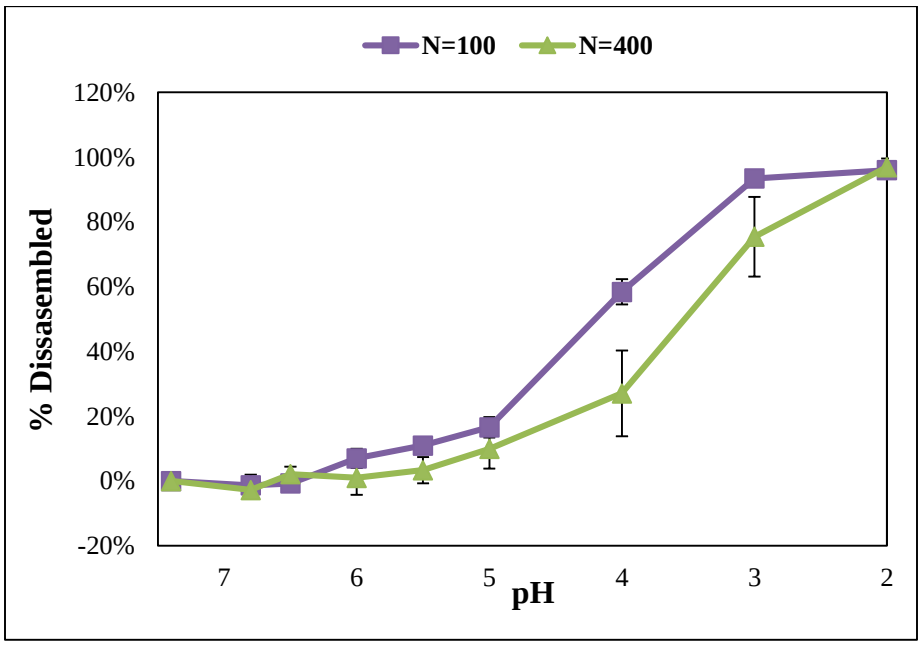

Figure 4.9: *In vitro* release of FITC-BSA from coacervates (N=400 and N=100) with decreasing pH.

4.3.5 *In Vitro* biocompatibility of polypeptide coacervates

Interaction of BSA loaded coacervates with NIH 3T3 cells was investigated. Cell viability was measured after incubation with BSA loaded coacervates, BSA, blank coacervates, PLys, PGlu and an untreated control. No significant toxicity was observed for BSA loaded coacervates, coacervates alone, BSA alone or PGlu alone (Figure 4.10). PLys alone showed a

slight toxicity, which was statistically significant compared to other treatment groups (ANOVA, Tukey $p<0.05$) (Figure 4.10). Direct inspection of cells incubated with FITC-BSA loaded coacervates for 24 hours show cells that were well spread and have a healthy appearance. BSA loaded coacervates appear to associate strongly with cell membranes, remaining attached despite multiple washing steps prior to imaging (Figure 4.11).

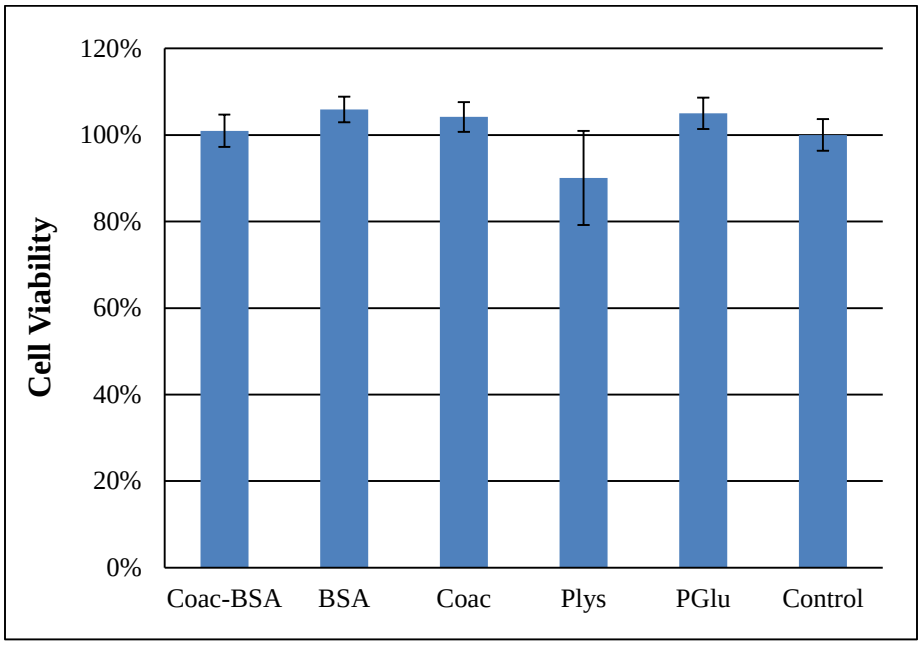

Figure 4.10: Cell viability after 24 hour incubation with BSA loaded coacervates (Coac-BSA), BSA alone, coacervates alone (Coac), PLys, or PGlu relative to a cell control. Only PLys showed slight toxicity.

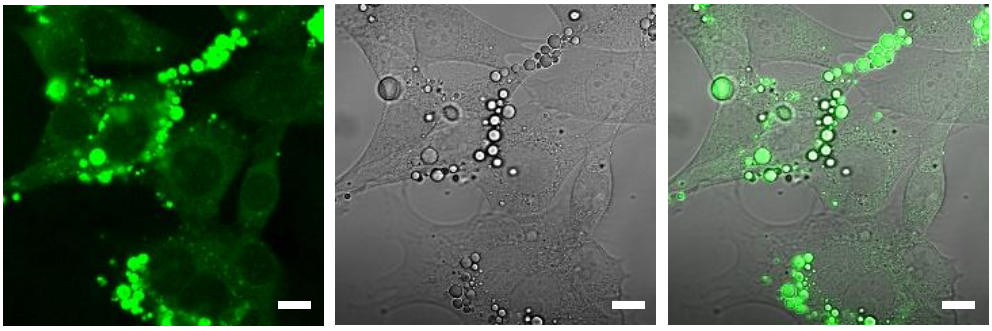

Figure 4.11: Optical micrographs of FITC-BSA coacervates incubated with NIH 3t3 cells shown in fluorescence (left), brightfield (center), and overlay (right). Scale bar represents 20 μm.

4.4 Discussion

Polypeptide complex coacervates have the potential to address the challenge of encapsulating and delivering proteins. Unlike the harsh processing conditions used to form many

other encapsulation technologies, complex coacervates are formed by simple mixing in benign, aqueous conditions. Complexation is driven by the electrostatic attraction between oppositely charged polypeptides. Proteins, which often have both local and net charges, can be easily added to the system and encapsulated via electrostatic interactions.

Polypeptide-based coacervates have unique mechanical properties that can be studied using rheology. In Figure 4.1 a decrease in the viscosity of the PEI/PGlu coacervates was seen as the salt concentration in the mixtures increased. The increased screening effect of the salt on the charged amino acids leads to coacervates with weaker intermolecular electrostatic interactions, higher water content and therefore lower viscosities. The influence of the electrostatic interactions on the viscosity of coacervates seen here is consistent with earlier observations on protein/gum Arabic coacervates.[20]

Stiffness of the material is a critical property for drug delivery, as it regulates cell interaction and uptake of the particles. Dynamic frequency sweep tests were used to evaluate the storage and loss modulus of PEI/PAsp coacervates formed at different salt concentrations. For coacervates formed with the lower salt concentration, the loss (viscous) modulus (G") had higher values compared to the storage (elastic) modulus (G'), for almost all frequencies tested. As the salt concentration was increased the loss modulus values decreased until they become lower than the storage modulus values, for almost all frequencies. These results indicate that coacervates prepared with lower salt are more viscous while coacervates prepared with higher salt are more elastic. Additionally, a shift in the crossover point of G' and G" was observed to shift to lower frequencies with increasing salt concentration. In a recent study of acrylamide gel particles it was found that soft particles (Young's modulus = 18 kPa) were preferentially internalized by macropinocytosis, while hard particles (Young's Modulus = 211 kPa) where internalized through clathrin-mediated routes. Particles with intermediate elasticity internalized via multiple mechanisms which resulted in larger overall uptake.[18] For comparison, coacervates formed with 100 mM NaCl had a Young's modulus of 0.7 kPa. A direct comparison here is confounded by the different methods used to measure the particles: acrylamide (indentation using atomic force microscopy) and coacervates (rotational rheometer). However, a conclusion can be made that the polypeptide coacervate system falls on the soft end of the particle spectrum meaning cell endocytosis would likely occur via macropinocytosis. An in vitro uptake assay would be necessary to confirm the route of uptake, however this link between uptake and stiffness is important to direct design and choice of biological application.

In an analogous fashion to the commonly used time–temperature superposition, Spruijt et al.[21] suggested that the frequency dependent modulus change of coacervates can be rescaled to create a master curve spanning many orders of time scale. As shown in Figure 4.3, frequency sweep curves were shifted to create master curves that can predict behavior at a wide range of time scales not accessible by conventional rheological measurements. Coacervate viscoelastic behavior, is in line with results on complex coacervates based on cellulose,[22] synthetic macromolecules[17] and other soft materials.[23]

For the application of protein encapsulation, PLys/PGlu coacervates were used, as both polymers have been extensively used in biological applications. Encapsulation of a model protein, BSA, was measured by separating the coacervates from the solution phase by centrifugation and then quantifying the amount of protein remaining in the solution phase (*i.e.*, not encapsulated). At a ratio of 0.05 BSA per polypeptide (or 20 polypeptides per BSA molecule), 100% of the added BSA is encapsulated. As the ratio of BSA to polypeptide is increased, the total amount of BSA encapsulated increases up to a maximum of 0.31 BSA per

polypeptide, representing 63% encapsulation efficiency. This decrease in loading with increased protein is likely due to the charged proteins competing with polypeptide for charge association. To increase the total loading, a ratio at which 100% of protein is encapsulated (0.05 BSA per polypeptide) should be used, and both components (BSA and polypeptides) increased. Other modifications could be made including changing the ratio of polypeptides, since BSA has a net negative charge, an excess of PLys to PGlu may increase loading. The loading efficiency of polypeptide coacervates is a vast improvement on PLGA systems which are typically limited to 1wt% therapeutic per particle.[6] Depending on the application needs, a choice can be made between efficiency and uptake, and thus reducing waste or amount of product loading. Where proteins are expensive to produce, the ability to control uptake efficiency is important for clinical success.[24]

Two main challenges in the field of protein delivery, are to preserve the secondary structure (and thus activity) of the protein, and to establish a method by which the protein will be released. No significant changes to the secondary structure of BSA encapsulated in the PLys/PGlu coacervates were observed, compared with free BSA in solution, demonstrating that no unfolding events occurred during encapsulation. In terms of protein release, polypeptide coacervates are electrostatic associations based on the attraction of charged amino acids. Release of BSA was demonstrated under conditions of decreasing pH. Lowering the pH of the solution, approaches the pKa of the carboxylic acid of PGlu causing it to be primarily neutral. This effectively weakens the association of the polypeptides and leads to the disassembly of the complex. Triggered release at low pH may be advantageous for delivering protein cargo once the assembly enters the cell.

Lastly the biocompatibility of coacervates were studied using a model cell line, NIH 3T3. No significant toxicity for BSA loaded coacervates, coacervates alone, BSA alone or PGlu acid alone (Figure 4.10). PLys alone showed a slight toxicity, which was statistically significant compared to other treatment groups. This result was expected as positively charged polymers such as PLys may coat or interact with the negatively charged membrane of cells, causing membrane disruption and cell death.[25] When incorporated in a complex coacervate, the positive amino acid side chain's of PLys are closely associated with the negative amino acid side chain of PGlu and thus are not free to interact negatively with the cell membrane. Fluorescence microscopy showed that the loaded coacervates interact well with cells and may be internalized. Further studies are necessary to determine the mechanism of the observed interaction as well as to quantify internalization. The viability and imaging studies presented here indicate a biocompatible and positive interaction with cells.

4.5 Conclusions

In conclusion, we present here a strategy for encapsulating proteins via the electrostatic association of charged polypeptides. Current encapsulation systems based on polymer such as PLGA are limited by harsh solvent processing conditions and low therapeutic loading. An ideal encapsulation system would have a simple method of particle formation, using benign aqueous conditions so as to preserve protein (or peptide) secondary structure (and thus function). A method to tune stiffness is also ideal, as stiffness can dictate how particles are internalized. Additionally, an encapsulation system should have a high loading efficiency and be biocompatible. Complex coacervates are formed via simple mixing in benign, aqueous conditions, making them advantageous for protein encapsulation. Additionally, a process driven

by simple mixing can be easily scaled to production scale. Rheological studies elucidated the viscoelastic behavior of the complex coacervates, and that the mechanics depend strongly on salt concentration. A model protein, BSA was encapsulated with a tunable efficiency with no observable impact on secondary structure. The ability to tune loading of the protein and control efficiency of uptake is particularly important for the use of protein therapeutics, which can be expensive to produce. Release of BSA was demonstrated under conditions of decreasing pH. Triggered release at low pH may be advantageous for delivering protein cargo once the assembly enters the cell. Lastly, protein loaded coacervates were shown to be non-toxic in a cell viability assay. The studies here present a simple and effective method for encapsulating proteins using polypeptide based complex coacervates. A system such as this could solve the problems with other protein delivery systems specifically in terms of process compatibility and scale up.

An important consideration that was not addressed in this work is the size of the complex coacervate droplets. As dynamic self-assemblies, these droplets can coalesce and grow in size up to several microns, or merge into one continuous phase over time. In the following chapter a method will be developed to control the coacervate size and prevent subsequent coalescence using a crosslinker.

4.6 References

1. DeWitt, D. E. & Hirsch, I. B. Outpatient insulin therapy in type 1 and type 2 diabetes mellitus. *J. Am. Med. Assoc.* **289,** 2254–2264 (2003).

2. Scott, A. M., Wolchok, J. D. & Old, L. J. Antibody therapy of cancer. *Nat. Rev. Cancer* **12,** 278–87 (2012).

3. Brown, L. R. Commercial challenges of protein drug delivery. *Expert Opin. Drug Deliv.* **2,** 29–42 (2005).

4. Jevsevar, S., Kunstelj, M. & Porekar, V. G. PEGylation of therapeutic proteins. *Biotechnol. J.* **5,** 113–28 (2010).

5. Torchilin, V. P. Recent advances with liposomes as pharmaceutical carriers. *Nat. Rev. Drug Discov.* **4,** 145–60 (2005).

6. Danhier, F. *et al.* PLGA-based nanoparticles: an overview of biomedical applications. *J. Control. Release* **161,** 505–22 (2012).

7. Kumar, P. S., Ramakrishna, S., Saini, T. R. & Diwan, P. V. Influence of microencapsulation method and peptide loading on formulation of poly(lactide-co-glycolide) insulin nanoparticles. *Pharmazie* **61,** 613–7 (2006).

8. Johnson, O. L. *et al.* A month–long effect from a single injection of microencapsulated human growth hormone. *Nat. Med.* **2,** 795–799 (1996).

9. Giteau, A. *et al.* Reversible protein precipitation to ensure stability during encapsulation within PLGA microspheres. *Eur. J. Pharm. Biopharm.* **70,** 127–36 (2008).

10. Bungenberg de Jong, H. B. & Kruyt, H. R. Coacervation (Partial Miscibility in Colloid Systems). *Proc. Sect. Sci, Koninkijke Ned. Akad. van Wet.* **32,** 849–856 (1929).

11. Sarmento, B. *et al.* Alginate/chitosan nanoparticles are effective for oral insulin delivery. *Pharm. Res.* **24,** 2198–206 (2007).

12. Shih, I.-L., Van, Y.-T. & Shen, M.-H. Biomedical applications of chemically and microbiologically synthesized poly(glutamic acid) and poly(lysine). *Mini Rev. Med. Chem.* **4,** 179–88 (2004).

13. Boussif, O. *et al.* A versatile vector for gene and oligonucleotide transfer into cells in culture and in vivo: polyethylenimine. *Proc. Natl. Acad. Sci. U. S. A.* **92,** 7297–301 (1995).

14. Priftis, D. & Tirrell, M. Phase behaviour and complex coacervation of aqueous polypeptide solutions. *Soft Matter* **8,** 9396–9405 (2012).

15. Priftis, D., Megley, K., Laugel, N. & Tirrell, M. Complex coacervation of poly(ethylene-imine)/polypeptide aqueous solutions: thermodynamic and rheological characterization. *J. Colloid Interface Sci.* **398,** 39–50 (2013).

16. Priftis, D., Farina, R. & Tirrell, M. Interfacial Energy of Polypeptide Complex Coacervates Measured via Capillary Adhesion. *Langmuir* **28,** 8721–9 (2012).

17. Spruijt, E., Sprakel, J., Cohen Stuart, M. A. & van der Gucht, J. Interfacial tension between a complex coacervate phase and its coexisting aqueous phase. *Soft Matter* **6,** 172–178 (2010).

18. Banquy, X. *et al.* Effect of mechanical properties of hydrogel nanoparticles on macrophage cell uptake. *Soft Matter* **5,** 3984–3991 (2009).

19. Holzwarth, G. & Doty, P. The Ultraviolet Circular Dichroism of Polypeptides. *J. Am. Chem. Soc.* **87,** 218–28 (1965).

20. Weinbreck, F., Wientjes, R. H. W., Nieuwenhuijse, H., Robijn, G. W. & de Kruif, C. G. Rheological properties of whey protein/gum arabic coacervates. *J. Rheol. (N. Y. N. Y).* **48,** 1215–1228 (2004).

21. Spruijt, E., Sprakel, J., Lemmers, M., Stuart, M. & van der Gucht, J. Relaxation Dynamics at Different Time Scales in Electrostatic Complexes: Time-Salt Superposition. *Phys. Rev. Lett.* **105,** 208301–1–4 (2010).

22. Liu, R. C. W. L., Orishima, Y. M. & Winnik, F. M. Rheological Properties of Mixtures of Oppositely Charged Polyelectrolytes . A Study of the Interactions between a Cationic Cellulose Ether and a Hydrophobically Modified Poly [sodium 2- (acrylamido) -2-methylpropanesulfonate]. *Polym. J.* **34,** 340–346 (2002).

23. De Kruif, C. G., Weinbreck, F. & de Vries, R. Complex coacervation of proteins and anionic polysaccharides. *Curr. Opin. Colloid Interface Sci.* **9,** 340–349 (2004).

24. Jain, R. A. The manufacturing techniques of various drug loaded biodegradable poly(lactide-co-glycolide) (PLGA) devices. *Biomaterials* **21,** 2475–90 (2000).

25. Kim, S. W. Polylysine copolymers for gene delivery. *Cold Spring Harb. Protoc.* **2012,** 433–8 (2012).

Chapter 5: Polypeptide Nanoparticles: Design and Stability

Associated Papers:
K Black, L Mlinar, and M Tirrell. "Polypeptide nanoparticles for drug delivery: Formulation and Stability" *(in preparation)*

Abstract:

Encapsulation is a useful strategy to delivery therapeutic proteins in the body. One major limitation of polymer encapsulation is the ability to control final size of the particles. Here a simple method controlling particle size by changing input conditions is presented. Polypeptide coacervates were formed by simple mixing and crosslinked using a zero length crosslinked to create a peptide bond between the amino acid side groups of poly(L-lysine) and poly(D/L-glutamic acid). By changing the ratio of PGlu to PLys colloidal stability was achieved without the need for an additional excipient. Surface charge of the particles was also controlled by this method. Final particle size was controlled by both molecular weight and concentration of the polypeptides. A span of particle diameter from to 272nm to 1.3 μm was achieved. Lastly, stability at low pH, where non-crosslinked coacervates disassemble, was demonstrated. A simple and tunable method to control particle size, such as the one presented here provides a possible solution to a major limitation in the field of drug delivery, control of particle size.

5.1 Introduction

Proteins and peptides represent a growing class of therapeutics which are difficult to deliver. Encapsulation is one emerging method with the potential to change the paradigm of drug delivery. Encapsulation in nanometer or micrometer scale particles can protect the protein therapeutic from degradation and removal from circulation by the body, as well as providing a method for controlled release. One of the most important characteristics is the size of the particles. Size can determine uptake, release rate, as well as degradation rate. Thus, ability to control the size of manufactured particles is an important goal.

Biodegradable particles have been formed from a variety of polymers, but the most well studied is poly(DL-lactide-co-glycolide) (PLGA). PLGA particles are formed using techniques such as precipitation[1], spray-drying[2], or emulsion[3,4]. Of these techniques, spray-drying and emulsifying have been used most commonly in scale up industrial processes. One successful example of commercialization of a PLGA product is Nutropin Depot®, developed by Alkermes and Genentech. Manufacture of Nutropin Depot® involved the creation of a complex, low temperature spraying method in order to preserve the activity of the encapsulated growth hormone.[5] One of the big challenges with this method on the commercial scale was that it resulted in a wide particle size distribution, which then required sieving to remove larger particles and aggregates. Sieving can greatly reduce the yield and increase the cost of production. This is especially problematic when the encapsulated protein is expensive to produce, like a growth hormone.[6] Ultimately the two companies decided to discontinue the manufacture of Nutropin Depot®, stating that the manufacturing costs were too great.

An important lesson can be learned from the example of Nutropin Depot®, and provide guidance to the development of new strategies to control particle size. An ideal system would have beneficial particle properties, and have a strategy for production that is simple and involves

easily tunable parameters that dictate final size. Particles should be biocompatible and not cause an immune response in the body. Particles should also have a mechanism for degradation or diffusion, so that they are able to release their therapeutic payload. The rate of release should be sustained over a period of time, appropriate for the disease condition. Ideally particles would be hydrophilic in order to avoid uptake by the reticulo-endothlial system (RES) which recognizes hydrophobic particles as foreign.[7] Size of the particles, as mentioned previously, is critically important and depends on the application. For oral delivery, 100 nm particles were shown to have the highest gastrointestinal uptake compared to particles of larger size.[8] For an injected product, between 70 and 200 nm is ideal for cancer therapeutics.[9] For applications in pulmonary delivery a larger particle size, 0.5 to 3 μm was found to be optimal for delivery of insulin to the aveoli in the lung.[10] Achievement of these particle properties should not come at a cost of an inefficient synthesis process in order for the system to be successful on the commercial scale.

One alternative to avoid the processing problems of PLGA is to use complex coacervation of oppositely charged polypeptides to form particles. Complex coacervates are formed when oppositely charged polyelectrolytes are mixed in aqueous solution, a process first observed in gelatin and gum Arabic.[11] Coacervation results in a liquid-liquid phase separation in which a dense polymer-rich phase (coacervate) separates from the dilute polymer-poor solution phase (aqueous phase). Coacervates can be formed using synthetic polypeptides, for example, poly(lysine) (PLys) and poly(glutamic acid) (PGlu), are biocompatible and have been used in a variety of biomaterial applications.[12] Previous work identified the conditions under which these polypeptides form complex coacervates in solution.[13,14] In addition to polymer chemistry, salt concentration, pH, the ratio of polycation to polyanion, total polymer concentration and temperature are important system parameters that can be tuned to control coacervate formation. It was also shown that PLys/PGlu coacervates can encapsulate proteins using a process driven by simple mixing and can be easily scaled to production scale. A model protein, BSA, was encapsulated with a tunable efficiency ranging from 100 to 63% corresponding to a protein to polypeptide ratio of 0.05 to 0.3. Since the process is carried out in aqueous conditions at physiological salt and pH, the encapsulation process did not affect the secondary structure of the protein, often an important condition for activity.[15] The protein loaded coacervates were also shown to be non-toxic in a cell viability assay. The studies here present a simple and effective method for encapsulating proteins using polypeptide based complex coacervates. A system such as this could solve the problems with other protein delivery systems specifically in terms of process compatibility and scale up.

One issue that has not been addressed with this system is the size of the complex coacervate droplets. As dynamic self-assemblies, these droplets can coalesce and grow in size up to several microns, or merge into one continuous phase over time (a few hours at room temperature). Here, a method to control the coacervate size and prevent subsequent coalescence using a crosslinker is demonstrated. 1-Ethyl-3-[3-dimethylaminopropyl]carbodiimide hydrochloride (EDC) is a water soluble carbodiimide crosslinker which provides a zero-length, carboxyl to amine conjugation. EDC has been used extensively in biomaterial surface modification including the layer by layer assembly of PLys/PGlu films.[16] Here, EDC is used to stabilize coacervate particles to prevent further recombination or absorption to surfaces by crosslinking the carboxyl group of PGlu to the primary amine of PLys. Using this approach, two methods of controlling particle size are studied, polypeptide length, and total concentration. In addition, colloidal stability is demonstrated by increasing the ratio of PGlu to PLys creating a negatively charged surface. Lastly, these crosslinked coacervate particles are shown to be stable

in conditions of decreasing pH, where non-crosslinked coacervates disassemble. Crosslinking is a useful tool to impart stability on the polypeptide complex coacervates. This method of allowing coacervation to occur and then crosslinking represents a simple and scalable method that could be employed to address the problems of PLGA particles.

5.2 Materials and Methods

Materials

All polypeptides used in this study (PLys and PGlu (N=400, 200 and 100)) were purchased from Alamanda Polymers, Inc. (Huntsville, AL). All other materials were purchased from Sigma-Aldrich (St. Louis, MO) unless otherwise noted. Water was dispensed from a Milli-Q water purification system at a resistivity of 18.2 MΩ cm. The polypeptides were used as received without any further purification. Separate stock solutions of 1 wt% of each polypeptide were prepared in water. The pH was then adjusted to 7.0 ± 0.05 by adding small amounts of 1M NaOH or HCl. EDC was prepared immediately before each use at a concentration of 1M in water.

Formation of Complex Coacervates

Complex coacervates were formed by mixing PLys with EDC in a concentrated phosphate buffered saline (PBS) solution followed by addition of PGlu to form the coacervate in aqueous solutions with a final salt concentration of 1x PBS and 0.1M EDC. PLys and PGlu were always used with equal degrees of polymerization (either N=400 or N=100). The polyelectrolyte mixtures are prepared in microcentrifuge vials and were vigorously vortexed after the addition of each component. The order of mixing was kept the same for all experiments. For non-crosslinked particles, water was used in place of the EDC solution. All complex coacervates were prepared immediately before use and studied at room temperature (25ºC).

Scanning Electron Microscopy (SEM)

Silicon wafers were coated with 0.01wt% PLys in water and allowed to dry to increase particle retention during processing. Samples were absorbed onto chips and fixed with 2% glutaraldehyde in 0.1M sodium cacodylate buffer, washed three times with 0.1M sodium cacodylate buffer, and post fixed in 1% osmium tetroxide in 0.1M sodium cacodylate buffer for 1 hour. Samples were again washed three times with 0.1M sodium cacodylate to remove excess osmium tetroxide and exposed to a gradient of increasing ethanol in water solutions until 100% ethanol was reached. Samples were then subjected to critical point drying on a Tousimis AutoSamdri-815, Series A. Dried samples were sputter coated with platinum using a Tousimis sputter coater. Scanning electron microscopy was performed on a Hiatchi S-5000 high resolution, cold field emission SEM.

Size Determination

ImageJ software was used to measure particle size. For each condition, size was measured from a minimum of 5 SEM images, using a minimum of 200 measurements. Average size +/- standard deviation was reported.

Turbidity

Turbidity, or the absorption of light at 500 nm, was used a measure of total coacervate formation. Turbidity (T) is defined by T=-ln(I/I0), with I0 = incident light intensity and I = intensity of light passed through the sample volume. Neither polypeptide absorbs light at 500 nm. A plate reader equipped with a UV spectrophotometer (Tecan, Infinite M200) was employed and samples were measured in triplicate.

Zeta Potential

Particles were formed and crosslinked as described above. For zeta pontential measurements samples were spun down with a microcentrifigure and washed with DI water three times prior to measurement. The zeta potential of crosslinked particles was measured using a Zetasizer Nano ZS (Malvern, Worcestershire, United Kingdom).

5.3 Results

5.3.1 Visual Evidence of Crosslinking

Oppositely charged polypeptides, PLys and PGlu, self-assemble into polypeptide rich droplets in aqueous solution, a phenomenon termed coacervation. Once formed, coacervates are dynamic structures and can collide and recombine with other neighbors. Coacervate droplets can also absorb and coalesce onto charged surfaces. Here the goal is to stabilize the coacervate droplets after they form, and prevent further recombination or absorption onto surfaces. To achieve this, EDC, a zero length crosslinker which reacts with primary amines and carboxylic acid groups creating peptide bonds, was used. Polypeptide coacervates were formed via self-assembly and then stabilized by crosslinking with EDC. Successful crosslinking stabilization can be visualized using SEM. In the case of crosslinked coacervates, which from here on will be referred to as polypeptide nanoparticles (PNPs), well-formed spherical particles are visualized in SEM on the silca chip surface. In the case of non-crosslinked coacervates, SEM revealed large merged and coalesced regions of amorphous coacervate (Figure 5.1).

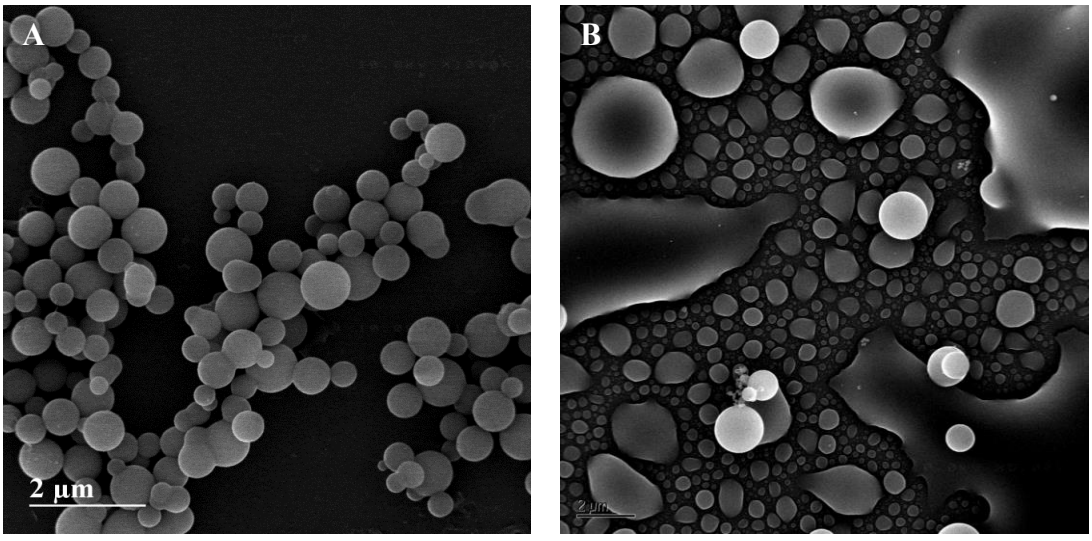

Figure 5.1: Polypeptide coacervates with (A) and without (B) crosslinking stabilization.

5.3.2 Surface charge colloidal stabilization

The ability to change surface charge of the particles and colloidal stability was investigated by varying the ratio of PGlu to PLys. Visually, neutral PNPs formed with an equal ratio of PGlu:PLys formed aggregates in solution (Figure 5.2A). At a ratio of 1.5:1 stability was improved and single stabilized particles can be seen in addition to small aggregates (Figure 5.2B). At a ratio of 1.75:1 stability is greatly improved and particles are stabilized in suspension as single particles. Increasing the ratio beyond this point 2:1, had no additional visual effect on stability Figure 5.3C-D). Thus surface charge, and also colloidal stability can be controlled by changing the ratio of the negative (PGlu) and positive (PLys) polypeptides. PNPs formed with an equal ratio of PLys and PGlu formed aggregates and were not able to be measured using zeta potential. It is assumed that these particles had increased aggregation due to their neutral surface charge. Increasing the ratio of PGlu:PLys led to a more negative surface charge as was reported by zeta potential surface charge measurements (Figure 5.3).

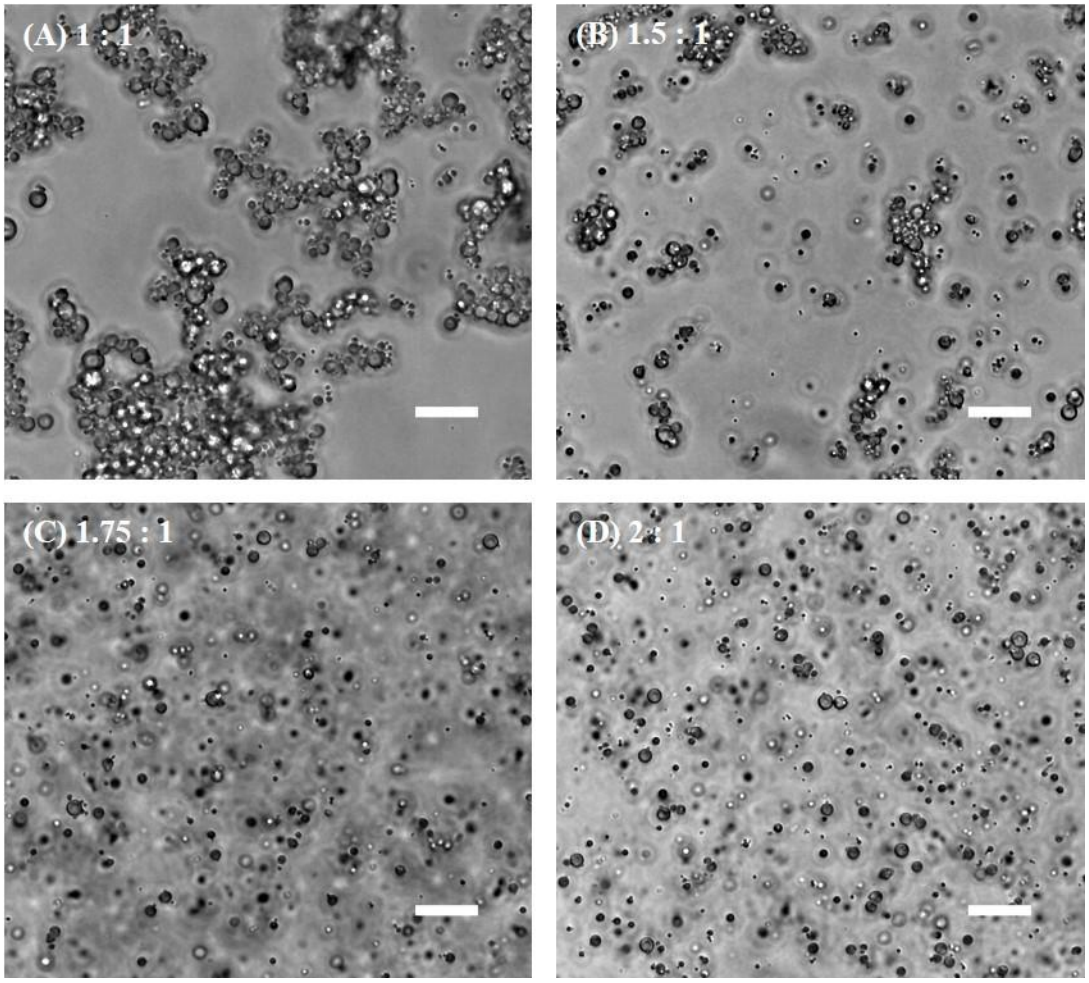

Figure 5.2: Representative images of PNPs made with varying ratios of PGlu: PLys (A) 1:1, (B) 1.5:1, (C) 1.75:1, and (D) 2:1. Scale bar represents 25 µm.

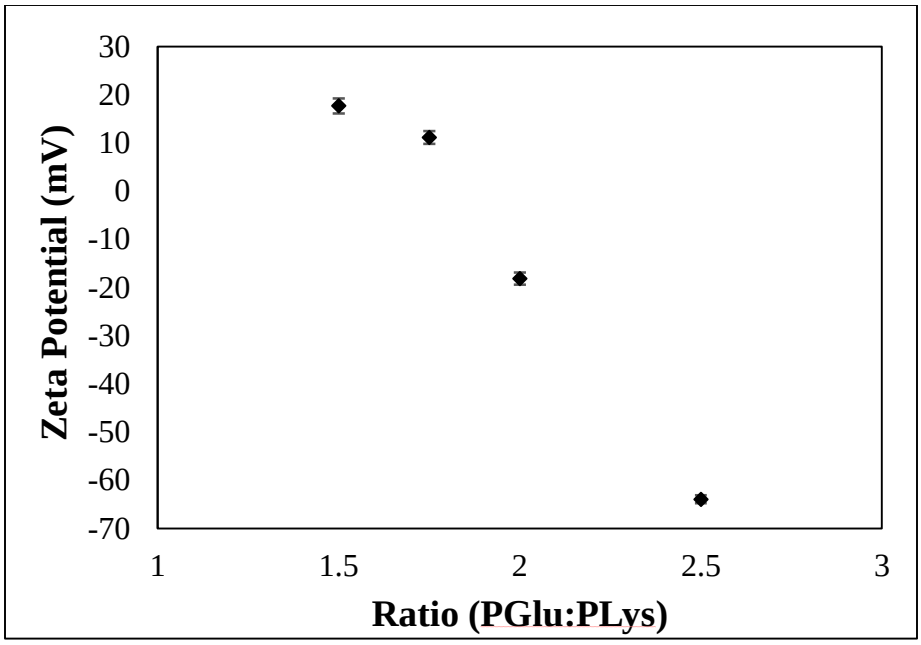

Figure 5.3: Zeta potential measurements of PNPs formed with varying rations of PGlu to PLys.

5.3.3 Design Parameters for Size Control

Size of the PNPs was controlled using both total polypeptide concentration and also molecular weight of the polypeptides. As total concentration was decreased from 20.1 to 5.2 µM as shown in Figure 5.4A-C, size of the PNPs also decreased. Similarly as molecular weight of the polypeptides is decreased from 60 to 15 kDa, size of the PNPs also decreased (Figure 5.4D-F). Summation of the results from this 2D parameter space can be seen in Figure 5.5. For each molecular weight, a graph of PNP size versus polypeptide concentration reveals a power-law based correlation.

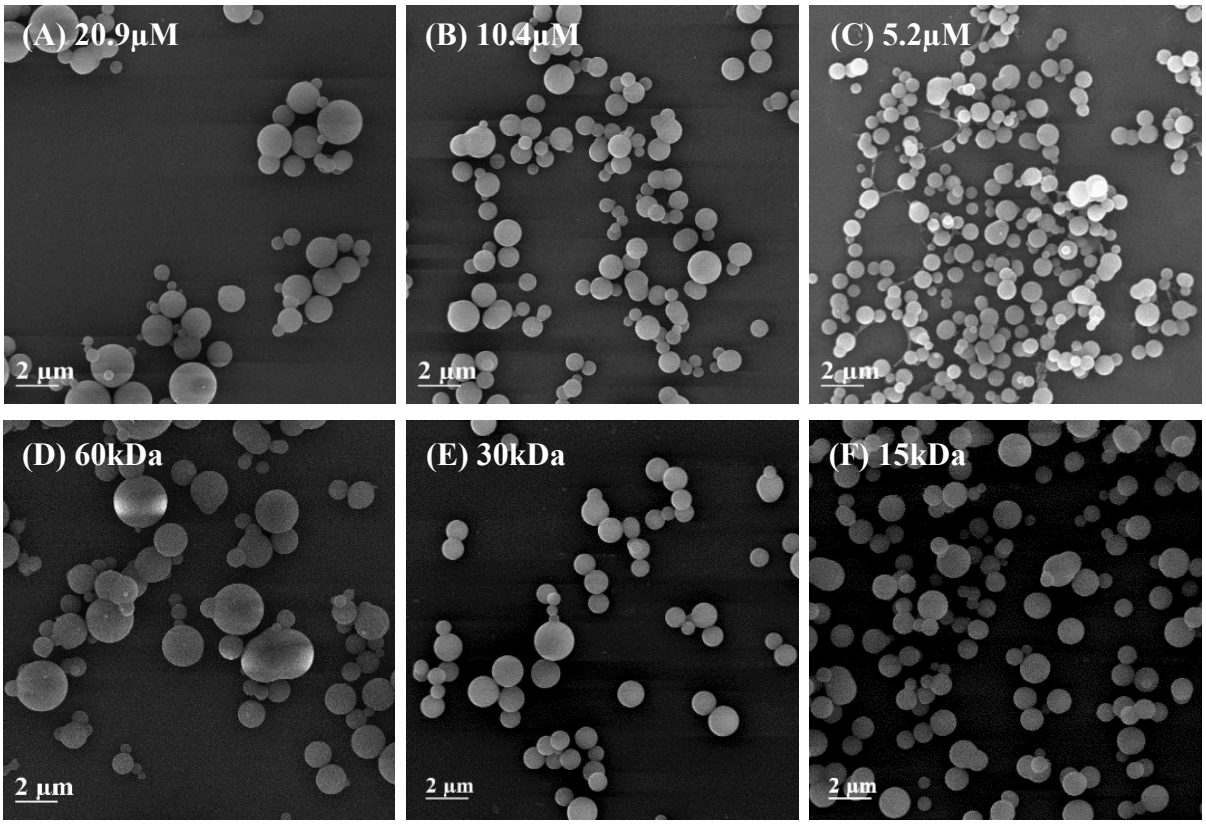

Figure 5.4: SEM images of PNPs formed with varying concentration and fixed molecular weight (60 kDa) (A-C) and varying molecular weight with fixed concentration (20.9 µM (D-F).

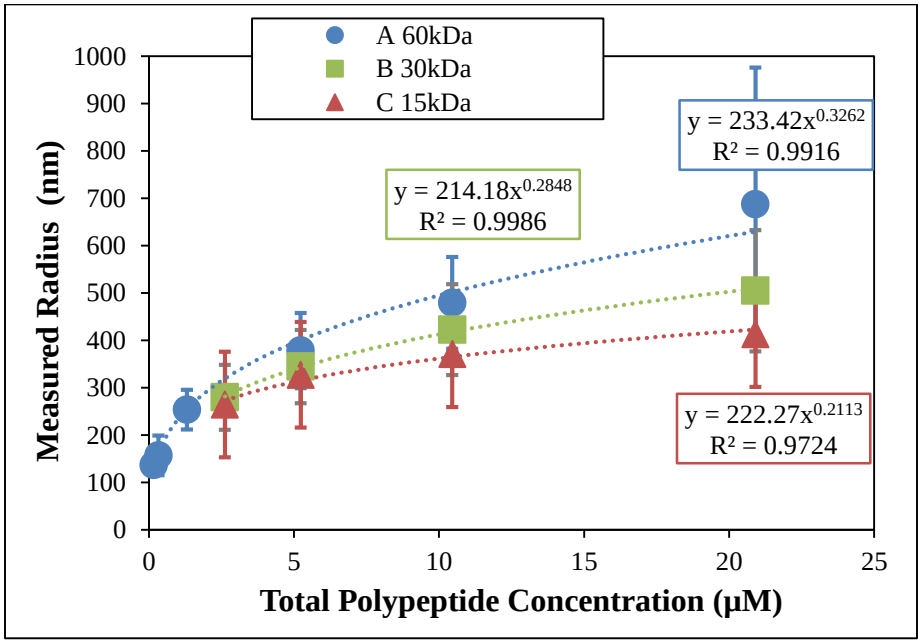

Figure 5.5: Summary of changes in PNP size versus concentration for three molecular weights, 60 kDa, 30 kDa, and 15 kDa.

5.3.4 Crosslinking Prevents Disassociation at Low pH

Polypeptide coacervates are electrostatic associations based on the attraction of oppositely charged amino acids. Thus, as pH changes, and the charge of the amino acid side chains are changed, the electrostatic association of the coacervates weaken and they ultimately disassemble. To test if the process of crosslinking with EDC increased the stability at low pH, turbidity was used as a measure of total coacervate formation. Turbidity of a solution of coacervates (with or without EDC crosslinking) was taken to be 100%. The pH was then titrated using 0.1M HCl and turbidity measured. At a pH of 4.5, non-crosslinked coacervates start to weaken and disassemble, shown as a decrease in turbidity. As pH is further decreased, non-crosslinked coacervates continue to disassemble until complete disassembly is reached at a pH of 2.5. Throughout the pH range tested, EDC crosslinked coacervates remain at 100% original turbidity, indicating no weakening or disassembly has occurred (Figure 5.6). Visually, the process of disassembly can be followed as shown in Figure 5.7. At pH 6, both coacervate and coacervate + EDC solutions show spherical particles. In the case of coacervate alone, droplets have merged to form larger droplets as they settled to the bottom of the tissue culture plate well. In the solution with coacervate +EDC, equilibrium size of the particles does not change as they settle in the well because they have been previously crosslinked to stabilize size. As pH is decreased to 3, a shrinking of the coacervates was observed and by pH 2, the coacervates have completely disassembled and the monomers have gone back into solution. In the coacervate + EDC, particles do not change shape, size or disassemble with decreasing pH (Figure 5.7).

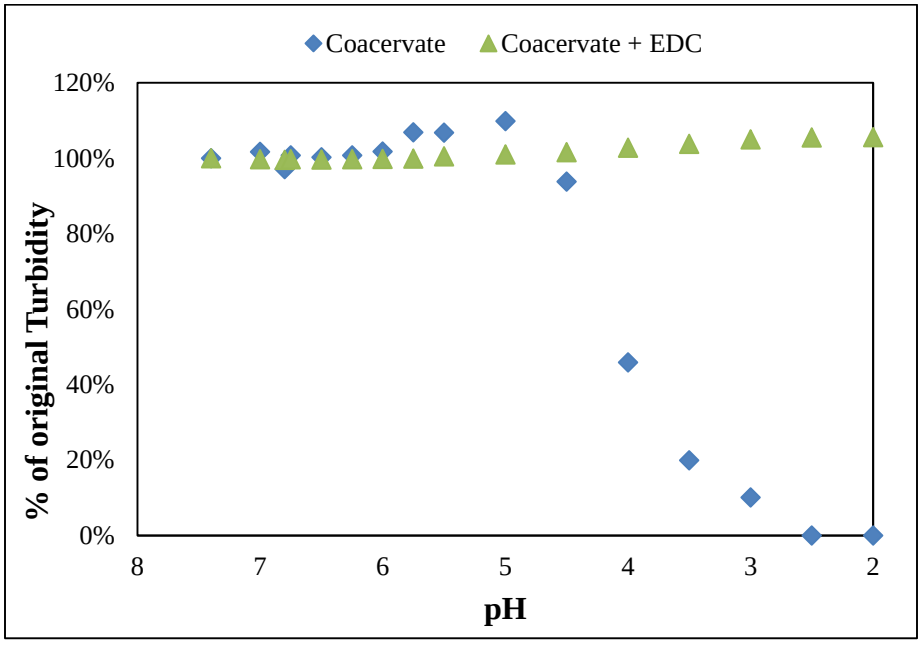

Figure 5.6: Turbidity versus pH for coacervate (non-crosslinked) and coacervate + EDC (crosslinked) solutions.

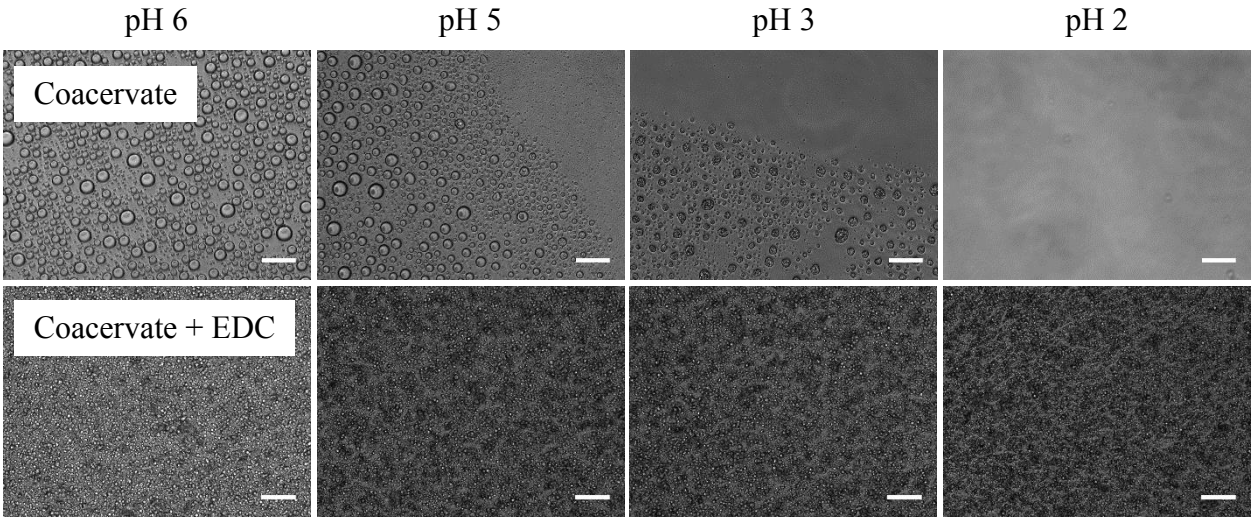

Figure 5.7: Microscopy images of coacervate and coacervate + EDC solutions at varying pH.

5.4 Discussion

Complex coacervate polypeptide nanoparticles (PNPs) can be easily created and stabilized by simple mixing. Unlike the harsh processing conditions used to form many other encapsulation technologies, PNPs are formed by simple mixing in benign, aqueous conditions. Complexation is driven by the electrostatic attraction between oppositely charged polypeptides, and crosslinking is achieved by creating a covalent bond between the polypeptide's amino acid R groups. Complex coacervates made of PLys/PGlu were previously shown to encapsulate a model protein, BSA, with high efficiency. Here we explore a method of controlling particle size and stability, important components for successful delivery.

Polypeptide complex coacervates are dynamic self-assembled structures, able to combine with neighboring droplets and absorb easily to charged surfaces. To prevent this rearrangement and lock in the self-assembled structure, EDC was used as a zero length crosslinker. As shown in Figure 5.1, particles that have been crosslinked have distinct spherical structure, and have not coalesced onto the silca surface of the SEM stub. In contrast, non-crosslinked coacervates merge and coalesce creating large amorphous droplets on the silca surface of the SEM stub. It was also found that changing the ratio of negative to positive polypeptides (PGlu to PLys) changed the surface charge of the particles and created colloidal stability, allowing the particles to be suspended without aggregating. In Figure 5.2, as the ratio of PGlu to PLys is increased, the surface charge of the nanoparticles becomes more negative. Interestingly, the zeta potential of particles with a ratio of 1.5:1 and 1.75:1 were slightly positive, which is unexpected given the excess of PGlu, a negatively charged polypeptide. This is likely due to residual counter-ion salts associated with the surface, and the difficulty in measuring particles which are not colloidally stable. The ability to control surface charge may be important based on the application of interest. Visually, at an equivalent ratio of PGlu to PLys, distinct spherical particles are formed, but aggregate easily likely due to their net neutral charge. At a ratio of 1.75:1 and 2:1, individual particles are suspended in solution. Achieving colloidal stability without the use of an additional surfactant or excipient is a positive attribute for a particle technology.

Control of size is a major focus of research in nanoparticles for biomedical applications. Changes in particle size can dictate where a particle might end up in the body and the rate at which cargo is released. Here, two methods of controlling particle size are studied, both the molecular weight of the polypeptide chains, and also the total polypeptide concentration. For this study, a ratio of 1.75:1 PGlu to PLys was used to ensure colloidal stability. In Figure 5.4A-C, as total concentration is decreased, smaller particles are formed. Similarly in Figure 5.4D-F, as the molecular weight of the polypeptides is decreased, particle size also decreases. Looking at a range of concentrations for each molecular weight, a master curve was created relating molecular weight, concentration, and size. For each molecular weight, a power law correlation was observed relating concentration and particle size. This result is consistent with results seen by Macoscko et. al. in the coalescence and breakup of droplets in polymer blends.[17] Briefly, both breakup and coalescence of droplets occur in equilibrium but as concentration is increased and neighboring droplets are brought closer together, the frequency of collisions and coalescence increases resulting in larger droplets with a larger size distribution. A decrease in molecular weight, shifts the curve of concentration versus size to smaller sizes. Here the concentration of amino acids was held constant, in other words, at concentration of 20 μM, the number of amino acids for both the 60 kDa and 30 kDa conditions would be the same, meaning for the 30 kDa there would be twice as many polymer chains as the 60 kDa. One possible explanation is that the longer length of the polypeptides leads to increased electrostatic attraction. This increased attraction could speed up the process of initial coacervate formation and prevent droplet breakup, thus increasing coalescence. Creation of this master curve of process conditions versus size illustrates how size could be tuned based on the requirements of the application.

Lastly, crosslinking the PNPs was shown to prevent disassembly at low pH. Complex coacervates are electrostatic associations and thus sensitive to changes in pH, which causes changes in the net charge of the polypeptide. In Figure 5.6 as pH was decreased, non-crosslinked coacervates began to disassemble as evident by a decrease in turbidity, a measure of coacervation. Crosslinked PNPs, however, where the electrostatic association of PLys and PGlu has been replaced by a covalent bond, are not sensitive to pH and stay fully intact down to a pH of 2. Visually, this process was monitored in Figure 5.7. Stability at low pH shows the conversion of electrostatic association to covalent bonding and may also be useful for applications where oral delivery is preferred and particles must survive in the harsh low pH environment of the gastrointestinal tract. Degradation of the particles then, would likely proceed through enzyme degradation.

5.5 Conclusions

Polypeptide complex coacervates are a useful polymer system able to encapsulate proteins in benign, aqueous conditions. One limitation of this system was that the coacervate phase is dynamic and can combine and coalesce over time. Here a method to prevent this coalescence and precisely tune particle size is presented. This system avoids many of the limitations present in the well-studied PLGA system, namely harsh solvent processing conditions, and inability to control size without implementation of a complex and costly process. The versatility of this PNP system could afford its use in a wide variety of applications where specific size and surface charge is needed.

5.6 References

1. Young, T. J., Johnston, K. P., Mishima, K. & Tanaka, H. Encapsulation of lysozyme in a biodegradable polymer by precipitation with a vapor-over-liquid antisolvent. *J. Pharm. Sci.* **88,** 640–50 (1999).

2. Lacasse, F., Hildgen, P. & Pérodin, J. Improved activity of a new angiotensin receptor antagonist by an injectable spray-dried polymer microsphere preparation. *Pharm. Res.* **14,** 887–891 (1997).

3. Kawashima, Y., Yamamoto, H., Takeuchi, H., Hino, T. & Niwa, T. Properties of a peptide containing DL-lactide/glycolide copolymer nanospheres prepared by novel emulsion solvent diffusion methods. *Eur. J. Pharm. Biopharm.* **45,** 41–8 (1998).

4. Aubert-Pouëssel, A., Venier-Julienne, M.-C., Saulnier, P., Sergent, M. & Benoît, J.-P. Preparation of PLGA microparticles by an emulsion-extraction process using glycofurol as polymer solvent. *Pharm. Res.* **21,** 2384–91 (2004).

5. Johnson, O. L. *et al.* A month–long effect from a single injection of microencapsulated human growth hormone. *Nat. Med.* **2,** 795–799 (1996).

6. Brown, L. R. Commercial challenges of protein drug delivery. *Expert Opin. Drug Deliv.* **2,** 29–42 (2005).

7. Kumari, A., Yadav, S. K. & Yadav, S. C. Biodegradable polymeric nanoparticles based drug delivery systems. *Colloids Surf. B. Biointerfaces* **75,** 1–18 (2010).

8. Desai, M. & Labhasetwar, V. Gastrointestinal uptake of biodegradable microparticles: effect of particle size. *Pharm. Res.* **13,** 1838–1845 (1996).

9. Storm, G., Belliot, S., Daemenb, T. & Lasic, D. D. Surface modification of nanoparticles to oppose uptake by the mononuclear phagocyte system. *Adv. Drug Deliv. Rev.* **17,** 31–48 (1995).

10. Patton, J., Bukar, J. & Nagarajan, S. Inhaled insulin. *Adv. Drug Deliv. Rev.* **35,** 235–247 (1999).

11. Bungenberg de Jong, H. B. & Kruyt, H. R. Coacervation (Partial Miscibility in Colloid Systems). *Proc. Sect. Sci, Koninkijke Ned. Akad. van Wet.* **32,** 849–856 (1929).

12. Shih, I.-L., Van, Y.-T. & Shen, M.-H. Biomedical applications of chemically and microbiologically synthesized poly(glutamic acid) and poly(lysine). *Mini Rev. Med. Chem.* **4,** 179–88 (2004).

13. Priftis, D. & Tirrell, M. Phase behaviour and complex coacervation of aqueous polypeptide solutions. *Soft Matter* **8,** 9396–9405 (2012).

14. Priftis, D., Megley, K., Laugel, N. & Tirrell, M. Complex coacervation of poly(ethylene-imine)/polypeptide aqueous solutions: thermodynamic and rheological characterization. *J. Colloid Interface Sci.* **398,** 39–50 (2013).

15. Tu, R. S. *et al*. Cooperative DNA binding and assembly by a bZip peptide-amphiphile. *Soft Matter* **6,** 1035–1044 (2010).

16. Boudou, T., Crouzier, T., Auzély-Velty, R., Glinel, K. & Picart, C. Internal composition versus the mechanical properties of polyelectrolyte multilayer films: the influence of chemical cross-linking. *Langmuir* **25,** 13809–19 (2009).

17. Sundararaj, U. & Macosko, C. Drop breakup and coalescence in polymer blends: the effects of concentration and compatibilization. *Macromolecules* **28,** 2647–2657 (1995).

Chapter 6: Future Work

In this dissertation nature's building block, peptides, were used to form self-assembled structures that address unmet medical needs in the field of biomaterials. Two classes of self-assembling materials were used, peptide amphiphiles and polypeptide coacervates in order to address unmet needs in regenerative medicine and drug delivery, respectively.

6.1 Peptide Amphiphiles for Regenerative Medicine

Shear induced gelation: C_{16}W3K

In this work, a novel method to induce multi-scale supramolecular structures in a PA solution through mechanical shear was studied. Upon dissolution, C_{16}-W3K PAs formed spherical micelles with a low solution viscosity. With the application of shear, the spherical micelles elongate to form worm-like micelles, which entangle and give rise to a viscoelastic hydrogel. Shear force is a trigger, which could be applied by injecting the solution through a thin needle, thus applying extensional shear, and forming a hydrogel at the site of an injury.

The principle issues with applying C_{16}-W3K *in vivo* is the low stiffness of the material and lack of biocompatibility. For the application of tissue engineering, biomaterials must match closely the stiffness, architecture, and function of native extracellular matrix of the tissues in question. With a maximum storage modulus of 72 Pa, the C_{16}-W3K system would not be suitable for repair of even the softest tissues in the body, such as brain tissue, which has a stiffness of 1,000 Pa.[1] In addition, at time points of 72 hours, a slight decline in cell viability was observed for cells grown on C_{16}-W3K gels. Though the C_{16}-W3K is an interesting system for the study of PA design, it is not suitable for the application of tissue engineering. Thus, a redesign of the C_{16}-W3K system is necessary. The toxicity is thought be caused by the positively charged lysine residues. Thus, a redesign should aim to replace the lysine residues with less toxic amino acids to avoid the toxicity. The alanine repeat sections should be conserved, as they are critical for the shear induced assembly. The detailed investigation of the conformational transitions in our designed C_{16}-W3K PAs can provide useful information about how to design other shear responsive peptide amphiphile systems.

pH induced gelation: C_{16}GSH

Keeping in mind the stiffness and biocompatibility limitations of C_{16}-W3K, a novel PA hydrogel that is stabilized by hydrogen bonding of the peptide headgroup was optimized for the application of peripheral nerve regeneration. C_{16}GSH assembles by hydrogen bonding at the peptide headgroup region. Because this hydrogen bonding occurs only at physiological pH and higher, due to the C_{16}GSH can be triggered to form hydrogels by manipulating the pH. An impressive span of stiffness (0.1-10 kPa) of the gel can be achieved by increasing the concentration of the PA molecules. In vitro tests were used to determine optimum concentration (and thus stiffness) of the gel to promote the activity of Schwann cells, a first responder of peripheral nerve injury, *in vitro*. For the purpose of the *in vivo* implantation experiments presented here, gels were pre crosslinked by raising the pH to 7.4 and then implanted. An important future step would be to optimize this system for in situ gelation. One possible method would be to use a dual injection syringe with PA solution on one side and a 2x concentrated

buffer in the other, such that upon injection (where the two solutions would be mixed), the final pH of the solution is 7.4.

The next step for this work is to evaluate the potential of C_{16}GSH in a small animal injury model as a conduit gel filler. Several conduits have been approved by the FDA for clinical use in humans, including NeuraGen® (Type I collagen), NeuroMatrix® (Type I collagen), Neurotube® (Polyglycolic acid), and Neurolac® (Polycaprolactone).[2] Surgically, when these tubes are implanted they are sutured to one nerve end, flushed with saline and sutured to close to the other nerve end. Clinically these tubes are limited to use in injuries of 3 cm or less. Our method would be to instead fill the conduits with a PA gel. By mimicking the natural ECM, the addition of a PA based fibrous hydrogel would give regenerating cells additional physical cues beyond the gross guidance provided by conduit. Any of the approved conduits would be appropriate to use in the animal model. Rat sciatic nerve injury is the most commonly used model in the field. Success can be measured by a variety of metrics including histology, electrical current, and gait analysis. Recent studies by Mark Van Dyke's group at Wake Forest and Kacey Marra's group at the University of Pittsburgh, detailed investigations of a keratin gel in a polycaprolactone conduit in a rat sciatic nerve model[3] and keratin gel in a collagen conduit in a rabbit sciatic nerve model.[4] These studies present a useful guideline for evaluating C_{16}GSH in a small animal model as a filler gel for an existing nerve guide conduit.

The unique properties of C_{16}GSH also could be studied to decouple the effects of fiber density and stiffness on cell spreading and migration *in vitro*. In the current system, increasing the concentration (and thus increasing fiber density and decreasing porosity) is coupled to increasing the stiffness. To separate this effect, mixed micelles of C_{16}GSH and C_{16}EoSH (a PEG linked variation) could be used to create a two parameter design space. Mixing in even a small amount of C_{16}EoSH to drastically reduced stiffness by orders of magnitude by preventing β-sheet bonding in the linker region of the PA (data not shown). An addition of a small percentage of C_{16}EoSH could be used to reduce the stiffness of a dense hydrogel. Thus it could be determined if Schwann cells prefer stiff and porous (full C_{16}GSH) or soft but dense (C_{16}GSH and C_{16}EoSH mix) hydrogels in migration assays.

Lastly, as shown in this work, C_{16}GSH hydrogels can be made with different stiffnesses that cover soft tissue, such as nerve or fat, up to very stiff tissues, such as collagenous bone. Thus, this system has potential to be used in a variety of other tissue engineering and regenerative medicine applications, such as difficult to solve cartilage and bone tissue injuries. Other PA systems have been tested in bone regeneration applications[5,6] but, C_{16}GSH, which has higher stability and stiffness, would likely be an improvement. A workflow similar to the workflow presented here for the peripheral nerve application should be followed: mechanical analysis, in vitro optimization and test design (as needed), and finally small animal injury model. This work demonstrated that C_{16}GSH can be formed, with a pH trigger, to form stable hydrogels with a wide range of stiffnesses that can be useful for a range of clinical applications. Future work should continue to study this molecule and bring it closer to the clinic.

6.2 Complex Coacervation for Drug Delivery

Protein Encapsulation via Polypeptide Complex Coacervation

A simple and powerful method of encapsulating proteins inside complex coacervates was demonstrated. It was demonstrated that there is tradeoff between loading efficiency and total

loading. Therefore, depending on the application, high loading capacity, up to 1:3 molar ratio of protein to polypeptide, or 100% loading of the protein can be achieved, depending on the process and cost of the protein which is often high. Encapsulated BSA, a model protein, retains its secondary structure when encapsulated and can be released under conditions of low pH due to disassembly of the coacervate.

One important consideration for using coacervates for protein encapsulation is to ensure that protein activity can be retained during encapsulation. In this work, retention of structure was studied as an indication of function, but function itself was not studied. A useful method to measure activity would be to encapsulate an enzyme with a colorimetric or conversion reporter. β-galactosidase is a useful enzyme for encapsulation as it cleaves a substrate which results in a product that can be monitored using absorbance of light at 420 nm.[7] Therefore, to protein function of β-galactosidase could be monitored before, during, and after disassembly of the coacervates. As complex coacervation is sensitive to salt and pH, further work could vary these factors to see how they affect enzyme function.

The purpose of encapsulating proteins, instead of delivering them freely in solution, is to protect them from degradation and clearance by the body. One major barrier to effective delivery is removal of particles in the bloodstream by the mononuclear phagocytic system, which includes Kupffer cells in the liver or spleen and bone-marrow macrophages.[8] An *in vitro* study that looks at the uptake of encapsulated proteins by macrophages would provide useful feedback. If it is found that complex coacervates are engulfed by macrophages, modifications to the design, such as the addition of a polyethylene glycol coating, could be added to help prevent uptake.[9] This work laid the foundation for using polypeptide coacervates as a method to encapsulate and delivery protein therapeutics, but challenges in controlling the size and stability of the coacervates still exist.

Polypeptide Nanoparticles: Design and Stability

To control the size and stability of polypeptide coacervates, the crosslinker EDC was used to create a peptide bond between the amino acid side groups of poly(L-lysine) (PLys) and poly(D/L-glutamic acid) (PGlu). By changing the ratio of PGlu to PLys colloidal stability was achieved without the need for an additional excipient. Surface charge of the particles was also controlled by this method. Final particle size was controlled by both molecular weight and concentration of the polypeptides. A span of particle diameter from to 272nm to 1.3 μm was achieved. Lastly, stability at low pH, where non-crosslinked coacervates disassemble, was demonstrated. A simple and tunable method to control particle size, such as the one presented here provides a possible solution to a major limitation in the field of drug delivery, control of particle size.

The primary idea behind allowing complex coacervates to form and then locking in the self-assembled species with a crosslinker is a powerful and versatile way to form nanoparticles with controlled size. In addition, it can be performed under aqueous conditions that are suitable for proteins. However, there are draw backs to the particular chemistry that was used in this work. EDC reacts with primary amines and carboxcylic acids, which are present on the primary amine group of lysine and the carboxylic acid of glutamic acid. Proteins contain these functional groups at their N and C terminus and may contain both lysine and glutamic acid amino acids as well. Thus, if a protein was encapsulated in the complex and then crosslinked, it is likely that the protein would be crosslinked to the polypeptides. This could potentially disrupt the structure of

the protein and impair function. Two possible solutions exist. By introducing the crosslinker after the coacervate is formed at the minimum necessary concentration, it is theorized that only the shell of the coacervate would be crosslinked and protein at the core of the coacervate would be unharmed. To determine if this is a viable solution, it would first need to determine if the protein resides on the outside or in the core of the coacervates. The alternative solution would be to use this work as a template, but switch the crosslinking chemistry and active groups. Amino acids with polymer groups susceptible to click chemistry could be included in the polypeptide that forms the coacervates and linked in a way that does not affect proteins.

In this work, it was demonstrated that polypeptide coacervates, which typically have poor stability and control over size, could be stabilized, and their size controlled, by crosslinking them. Future work should continue to optimize this as a platform for protein delivery.

6.3 References

1. Pettikiriarachchi, J. T. S., Parish, C. L., Shoichet, M. S., Forsythe, J. S. & Nisbet, D. R. Biomaterials for Brain Tissue Engineering. *Aust. J. Chem.* **63,** 1143–1154 (2010).

2. Meek, M. F. & Coert, J. H. US Food and Drug Administration/Conformit Europe-approved absorbable nerve conduits for clinical repair of peripheral and cranial nerves. *Ann. Plast. Surg.* **60,** 110–6 (2008).

3. Lin, Y.-C. *et al.* Keratin gel filler for peripheral nerve repair in a rodent sciatic nerve injury model. *Plast. Reconstr. Surg.* **129,** 67–78 (2012).

4. Hill, P. *et al.* Repair of peripheral nerve defects in rabbits using keratin hydrogel scaffolds. *… Eng. Part A* **17,** 1500–1505 (2011).

5. Sargeant, T. D. *et al.* Hybrid bone implants: self-assembly of peptide amphiphile nanofibers within porous titanium. *Biomaterials* **29,** 161–71 (2008).

6. Hartgerink, J. D., Beniash, E. & Stupp, S. I. Self-assembly and mineralization of peptide-amphiphile nanofibers. *Science* **294,** 1684–8 (2001).

7. Kunkel, J. & Asuri, P. Function, structure, and stability of enzymes confined in agarose gels. *PLoS One* **9,** 2–6 (2014).

8. Stolnik, S., Illum, L. & Davis, S. S. Long circulating microparticulate drug carriers. *Adv. Drug Deliv. Rev.* **16,** 195–214 (1995).

9. Immordino, M. L., Dosio, F. & Cattel, L. Stealth liposomes: review of the basic science, rationale, and clinical applications, existing and potential. *Int. J. Nanomedicine* **1,** 297–315 (2006).